iScience

CellPress

Article

Pd-Catalyzed Aerobic Oxidative Heck Cross-Coupling for the Straightforward Construction of Indole δ-Lactams

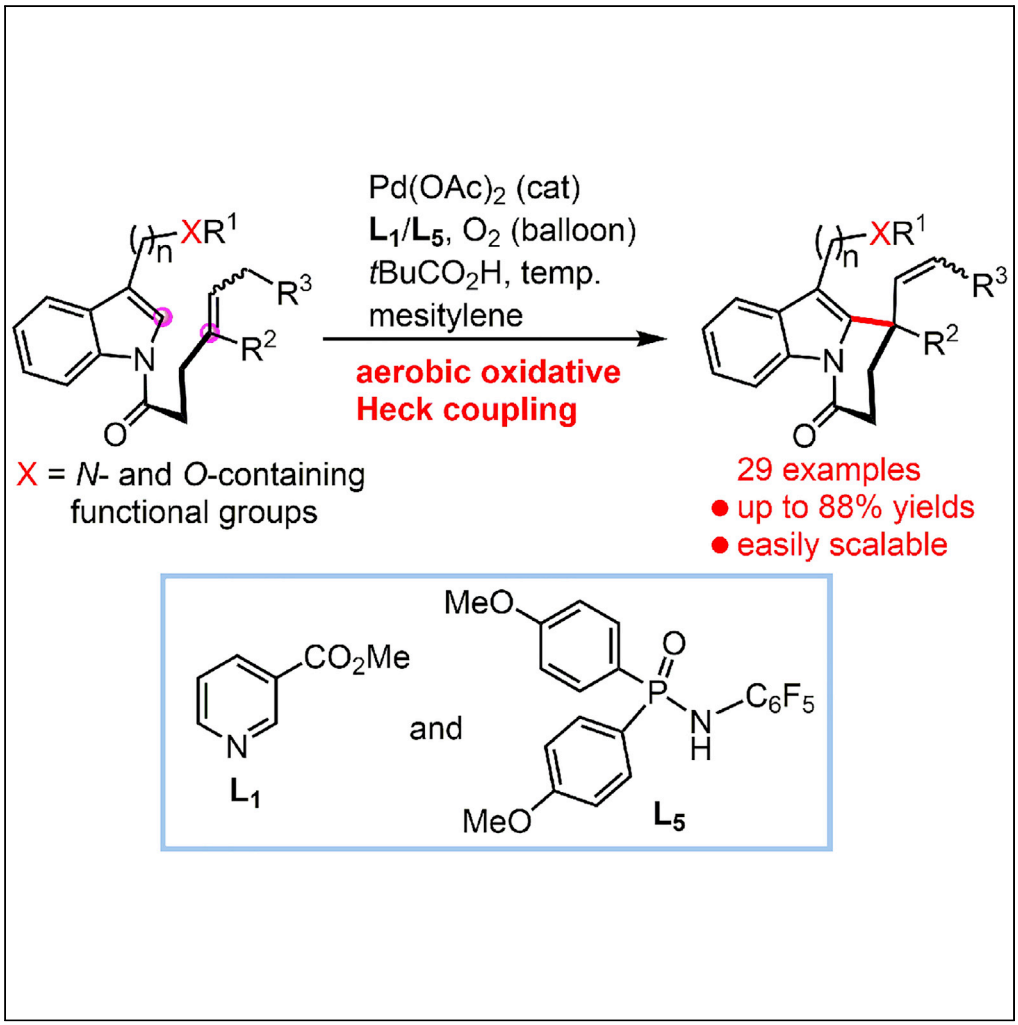

Jing Zhang, Fu-She Han

fshan@ciac.ac.cn

HIGHLIGHTS

Construction of indole δ-lactams enabled by a Pd-catalyzed oxidative Heck coupling

The phosphinamide L_5 was crucial as a co-ligand for prompting the reaction

A $Pd^{(I)}/Pd^{(III)}$ catalytic cycle is proposed to be responsible

Zhang & Han, iScience 17, 256–266
July 26, 2019
https://doi.org/10.1016/j.isci.2019.06.037

iScience

CellPress

Article

Pd-Catalyzed Aerobic Oxidative Heck Cross-Coupling for the Straightforward Construction of Indole δ-Lactams

Jing Zhang[1,2] and Fu-She Han[1,3,*]

SUMMARY

The [6.5.6]-tricyclic indole δ-lactam represents a common key intermediate for the synthesis of a broad variety of structurally intriguing indole alkaloids. The development of a method for the versatile and straightforward construction of such structural motif is of great importance for potential synthetic applications. Herein, we present a co-ligand-prompted Pd-catalyzed *6-exo-trig* intramolecular cyclization of indolyl amides via the aerobic oxidative Heck cross-coupling. The method provided a general and efficient way for the construction of [6.5.6]-tricyclic indole δ-lactams. A mechanistic study suggests that a $Pd^{(I)}/Pd^{(III)}$ catalytic cycle should be responsible for effective coupling, which represents a mechanistically alternative pathway when compared with the $Pd^{(0)}/Pd^{(II)}$ cycle proposed for other related coupling reactions.

INTRODUCTION

The leuconoxine subfamily of aspidosperma-derived monoterpene indole alkaloids (e.g., **1**–**8** in Figure 1) was isolated from the plants of the genus *Leuconotis* (*Apocynaceae*) (Pfaffenbach and Gaich, 2016; Geng et al., 2016; Tokuyama, 2015). These natural products possess a unique diaza-[5.5.6.6]-fenestrane structural motif that is extremely rare in indole natural products. The latex of the plants was used traditionally to treat worm infections and yaws diseases. Owing to their high structural complexity and interesting biological properties, these and the related natural products have attracted much attention in the synthetic community. The efficient construction of the δ-lactam-containing (Figure 1, highlighted in red) ring-fused system has been the key issue of intensive synthetic efforts. The reported methods include free radical-induced cyclization (Magolan and Kerr, 2006; Magolan et al., 2008; Biechy and Zard, 2009; Zhu et al., 2015; Yu et al., 2016a, 2016b), Heck cross-coupling (Umehara et al., 2014; Iwama et al., 2013), and Friedel-Crafts reactions (Feng et al., 2015; Lv et al., 2014; Zhong et al., 2012, 2014, 2015; Liang et al., 2016; Zheng et al., 2018) at $C_{20}-C_{21}$; the amidation of ester (Xu et al., 2013, 2015; Nakajima et al., 2010; Higuchi et al., 2015; Li et al., 2015) or oxidative amidation of alcohol (Pfaffenbach and Gaich, 2015) at N_1-C_2; and the transannular cyclization (Yang et al., 2014a, 2014b; Dagoneau et al., 2016) of an aryl amide with ketone functionality via N_1-C_{21}.

Having experienced the synthetic studies on tronoharine (Zhong et al., 2015) and mersicarpine indole alkaloids (Zhong et al., 2012, 2014), we recently became interested in the leuconoxine subfamily, a class of structurally more intriguing and synthetically more challenging indole alkaloids. As mentioned, the key issue toward the efficient synthesis of this class of natural products and potential analogs with structural diversity is the establishment of a straightforward method for effective construction of the common intermediate [6.5.6]-tricyclic indole δ-lactam. To this end, we conceived of a transition-metal-catalyzed oxidative Heck coupling (i.e., dual dehydrogenative coupling) protocol, which, conceptually and strategically, would provide an ideal platform for accessing such structural skeletons as witnessed by the recent great advance in transition-metal-catalyzed oxidative C–C bonding formation (Shi et al., 2011; Liu et al., 2011, 2015). In fact, there has been rapidly growing interest in oxidative Heck-type coupling of indole and other classes of substrates (Abbiati et al., 2003; Ferreira and Stoltz, 2003; Ferreira et al., 2008; Schiffner et al., 2010; Pintori and Greaney, 2011; Kandukuri et al., 2012; Kandukuri and Oestreich, 2012; Broggini et al., 2012; Yang et al., 2014a, 2014b; Ikemoto et al., 2014; Gao et al., 2016; Meng et al., 2013, 2014), and the great advantage of the related reaction in natural product synthesis has been demonstrated early by the synthesis of a few indole-type natural products (Baran et al., 2003; Meng et al., 2015; Lu et al., 2014).

However, surprisingly, a literature survey showed that among the related reports, methods for the construction of six-membered cycles through oxidative Heck coupling at indole N_1 and C_2 have been rarely

[1]CAS Key Lab of High-Performance Synthetic Rubber and Its Composite Materials, Changchun Institute of Applied Chemistry, Chinese Academy of Sciences, 5625 Renmin Street, Changchun, Jilin 130022, China

[2]The University of Chinese Academy of Sciences, Beijing 100864, China

[3]Lead Contact

*Correspondence: fshan@ciac.ac.cn

https://doi.org/10.1016/j.isci.2019.06.037

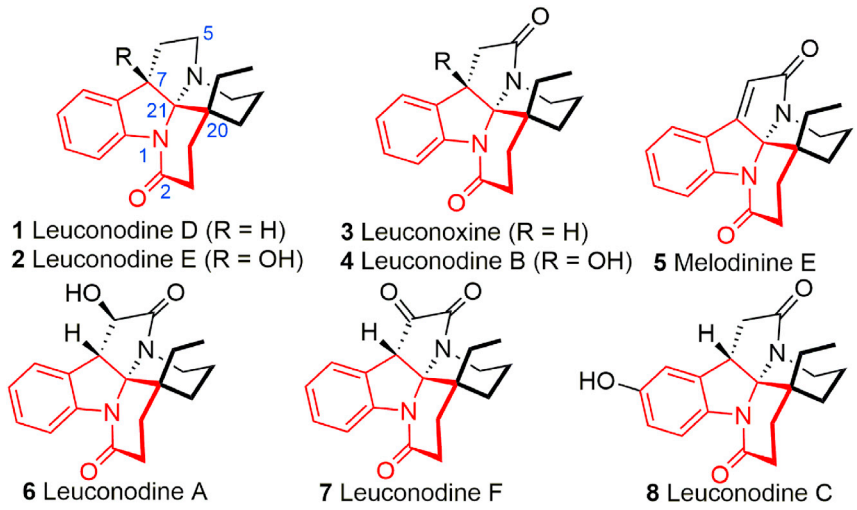

Figure 1. Selected Structures of Leuconoxine Subfamily

reported. Of the very few relevant examples investigated so far, the attempted oxidative Heck coupling of **9** (n = 2) afforded the 6-*exo-trig* product **11** only in poor yield under a variety of conditions (Schiffner et al., 2010) (Figure 2A). More interestingly, it was found that the substrate **10** (n = 1) with one carbon less than **9** produced exclusively the 5-*exo-trig* product **12** in moderate to good yields without, however, the observation of the sterically more favored six-membered 6-*endo-trig* isomers **12a** and **12b** (Ferreira et al., 2008; Schiffner et al., 2010). Apparently, these unsuccessful precedents imply that the construction of six-membered cycles at indole N_1 and C_2 by means of oxidative Heck coupling is exceptionally challenging.

Nevertheless, we decided to investigate this challenging reaction because of the great potential utility in versatile synthesis of various indole natural products such as shown in Figure 1. In our study, a directing group-oriented oxidative coupling of indole derivatives **13** was devised (Figure 2B). Conceptually, we envisaged that the presence of a heteroatom-containing side chain tethered to indole C_3 may serve to act as a directing group to prompt the C–H activation through a geometrically favored intermediate **14**, and ultimately, driving the coupling reaction with the olefin functionality to afford the δ-lactam **15**. On the other hand, the side chain in the cross-coupled products, without the need to remove, can be further manipulated at the late stage as a latent functionality toward the synthesis of various indole natural products and their analogs. Taking together these advantages, the protocol proposed herein would provide not only a strategically distinctive but also a methodologically much more efficient tool for the construction of indole δ-lactams. The successful demonstration of the devised oxidative Heck cross-coupling protocol and mechanistic study will be presented herein.

RESULTS AND DISCUSSION

The Development of Method for Oxidative Heck Coupling

Optimization of the reaction parameters was carried out using indole derivative **13a** as a model compound (Table 1). Based on the conditions reported by Stoltz (Ferreira and Stoltz, 2003; Ferreira et al., 2008) and Oestreich (Schiffner et al., 2010; Kandukuri et al., 2012), a broad array of pyridine ligands was examined with the presence of different palladium catalysts in our initial screening because it was suggested that the basicity of pyridine nitrogen was critical to the catalytic activity of metal catalysts owing to their different coordination properties. Disappointedly, an exhaustive optimization of the reaction conditions by means of a free combination of various reaction parameters including ligands, catalysts, oxidants, additives, temperature, and solvents showed that the coupling reaction was almost ineffective in most cases (data not shown). Only a few sets of conditions could afford the desired product **15a** in low to moderate yields with 43% as the best outcome in the presence of L_1 ligand (Table 1, entry 1). In addition, L_2 afforded **15a** at an yield similar to L_1 (entry 2). In contrast, only a trace amount of product was detected for bidentate L_3 (entry 3).

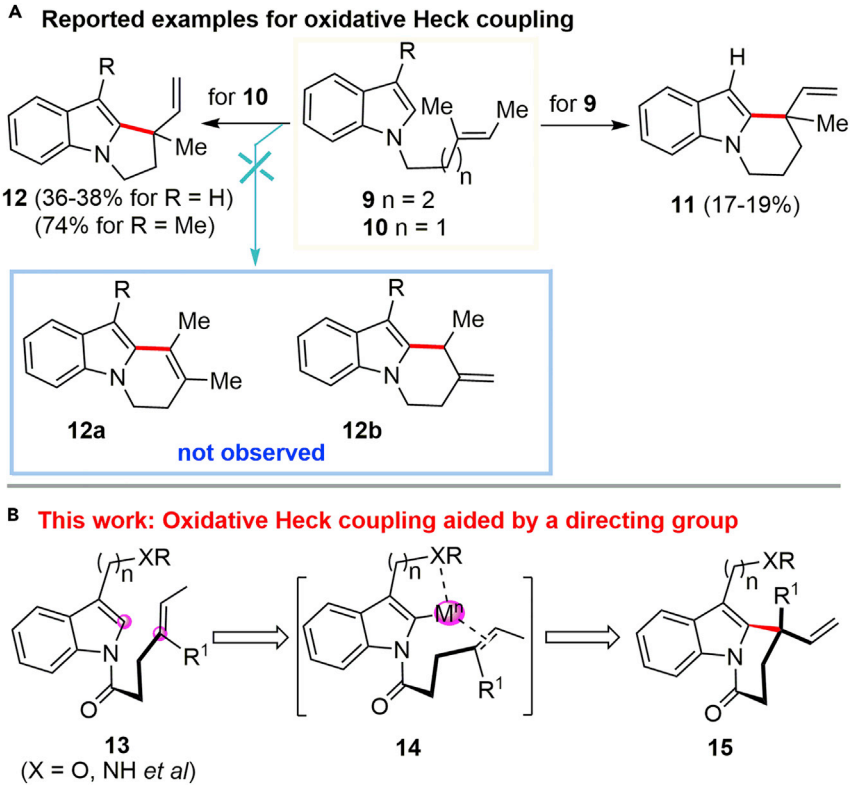

Figure 2. Oxidative Heck coupling at indole N_1 and C_2
Reported (A) and our proposed (B) oxidative Heck coupling.

The dramatic effect of the structural nature of ligands on this reaction prompted us to turn our attention to search an alternative catalyst system or ligand. Accordingly, we shifted our focus to a phosphinamide-based palladacycle catalyst **16,** which was developed previously by our group (Du et al., 2015; Guan et al., 2014). A supportive clue, albeit not tightly related with the proposed Heck-type reaction, that encouraged us to inspect this catalyst herein is that **16** exhibited extremely high catalytic activity for mild Suzuki coupling of a broad range of arene (*pseudo*)halides (Wu et al., 2015, 2018; Cao et al., 2018). To our delight, the use of **16** as catalyst did improve substantially the yield of **15a** to 72% (entry 4). In addition, it was found that the presence of O_2 was essential because the yield was markedly decreased under air atmosphere (entries 4 versus 5). A brief screening of solvents showed that mesitylene was superior to others (entries 4 versus 6–10). Interestingly, a further comparison revealed that the direct addition of $Pd(OAc)_2$ and phosphinamide ligand L_4 to the reaction system gave the product **15a** in identical yield to that of utilizing the pre-formed palladium complex **16** (entries 4 versus 11). Finally, an orthogonal evaluation on pyridine and phoshinamide ligands (entries 11–16) demonstrated that an appropriate combination of a catalytic amount of L_1 and L_5 (molar ratio = 4:1) was optimal, affording **15a** in 76% yield (entry 14). Notably, the reaction could be reliably performed on gram scale in 70% yield (entry 14). Of note is that when the ligands L_1 and L_5 were used independently, the reaction efficiency was dramatically diminished (entries 1 and 17). Our further control experiments showed that when the pre-formed palladacycle **16** was used, L_4 was dissociated from palladacycle **16** to recover the ligand in quantitative yield after the reaction was completed. On the other hand, a comparison study demonstrated that palladacycle **16** did not form *in situ* from $Pd(OAc)_2$ and L_4 either in the presence or absence of substrate **13a**. These results coupled with the detection of free L_4 by HRMS (see Figure S5) in the reaction system imply that L_4 may serve to act as a co-ligand rather than the formation of palladacycle **16** with $Pd(OAc)_2$ in the reaction system. In the case of using palladacycle **16**, the protonolysis of C–Pd bond may occur to release the phosphinamide ligand. Thus the effective coupling by using mixed ligands is presumably due to the well-balanced basicity of the two ligands (Ferreira et al., 2008; Kandukuri et al., 2012).

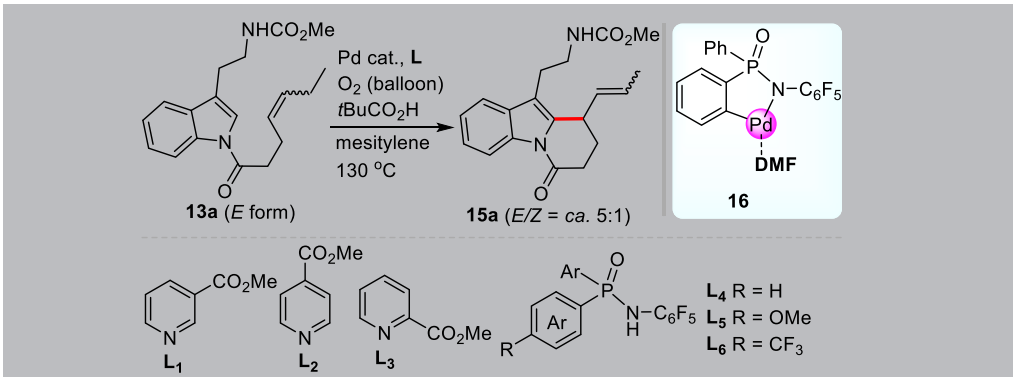

Entry	Catalyst (10 mol %)	Ligand (mol %)	Solvent	Yield (%)[a]
1	$Pd(OAc)_2$	L_1 (40)	Mesitylene	43
2	$Pd(OAc)_2$	L_2 (40)	Mesitylene	40
3	$Pd(OAc)_2$	L_3 (40)	Mesitylene	Trace
4	**16**	L_1 (40)	Mesitylene	72
5	**16**	L_1 (40)	Mesitylene	30[b]
6	**16**	L_1 (40)	$tBuO_2H$	54
7	**16**	L_1 (40)	DMF	45
8	**16**	L_1 (40)	DMSO	30
9	**16**	L_1 (40)	*p*-Cylene	23
10	**16**	L_1 (40)	PhCl	Trace
11	$Pd(OAc)_2$	L_1/L_4 (40/10)	Mesitylene	72
12	$Pd(OAc)_2$	L_2/L_4 (40/10)	Mesitylene	74
13	$Pd(OAc)_2$	L_3/L_4 (40/10)	Mesitylene	Trace
14	$Pd(OAc)_2$	L_1/L_5 (40/10)	Mesitylene	76 (**70**)[c]
15	$Pd(OAc)_2$	L_2/L_5 (40/10)	Mesitylene	74
16	$Pd(OAc)_2$	L_1/L_6 (40/10)	Mesitylene	42
17	$Pd(OAc)_2$	L_5 (10)	Mesitylene	20

Table 1. Optimization of the Reaction Conditions

Conditions: **13a** (60 mg, 0.18 mmol), catalyst (10 mol %), ligand (x mol %), O_2 (balloon), and $tBuCO_2H$ (30.0 equiv.) in solvent (0.1 mol/L) at 130°C for 16 h.

[a]Isolated yield.

[b]The reaction was performed under air atmosphere.

[c]The data in parentheses was the yield using 1.50 g of **13a**.

With the optimized conditions established, we then examined the substrate scope (Table 2). Various substrates modified by electron-neutral (**15a**), electron-donating (**15b**), and electron-withdrawing (**15c**–**15e**) substituents at different positions in indole ring were well tolerated. In addition, different substituents such as Me (**15f**), Et (**15a**–**15e**, **15h**–**15n**), and ester (**15g**) at olefin terminal were also competent. Importantly, a broad compatibility was also observed for the functional groups at the indole C_3 side chain, including a range of amino functionalities protected by MeOC(O) (**15a**–**15g**, **15k**), Cbz (**15h**), Ts (**15i**), Tf (**15j**), hydroxy group (**15l**), and ester groups (**15m** and **15n**). This would be an important advantage for a late-stage flexible manipulation when synthesis of indole alkaloids and potential analogs with structural diversity is under consideration. Of note is that substrates having a simple Me or H at indole C_3 were intact

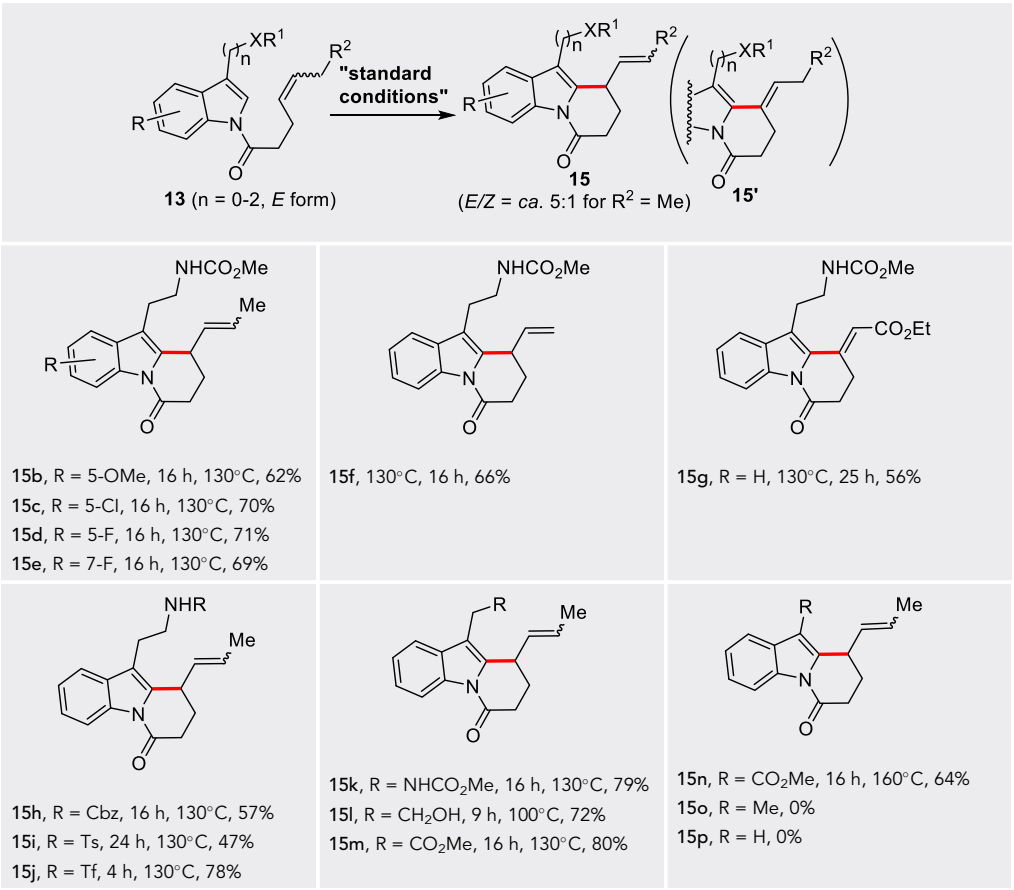

Table 2. Substrate Scope for the Construction of Tertiary Carbon Center

Conditions: **13** (100 mg), $Pd(OAc)_2$ (10 mol %), $\mathbf{L_1}$ (40 mol %), $\mathbf{L_5}$ (10 mol %), O_2 (balloon), and tBuCO$_2$H (30.0 equiv.) in mesitylene (0.1 mol/L); isolated yield; *E/Z* was determined by ^{1}H NMR.

(**15o** and **15p**). These results are in good agreement with our hypothesis that the presence of a heteroatom-containing directing group at C_3 is essential for effective coupling (*vide supra*). Here, an interesting observation was that except for **15g** whose β-hydride elimination took place at the tertiary carbon, the β-hydride elimination for other reactions proceeded exclusively at the secondary or primary carbon to produce the thermodynamically less stable products with non-conjugated double bonds. The outcomes could be rationally explained based on the C–H activation mechanism and coordination effect at C_3 side chain (see mechanistic study vide infra).

Next, we expanded the methodology to the construction of quaternary carbon center and bridged cycle. Gratifyingly, the reaction proceeded smoothly to give both types of products in high yields under the standard conditions (Table 3). As for the construction of quaternary carbon center, the substrates decorated by various substituents in indole ring as well as at the C_3 side chain and olefinic positions displayed good viability (**15q**–**15x**). Notably, the reaction could be uneventfully performed on gram scale as exemplified by the synthesis of **15w** bearing an Et group at the quaternary carbon center, which appears as a common group in a number of related natural products (Figure 1, **1**–**8**). Concerning the construction of aza[3.3.1]-bridged cycle, the substrates tethered with an aminoethyl group at C_3 position were less effective under the standard conditions. For instance, a Tf-protected substrate afforded the product **15y** in 21% yield containing a minor amount of inseparable by-products. However, substrates bearing a hydroxyethyl group reacted facilely. The electron-neutral (**15z** and **15aa**), electron-donating (**15ab**), and electron-withdrawing (**15ac**) groups in indole cycle had little effect on the reactivity. The reaction could also be reliably performed on large scale (**15z**). As the aza[3.3.1]-bridged skeleton exists in a range of chippiine-type indole natural products (Kam et al., 1992, 1993, 2000, 2004), the method would also be potentially useful in the synthesis

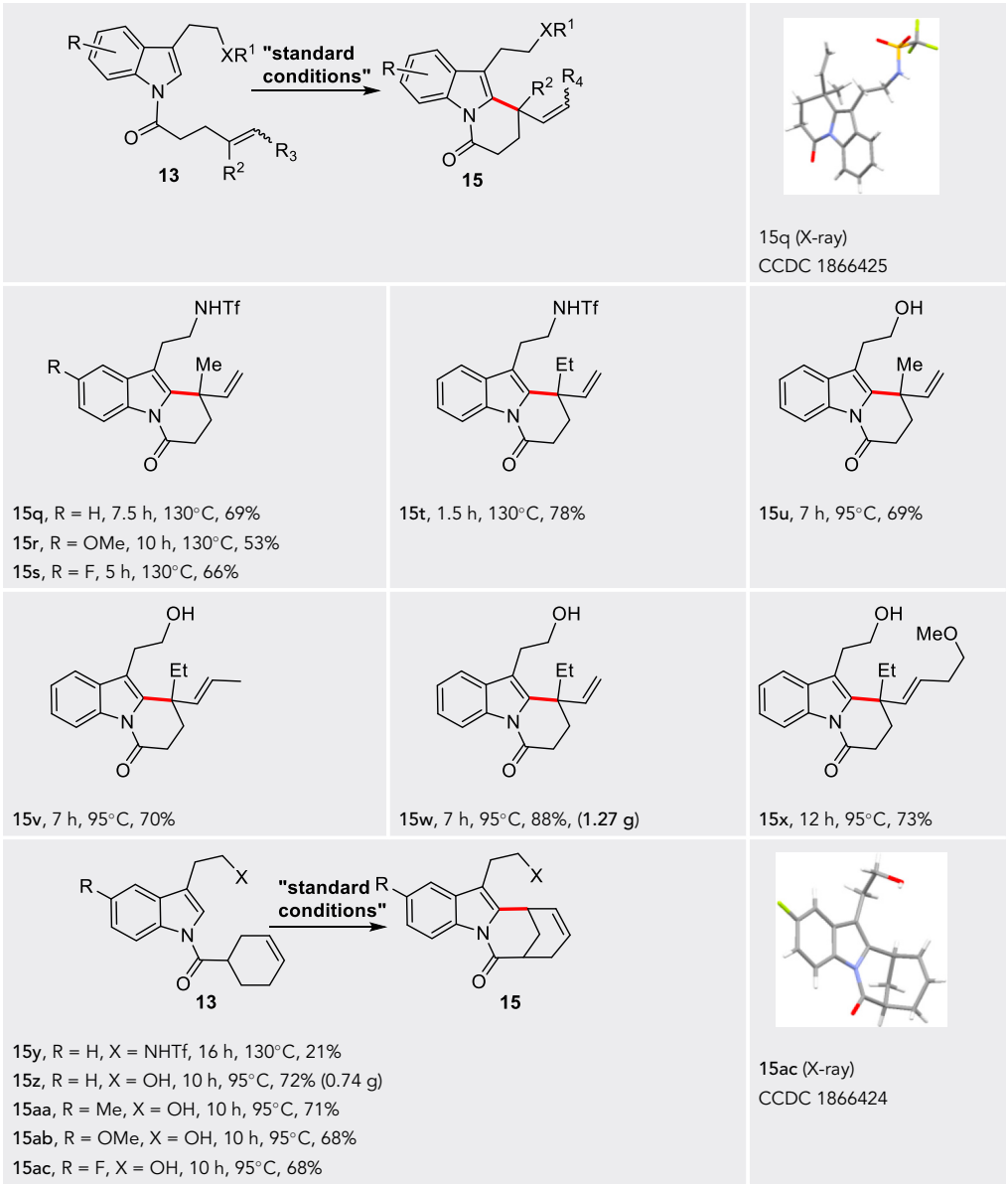

Table 3. Substrate Scope for the Construction of Quaternary Carbon and Aza[3.3.1]-Bridged Cycle

Conditions: **13** (100 mg), $Pd(OAc)_2$ (10 mol %), L_1 (40 mol %), L_5 (10 mol %), O_2 (balloon), and $tBuCO_2H$ (30.0 equiv.) in mesitylene (0.1 mol/L); isolated yield.

of related natural products. The structures of both types of compounds were confirmed by NMR and HRMS, and were further clarified by the single X-ray crystallography of **15q** (CCDC 1866425) and **15ac** (CCDC 1866424).

Mechanistic Study of Oxidative Heck Coupling

Having verified the broad generality of the methodology, we investigated the reaction mechanism. First, three control experiments by using **13a**, deuterated **13a-D** (*ca.* 92% D, see Figure S2), and a 1:1 mixture of **13a** and **13a-D** as substrates were carried out to confirm whether the C−H bond or alkene activation is involved in the catalytic cycle. Surprisingly, almost identical yields were obtained for the three reactions under standard conditions, indicating no isotopic effect. However, a further analysis on the recovered starting materials revealed that the undeuterated **13a** was the major component for the reaction

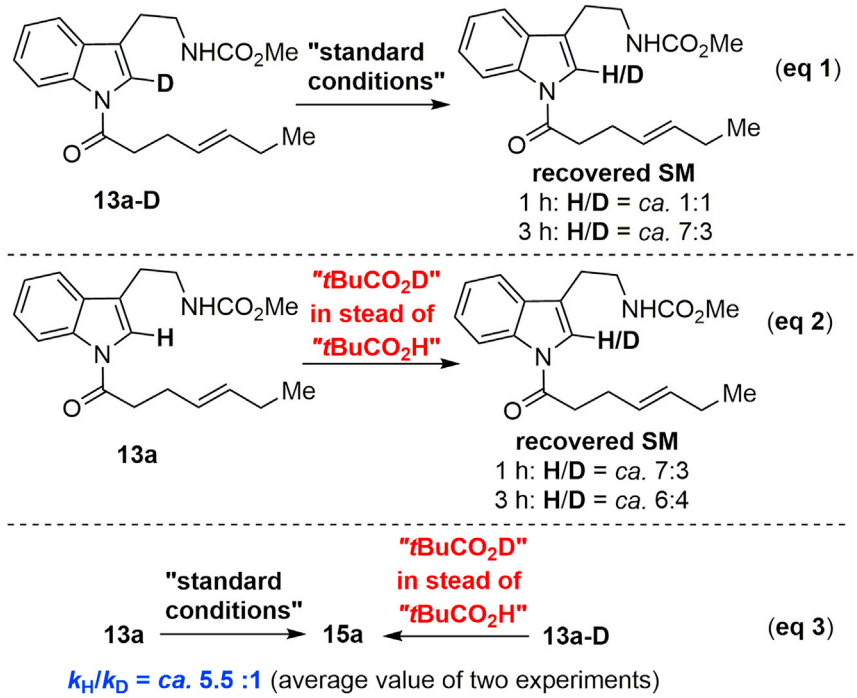

Scheme 1. The Control Experiments of H/D Exchange (Equations 1 and 2) and Kinetic Isotopic Effect (Equation 3)

using **13a-D** as substrate. The serendipitous result indicates that H/D exchange at indole C_2 may take place during the reaction, which should interrupt the actual observation of isotopic effect. To clarify this point, further detailed control experiments were performed. Accordingly, treatment of the deuterated substrate **13a-D** (Scheme 1, Equation 1) under the standard conditions followed by the quantitative NMR and HRMS analyses of the recovered starting material revealed that H/D interchange took place at indole C_2 position (see Figure S3). Moreover, the ratio of H/D interchange increases with the elongation of reaction time (i.e., H/D = *ca.* 1:1 for 1 h, and *ca.* 7:3 for 3 h). Alternatively, treatment of undeuterated **13a** under conditions identical to that of Equation 1 but just replacing *t*BuCO$_2$H with *t*BuCO$_2$D (*ca.* 90% D) resulted in an H/D = *ca.* 7:3 and 6:4 of the recovered **13a** (Scheme 1, Equation 2) after 1 h and 3 h, respectively (See Figure S4). The orthogonal experiments clearly exemplified that significant H/D exchange between the indole C_2–H of the substrate and *t*BuCO$_2$H takes place.

Thus, to avoid the interruption of proton scrambling between the substrate and *t*BuCO$_2$H in the study of kinetic isotopic effect (KIE), we designed two experiments. One was performed using **13a** as substrate under standard conditions and the other one was carried out using deuterated **13a-D** as substrate but replacing *t*BuCO$_2$H with *t*BuCO$_2$D (Scheme 1, Equation 3). As slow decomposition of product **15a** was detected (Ferreira et al., 2008), the time-dependent conversion of substrates rather than the formation of product was monitored by high-performance liquid chromatography (Figure 3, left and see also Table S1). The KIE was deduced based on the conversion of substrates versus the reaction time (Figure 3, right). The observation of a large primary KIE with k_H/k_D = *ca.* 5.5:1 indicates that C–H activation should be the rate-determining step of the oxidative Heck coupling.

Next, we investigated the redox cycle of palladium catalyst. Although a $Pd^{(0)}/Pd^{(II)}$ cycle was tentatively proposed in the literature (Ferreira et al., 2008; Kandukuri et al., 2012) for the five-membered cyclization reaction, we envisioned that our 6-*exo*-*trig* annulation should undergo an alternative pathway based on the experimental phenomena, such as color change of the reaction system (*vide infra*). We used HRMS to detect any possible Pd-containing species. Four strong peaks and several weak ones related with palladium complexes were captured for the reaction under oxygen atmosphere (see Figure S5). The strong peaks at *m/z* = 365.9951 and 385.0353 can be assigned to a $Pd^{(III)}$ species with a formula of

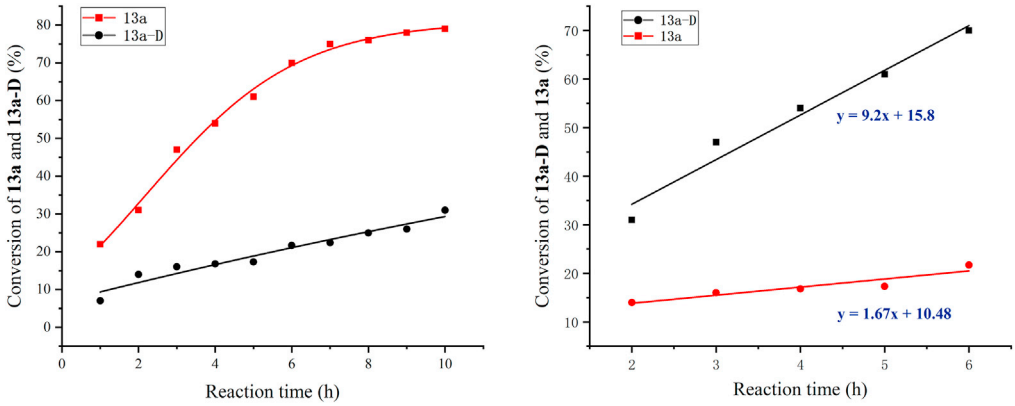

Figure 3. Kinetic Isotopic Effect

Conversion profile (left) and the linear fitting (right) of the substrates **13a** and **13a-D**.

$[Pd^{(III)}(MeCO_2^-)_2(tBuCO_2^-)(H_2O)Na^+]$ (calculated for $C_9H_{17}NaO_7Pd^+$: *m/z* 365.9901) and a $Pd^{(II)}$ complex $[Pd^{(II)}(tBuCO_2^-)\mathbf{L_1}(MeCN)]$ (calculated for $C_{14}H_{19}N_2O_4Pd^+$: *m/z* 385.0374), respectively. In addition, all the weak peaks can also be well assigned. However, the other two strong peaks at *m/z* = 468.0598 and 481.0558 cannot be rationally assigned because either the $Pd^{(III)}$ complexes $[Pd^{(III)}(MeCO_2^-)_2(tBuCO_2^-)(tBuCO_2H)(H_2O)Na^+]$ (calculated for $C_{14}H_{27}NaO_9Pd^+$: *m/z* 468.0582) and $[Pd^{(III)}(MeCO_2^-)_2(tBuCO_2H)(H_2O)\mathbf{L_1}]$ (calculated for $C_{16}H_{25}NO_9Pd^+$: *m/z* 481.0559) or the $Pd^{(II)}$ complexes $[Pd^{(II)}(tBuCO_2^-)_2\mathbf{L_1}Na^+]$ (calculated for $C_{17}H_{25}NNaO_6Pd^+$: *m/z* 468.0609) and $[Pd^{(II)}(tBuCO_2^-)(\mathbf{L_1})_2]$ (calculated for $C_{19}H_{23}N_2O_6Pd^+$: *m/z* 481.0586) are possible. For a further clarification, we inspected the reaction under argon atmosphere. Three signals were detected involving a strong signal of $Pd^{(II)}$ complex at *m/z* = 385.0362. In addition, the two peaks at *m/z* = 468.0609 and 481.0589 as those that appeared under oxygen atmosphere were also observed. However, they were remarkably much weaker than those under oxygen atmosphere. Thus, a comparison of the HRMS analysis under different conditions implies that most probably the two signals should belong to $Pd^{(III)}$ complexes. The detection of these signals under argon atmosphere may be resulted from the oxidation of some minor oxidants involved in the reaction system. All the above experiments displayed good reproducibility.

Further support for the generation of $Pd^{(III)}$ complexes is the apparent color change of the reaction solution. Namely, the color changed from pale yellow to deep red-brown for the solution under oxygen atmosphere (see Figures S24 and S25), which indicates typically the generation of $Pd^{(III)}$ ion according to the literature (Powers and Ritter, 2009; Powers et al., 2009). In comparison, the Pd black that was precipitated out with the pale yellow solution almost remained unchanged for the reaction under argon atmosphere. Moreover, it was found that when the reaction was performed under argon atmosphere in the presence of stoichiometric amount $Pd(OAc)_2$ and the corresponding ratio of ligands, **15a** was obtained only in lower than 20% yield. These results clearly suggest that a $Pd^{(I)}/Pd^{(III)}$ should be involved in the catalytic cycle, although a $Pd^{(0)}/Pd^{(II)}$ cycle cannot be entirely ruled out as a minor catalytic process.

Thus, through an extensive mechanistic study, we could propose a catalytic cycle for the 6-*exo*-*trig* annulation. Namely, oxidation of $Pd^{(II)}$ by oxygen generates the $Pd^{(III)}$ complexes, which then form an infant transition state **I** with substrate **13** under the direction of the heteroatom-containing C_3 side chain (Figure 4). Subsequently, C–H bond activation proceeds to produce the intermediate **II**. Migratory *syn* insertion followed by *syn* β-hydride elimination via **III** delivered the product **15**. The sensitive $Pd^{(I)}$ was reoxidized to $Pd^{(III)}$ via the more stable $Pd^{(II)}$ to bring the reaction into the next cycle. Based on the proposed mechanism, the *syn* insertion results in an *anti*-orientated R^1 group and $Pd^{(III)}$ ion. Subsequently, the $Pd^{(III)}$ coordinates with the heteroatom at the C_3 side chain to form a closed intermediate **III**, which prevents the elimination of *anti*-β-hydride at the tertiary carbon (for R^1 = H). As a result, the products with non-conjugated double bonds as shown in Table 2 are formed exclusively. As an exceptional example, the production of **15g** (Table 2) should undergo epimerization via an oxa-π-allylpalladium intermediate **IV** to form **V**, and ultimately, allowing for *anti*-β-hydride elimination at the tertiary carbon (Kandukuri et al., 2012).

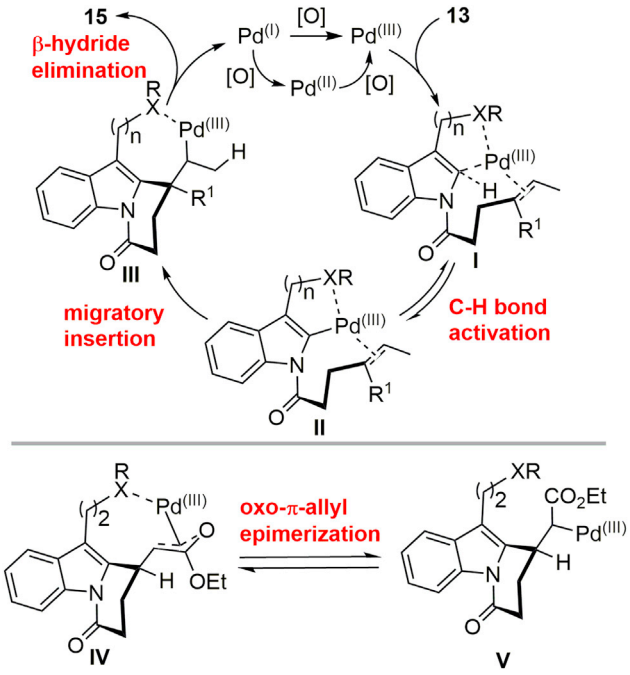

Figure 4. Proposed $Pd^{(I)}/Pd^{(III)}$ as the Major Catalytic Cycle

Limitations of the Study

A brief examination showed that the present method is not compatible for the construction of seven-membered indole lactams from the corresponding indolyl 5-enamide.

Conclusion

Targeted toward the efficient and collective synthesis of an array of structurally intriguing indole alkaloids as well as their potential analogs, we have designed and developed a Pd-catalyzed aerobic oxidative Heck coupling reaction that could achieve the previously challenging 6-*exo*-*trig* annulation using indolyl amides as substrates. The method provides a straightforward pathway for accessing [6.5.6]-tricyclic indole lactams, which may serve as a common intermediate for the synthesis of various indole alkaloids and their analogs. The method also displays a broad generality and could be reliably performed over gram scale as demonstrated by several different types of substrates. The keys for the successful realization of the coupling reaction are highlighted by a mechanism-based design of incorporating a heteroatom-containing directing group at indole C_3 and the utilization of phosphinamide compounds as novel co-ligands. Extensive experimental results revealed that C–H activation should be the rate-determining step and that $Pd^{(III)}$ complexes may be responsible for effective reaction. This catalytic cycle differs from the previously proposed $Pd^{(0)}/Pd^{(II)}$ cycle for the construction of five-membered rings and would be important for the mechanism-based *de novo* design of relevant reactions. We believe that the method could find extensive applications for the flexible synthesis of various indole alkaloids. The investigations into the enantioselective version of the cross-coupling reaction, as well as its application in the collective synthesis of relevant natural products, are the focus of our future work.

METHODS

All methods can be found in the accompanying Transparent Methods supplemental file.

SUPPLEMENTAL INFORMATION

Supplemental Information can be found online at https://doi.org/10.1016/j.isci.2019.06.037.

ACKNOWLEDGMENTS

Financial support from the National Natural Science Foundation of China (21772191 and 21572215) is acknowledged.

AUTHOR CONTRIBUTIONS

F.-S.H. conceived the synthetic strategy, directed the project, and wrote the manuscript. F.-S.H. and J.Z. discussed the experimental results and commented on the manuscript. J.Z. conducted the experimental works.

DECLARATION OF INTERESTS

The authors declare no competing interests.

Received: April 1, 2019
Revised: June 3, 2019
Accepted: June 28, 2019
Published: July 26, 2019

REFERENCES

Abbiati, G., Beccalli, E.M., Broggini, G., and Zoni, C. (2003). Regioselectivity on the palladium-catalyzed intramolecular cyclization of indole derivatives. J. Org. Chem. *68*, 7625–7628.

Baran, P.S., Guerrero, C.A., and Corey, E.J. (2003). Short, enantioselective total synthesis of okaramine N. J. Am. Chem. Soc. *125*, 5628–5629.

Biechy, A., and Zard, S.Z. (2009). A flexible, convergent approach to polycyclic indole structures: formal synthesis of (±)-mersicarpine. Org. Lett. *11*, 2800–2803.

Broggini, C., Barbera, V., Beccalli, E.M., Borsini, E., Galli, S., Lanza, G., and Zecchi, G. (2012). Palladium$^{(II)}$/copper halide/solvent combination for selective intramolecular domino reactions of indolecarboxylic acid allylamides: an unexpected arylation/esterification sequence. Adv. Synth. Catal. *354*, 159–170.

Cao, B.-C., Wu, G.-J., Yu, F., He, Y.-P., and Han, F.-S. (2018). A total synthesis of (−)-hamigeran B and (−)-4-bromohamigeran B. Org. Lett. *20*, 3687–3690.

Dagoneau, D., Xu, Z., Wang, Q., and Zhu, J. (2016). Enantioselective total synthesis of (–)-rhazinilam, (–)-leucomidine B, and (+)-leuconodine F. Angew. Chem. Int. Ed. *55*, 760–763.

Du, Z.-J., Guan, J., Wu, G.-J., Xu, P., Gao, L.-X., and Han, F.-S. (2015). Pd(II)-catalyzed enantioselective synthesis of P-stereogenic phosphinamides via desymmetric C−H arylation. J. Am. Chem. Soc. *137*, 632–635.

Feng, X., Jiang, G., Xia, Z., Hu, J., Wan, X., Gao, J.-M., Lai, Y., and Xie, W. (2015). Total synthesis of (–)-conolutinine. Org. Lett. *17*, 4428–4431.

Ferreira, E.M., and Stoltz, B.M. (2003). Catalytic C-H bond functionalization with palladium(II): aerobic oxidative annulations of indoles. J. Am. Chem. Soc. *125*, 9578–9579.

Ferreira, E.M., Zhang, H., and Stoltz, B.M. (2008). C-H bond functionalizations with palladium(II): intramolecular oxidative annulations of arenes. Tetrahedron *64*, 5987–6001.

Gao, S., Yang, C., Huang, Y., Zhao, L., Wu, X., Yao, H., and Lin, A. (2016). Pd(II)-catalyzed intramolecular oxidative Heck dearomative reaction: approach to thiazole-fused pyrrolidinones with a C2-azaquarternary center. Org. Biomol. Chem. *14*, 840–843.

Geng, Q., Li, Z., Lv, Z., and Liang, G. (2016). Progress in total synthesis of leuconolam-leuconoxine-mersicarpine alkaloids. Chin. J. Org. Chem. *36*, 1447.

Guan, J., Wu, G.-J., and Han, F.-S. (2014). Pd^{II}-catalyzed mild C−H ortho arylation and intramolecular amination oriented by a phosphinamide group. Chem. Eur. J. *20*, 3301–3305.

Higuchi, K., Suzuki, S., Ueda, R., Oshima, N., Kobayashi, E., Tayu, M., and Kawasaki, T. (2015). Asymmetric total synthesis of (–)-leuconoxine via chiral phosphoric acid catalyzed desymmetrization of a prochiral diester. Org. Lett. *17*, 154–157.

Ikemoto, H., Yoshino, T., Sakata, K., Matsunaga, S., and Kanai, M. (2014). Pyrroloindolone synthesis via a Cp*CoIII-catalyzed redox-neutral directed C-H alkenylation/annulation sequence. J. Am. Chem. Soc. *136*, 5424–5431.

Iwama, Y., Okano, K., Sugimoto, K., and Tokuyama, H. (2013). Enantiocontrolled total synthesis of (–)-mersicarpine. Chem. Eur. J. *19*, 9325–9334.

Kam, T.-S., Loh, K.-Y., and Chen, W. (1993). Conophylline and conophyllidine-new dimeric alkaloids from tabernaemontana divaricata. J. Nat. Prod. *56*, 1865–1871.

Kam, T.-S., Loh, K.-Y., Lim, L.-H., Yoong, W.-L., Chuah, C.-H., and Chen, W. (1992). New alkaloids from the leaves of tabernaemontana divaricata. Tetrahedron Lett. *33*, 969–972.

Kam, T.-S., Pang, H.-S., Choo, Y.-M., and Komiyama, K. (2004). Biologically active ibogan and vallesamine derivatives from tabernaemontana divaricata. Chem. Biodivers. *1*, 646–656.

Kam, T.-S., Sim, K.-M., and Lim, T.-M. (2000). Tronocarpine, a novel pentacyclic indole incorporating a seven-membered lactam moiety. Tetrahedron Lett. *41*, 2733–2736.

Kandukuri, S.R., and Oestreich, M. (2012). Aerobic palladium(II)-catalyzed dehydrogenation of cyclohexene-1-carbonyl indole amides: an indole-directed aromatization. J. Org. Chem. *77*, 8750–8755.

Kandukuri, S.R., Schiffner, J.A., and Oestreich, M. (2012). Aerobic palladium(II)-catalyzed 5-endo-trig cyclization: an entry into the diastereoselective C-2 alkenylation of indoles with tri- and tetrasubstituted double bonds. Angew. Chem. Int. Ed. *51*, 1265–1269.

Li, Z., Geng, Q., Lv, Z., Pritchett, B.P., Baba, K., Numarjiri, Y., Stoltz, B.M., and Liang, G. (2015). Selective syntheses of leuconolam, leuconoxine, and mersicarpine alkaloids from a common intermediate through regiocontrolled cyclizations by Staudinger reactions. Org. Chem. Front. *2*, 236–240.

Liang, X., Jiang, S.-Z., Wei, K., and Yang, Y.-R. (2016). Enantioselective total synthesis of (–)-alstoscholarisine A. J. Am. Chem. Soc. *138*, 2560–2562.

Liu, C., Yuan, J., Gao, M., Tang, S., Li, W., Shi, R., and Lei, A. (2015). Oxidative coupling between two hydrocarbons: an update of recent C–H functionalizations. Chem. Rev. *115*, 12138–12204.

Liu, C., Zhang, H., Shi, W., and Lei, A. (2011). Bond formations between to nucleophiles: transition metal catalyzed oxidative cross-coupling reactions. Chem. Rev. *111*, 1780–1824.

Lu, Z., Yang, M., Chen, P., Xiong, X., and Li, A. (2014). Total synthesis of hapalindole-type natural products. Angew. Chem. Int. Ed. *53*, 13840–13844.

Lv, Z., Li, Z., and Liang, G. (2014). Total synthesis of mersicarpine through a cationic cyclization approach. Org. Lett. *16*, 1653–1655.

Magolan, J., and Kerr, M.A. (2006). Expanding the scope of $Mn(OAc)_3$–mediated cyclizations: synthesis of the tetracyclic core of tronocarpine. Org. Lett. *8*, 4561–4564.

Magolan, J., Carson, C.A., and Kerr, M.A. (2008). Total synthesis of (±)-mersicarpine. Org. Lett. *10*, 1437–1440.

Meng, L., Liu, C., Zhang, W., Zhou, C., and Lei, A. (2014). Palladium catalysed β-selective oxidative Heck reaction of an electron-rich olefin. Chem. Commun. (Camb.) *50*, 1110–1112.

Meng, L., Wu, K., Liu, C., and Lei, A. (2013). Palladium-catalyzed aerobic oxidative Heck-type alkenylation of Csp^3–H for pyrrole synthesis. Chem. Commun. (Camb.) *49*, 5853–5855.

Meng, Z., Yu, H., Li, L., Tao, W., Chen, H., Wang, M., Yang, P., Edmonds, D.J., Zhong, J., and Li, A. (2015). Total synthesis and antiviral activity of indolosesquiterpenoids from the xiamycin and oridamycin families. Nat. Commun. *6*, 6096.

Nakajima, R., Ogino, T., Yokoshima, S., and Fukuyama, T. (2010). Total synthesis of (–)-mersicarpine. J. Am. Chem. Soc. *132*, 1236–1237.

Pfaffenbach, M., and Gaich, T. (2015). A photoinduced cyclization cascade–total synthesis of (–)-leuconoxine. Chem. Eur. J. *21*, 6355–6357.

Pfaffenbach, M., and Gaich, T. (2016). The diaza [5.5.6.6]fenestrane skeleton–synthesis of leuconoxine alkaloids. Chem. Eur. J. *22*, 3600–3610.

Pintori, D.G., and Greaney, M.F. (2011). Intramolecular oxidative C-H coupling for medium-ring synthesis. J. Am. Chem. Soc. *133*, 1209–1211.

Powers, D.C., and Ritter, T. (2009). Bimetallic Pd(III) complexes in palladium catalysed carbon-heteroatom bond formation. Nat. Chem. *1*, 302–309.

Powers, D.C., Geibel, M.A.L., Klein, J.E.M.N., and Ritter, T. (2009). Bimetallic palladium catalysis: direct observation of Pd(III)–Pd(III) intermediates. J. Am. Chem. Soc. *131*, 17050–17051.

Schiffner, J.A., Wöste, T.H., and Oestreich, M. (2010). Enantioselective Fujiwara-Moritani indole and pyrrole annulations catalyzed by chiral palladium(II)-NicOx complexes. Eur. J. Org. Chem. *174*, 174–182.

Shi, W., Liu, C., and Lei, A. (2011). Transition-metal catalyzed oxidative cross-coupling reactions to form C–C bonds involving organometallic reagents as nucleophiles. Chem. Soc. Rev. *40*, 2761.

Tokuyama, H. (2015). The total synthesis of biosynthetically related monoterpene indole alkaloids. J. Syn. Org. Chem. Jpn. *73*, 66.

Umehara, A., Ueda, H., and Tokuyama, H. (2014). Total synthesis of leuconoxine, leuconodine B, and melodinine E by oxidative cyclic aminal formation and diastereoselective ring-closing metathesis. Org. Lett. *14*, 2526–2529.

Wu, G.-J., Han, F.-S., and Zhao, Y.-L. (2015). Palladacycles derived from arylphosphinamides for mild Suzuki–Miyaura cross-couplings. RSC Adv. *5*, 69776–69781.

Wu, G.-J., Zhang, Y.-H., Tan, D.-X., and Han, F.-S. (2018). Total synthesis of cyrneines A–B and glaucopine C. Nat. Commun. *9*, 2148.

Xu, Z., Wang, Q., and Zhu, J. (2013). Enantioselective total synthesis of leuconolam-leuconoxine-mersicarpine group monoterpene indole alkaloids. J. Am. Chem. Soc. *135*, 19127–19130.

Xu, Z., Wang, Q., and Zhu, J. (2015). Total syntheses of (−)-mersicarpine, (−)-scholarisine G, (+)-melodinine E, (−)-leuconoxine, (−)-leuconolam, (−)-leuconodine A, (+)-leuconodine F, and (−)-leuconodine C: self-induced diastereomeric anisochronism (SIDA) phenomenon for scholarisine G and leuconodines A and C. J. Am. Chem. Soc. *137*, 6712–6724.

Yang, J.-M., Zhu, C.-Z., Tang, X.-Y., and Shi, M. (2014a). Rhodium(II)-catalyzed intramolecular annulation of 1-sulfonyl-1,2,3-triazole with pyrrole and indole rings: facile synthesis of N-bridged azepine skeletons. Angew. Chem. Int. Ed. *53*, 5142–5146.

Yang, Y., Bai, Y., Sun, S., and Dai, M. (2014b). Biosynthetically inspired divergent approach to monoterpene indole alkaloids: total synthesis of mersicarpine, leuconodines B and D, leuconoxine, melodinine E, leuconolam, and rhazinilam. Org. Lett. *16*, 6216–6219.

Yu, K., Gao, B., and Ding, H. (2016a). Asymmetric total synthesis and absolute configuration reassignment of indole alkaloid (+)-alsmaphorazine D. Acta Chim. Sin. *74*, 410.

Yu, K., Gao, B., Liu, Z., and Ding, H. (2016b). Enantioselective total synthesis and structural reassignment of (+)-alsmaphorazine E via a traceless chirality transfer strategy. Chem. Commun. (Camb.) *52*, 4485–4488.

Zheng, Y., Yue, B.-B., Wei, K., and Yang, Y.-R. (2018). Short synthesis of the monoterpene indole alkaloid (±)-arbornamine. J. Org. Chem. *83*, 4867–4870.

Zhong, X., Li, Y., and Han, F.-S. (2012). Al-catalyzed facile construction of quaternary C–C bonds by the allylic substitution of tertiary alcohols: a concise and formal synthesis of (±)-mersicarpine. Chem. Eur. J. *18*, 9784–9788.

Zhong, X., Li, Y., Zhang, J., and Han, F.-S. (2015). Synthetic study toward the misassigned (±)-tronoharine. Org. Lett. *17*, 720–723.

Zhong, X., Qi, S., Li, Y., Zhang, J., and Han, F.-S. (2014). A study in indol-2-yl carbinol chemistry and the application for the total synthesis of mersicarpine. Tetrahedron *70*, 3724–3740.

Zhu, C., Liu, Z., Chen, G., Zhang, K., and Ding, H. (2015). Total synthesis of indole alkaloids alsmaphorazine D. Angew. Chem. Int. Ed. *54*, 879–882.

ISCI, Volume *17*

Supplemental Information

Pd-Catalyzed Aerobic Oxidative Heck Cross-Coupling for the Straightforward Construction of Indole δ-Lactams

Jing Zhang and Fu-She Han

Transparent Methods

General procedure for the synthesis of reaction substrates 13 (Figure S1) and oxidative coupling (Figure S23), the theoretical and experimental isotopic distribution of Pd complexes as detected by high resolution mass spectrometer (Figures S6-22), and copies of NMR spectra of reaction substrates and products (Figures S26-81)

1. General information:

Unless otherwise noted, all commercial reagents were used without further purification. Anhydrous solvents were distilled according to standard methods. Analytical thin layer chromatography (TLC) was performed on 0.2 mm thick silica gel 60-F254 plates (Merck). Chromatographic purification of products was accomplished using forced-flow chromatography on 230-400 mesh silica gel. The ^{1}H NMR spectra were recorded at 300 MHz or 400 MHz (Bruker AV) and the ^{13}C NMR spectra were recorded at 75, 101, or 126 MHZ with TMS as internal standard. All chemical shifts are given in ppm. All coupling constants (*J* values) were reported in Hertz (Hz). High resolution mass spectra (HRMS) were obtained on an IonSpec Ultima 7.0 T FT-ICR-MS (IonSpec, USA) with a Waters Z-spray source. X-ray crystallographic analysis was performed on a Bruker D8 ADVANCE diffractometer with MoKα radiation (λ = 0.71073).

2. General procedure for the synthesis of indolyl amides (Hartung et al., 2003)

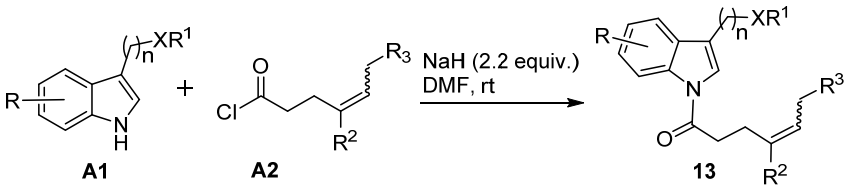

Figure S1. Synthesis of substrates **13**, related to **Table 1-3**

To a solution of **A1** and NaH in DMF was added **A2** (1.5 equiv) dropwise at 0 °C. The mixture was allowed to warm to room temperature and stirred for 10 min. To this mixture was added aqueous NH_4Cl. The reaction mixture was extracted with ethyl acetate (2 × 50 mL). The combined organic layers were washed successively with H_2O (4 × 50 mL) and brine (50 mL), dried over Na_2SO_4, and concentrated under reduced pressure. The crude reaction mixture was purified by silica-gel column chromatography.

3. General procedure for oxidative C–H Heck cross-coupling

To a dried Schlenck tube equipped with a magnetic bar was charged with **13**, $Pd(OAc)_2$ (10 mol%), methyl nicotinate (**L_1**, 40 mol%), phosphinamide **L_5** (10 mol %), and *t*$BuCO_2H$ (30 equiv.). The reaction tube was evacuated and back-filled with O_2 for three times. Then mesitylene was added (0.1mol/L) and the reaction mixture was stirred at the optimized temperature until the substrates **13** had disappeared as monitored by TLC. Purification of the reaction mixture by column chromatography on silica gel provided the desired product **15**.

4. Characterization data of substrates and products

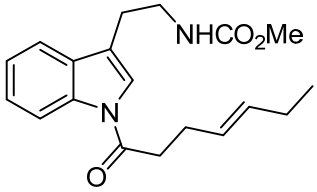

13a

13a was purified by column chromatography on silica gel (petroleum ether/EtOAc = 7/1) to give a white solid in 80% yield. ^{1}H NMR (300 MHz, $CDCl_3$) δ 8.44 (d, *J* = 8.1 Hz, 1H), 7.52 (d, *J* = 7.6 Hz, 1H), 7.40–7.23 (m, 3H), 5.64–5.43 (m, 2H), 5.05 (s, 1H), 3.67 (s, 3H), 3.52 (q, *J* = 6.8 Hz, 2H), 2.89 (m, 4H), 2.46 (q, *J* = 7.1 Hz, 2H), 2.03–1.93 (m, 2H), 0.97 (t, *J* = 7.5 Hz, 3H). ^{13}C NMR (126 MHz, $CDCl_3$) δ 170.79, 157.16, 136.06, 133.85, 130.30, 126.79, 125.40, 123.54, 122.11, 119.41, 118.79, 116.84, 52.16, 40.51, 35.97, 27.50, 25.80, 25.60, 13.79. HRMS Calcd for $C_{19}H_{24}N_2NaO_3$ ([M+Na]$^+$): 351.1679; Found: 351.1676.

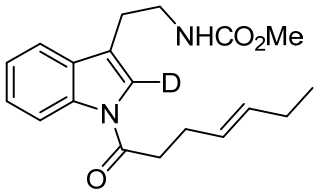

13a-D

13a-D was purified by column chromatography on silica gel (petroleum ether/EtOAc = 7/1) to give a white solid in 80% yield. ^{1}H NMR (300 MHz, DMSO-d_6) δ 8.34 (dd, *J* = 7.4, 1.6 Hz, 1H), 7.74 (s, 0.15H), 7.65–7.56 (m, 1H), 7.43–7.23 (m, 3H), 5.63–5.44 (m, 2H), 3.53 (s, 3H), 3.30 (d, *J* = 6.8 Hz, 2H), 3.05 (t, *J* = 7.4 Hz, 2H), 2.80 (t, *J* = 7.2 Hz, 2H), 2.38 (q, *J* = 6.8 Hz, 2H), 2.03–1.91 (m, 2H), 0.91 (t, *J* = 7.4 Hz, 3H). HRMS Calcd for $C_{19}H_{23}DN_2NaO_3$ ([M+Na]$^+$): 352.1742; Found: 352.1739.

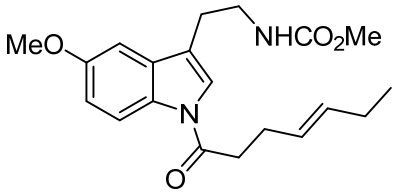

13b

13b was purified by column chromatography on silica gel (petroleum ether/EtOAc = 7/1) to give a white solid in 60% yield. ^{1}H NMR (300 MHz, $CDCl_3$) δ 8.34 (d, *J* = 8.9 Hz, 1H), 7.27 (s, 1H), 6.97 (s, 2H), 5.63–5.44 (m, 2H), 4.84 (s, 1H), 3.86 (s, 3H), 3.68 (s, 3H), 3.52 (q, *J* = 6.8 Hz, 2H), 2.89 (q, *J* = 7.0, 6.4 Hz, 4H), 2.50 (t, *J* = 7.1 Hz, 2H), 2.09–1.95 (m, 2H), 1.02–0.89 (m, 3H). ^{13}C NMR (75 MHz, $CDCl_3$) δ 170.46, 157.16, 156.50, 133.89, 131.36, 130.80, 126.86, 122.79, 119.24, 117.71, 113.56, 101.83, 55.80, 52.26, 40.51, 35.79, 27.64, 25.87, 25.6, 13.84. HRMS Calcd for $C_{20}H_{27}N_2O_4$ ([M+H]$^+$): 359.1965; Found: 359.1968.

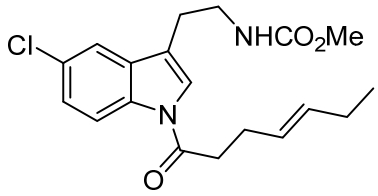

13c

13c was purified by column chromatography on silica gel (petroleum ether/EtOAc = 6/1) to give a yellow solid in 65% yield. ^{1}H NMR (300 MHz, $CDCl_3$) δ 8.38 (d, *J* = 8.8 Hz, 1H), 7.48 (s, 1H), 7.33–7.23 (m, 2H), 5.66–5.42 (m, 2H), 4.82 (s, 1H), 3.68 (s, 3H), 3.51 (d, *J* = 6.3 Hz, 2H), 2.90 (dt, *J* = 12.5, 7.1 Hz, 4H), 2.49 (q, *J* = 6.8 Hz, 2H), 2.06–1.96 (m, 2H), 0.96 (t, *J* = 7.4 Hz, 3H). ^{13}C NMR (75 MHz, $CDCl_3$) δ 170.73, 157.17, 134.40, 134.07, 131.64, 129.24, 126.62, 125.53, 123.36, 118.85, 118.55, 117.93, 52.3, 40.49, 35.89, 27.48, 25.64 (2C), 13.81. HRMS Calcd for $C_{19}H_{24}ClN_2O_3$ ($[M+H]^+$): 363.1470; Found: 363.1472.

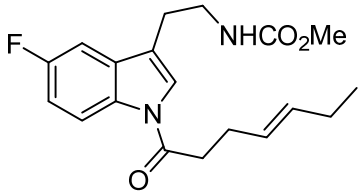

13d

13d was purified by column chromatography on silica gel (petroleum ether/EtOAc = 6/1) to give a yellow solid in 65% yield. ^{1}H NMR (300 MHz, $CDCl_3$) δ 8.42 (dd, *J* = 9.1, 4.7 Hz, 1H), 7.35 (s, 1H), 7.18 (d, *J* = 8.8 Hz, 1H), 7.08 (t, *J* = 9.2 Hz, 1H), 5.66–5.44 (m, 2H), 4.80 (s, 1H), 3.68 (s, 3H), 3.52 (q, *J* = 6.8 Hz, 2H), 2.99–2.84 (m, 4H), 2.52 (t, *J* = 7.1 Hz, 2H), 2.12–1.95 (m, 2H), 0.97 (t, *J* = 7.5, 3H). ^{13}C NMR (75 MHz, $CDCl_3$) δ 170.62, 159.66 (d, *J* = 240.6 Hz), 157.21, 134.00, 132.41, 131.45 (d, *J* = 10.4 Hz), 126.66, 123.59, 119.14 (d, *J* = 3.4 Hz), 117.96 (d, *J* = 8.9 Hz), 113.00 (d, *J* = 24.5 Hz), 104.56 (d, *J* = 23.9 Hz), 52.25, 40.42, 35.76, 27.52, 25.76, 25.61, 13.79. HRMS Calcd for $C_{19}H_{23}FN_2NaO_3$ ($[M+Na]^+$): 369.1585; Found: 369.1586.

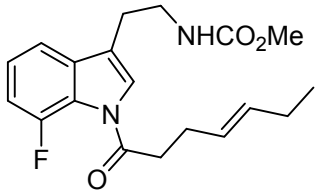

13e

13e was purified by column chromatography on silica gel (petroleum ether/EtOAc = 4/1) to give a yellow solid in 70% yield. ^{1}H NMR (300 MHz, $CDCl_3$) δ 7.45 (s, 1H), 7.33 (d, *J* = 7.5 Hz, 1H), 7.26–7.17 (m, 1H), 7.17–7.03 (m, 1H), 5.67–5.41 (m, 2H), 4.82 (s, 1H), 3.68 (s, 3H), 3.51 (q, *J* = 6.4 Hz, 2H), 2.96 (dt, *J* = 31.9, 7.1 Hz, 4H), 2.51 (q, *J* = 7.0 Hz, 2H), 2.06–1.96 (m, 2H), 0.96 (t, *J* = 7.4 Hz, 3H). ^{13}C NMR (75 MHz, $CDCl_3$) δ 169.60, 157.17, 150.29 (d, *J* = 252.7 Hz), 134.84 (d, *J* = 3.6 Hz), 133.84, 126.69, 124.37, 124.27, 122.28 (d, *J* = 10.6 Hz), 118.98, 114.79 (d, *J* = 3.5 Hz), 112.33 (d, *J* = 22.6 Hz), 52.14, 40.39, 36.36, 27.89, 25.69, 25.56, 13.75. HRMS Calcd for $C_{19}H_{23}FN_2NaO_3$ ($[M+Na]^+$): 369.1585; Found: 369.1587.

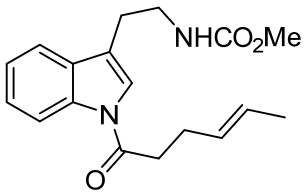

13f

13f was purified by column chromatography on silica gel (petroleum ether/acetone = 17/1) to give a yellow solid in 40% yield. ^{1}H NMR (300 MHz, $CDCl_3$) δ 8.45 (d, *J* = 8.2 Hz, 1H), 7.54 (d, *J* = 7.6 Hz, 1H), 7.41–7.27 (m, 3H), 5.54 (t, *J* = 5.2 Hz, 2H), 4.85 (s, 1H), 3.68 (s, 3H), 3.54 (q, *J* = 6.7 Hz, 2H), 2.98–2.88 (m, 4H), 2.53–2.46 (m, 2H), 1.68 (s, 3H). ^{13}C NMR (75 MHz, $CDCl_3$) δ 170.79, 157.24, 136.04, 130.31, 129.07, 126.71, 125.41, 123.55, 122.10, 119.44, 118.80, 116.83, 52.18, 40.50, 35.87, 27.47, 25.79, 18.00. HRMS Calcd for $C_{18}H_{23}N_2O_3$ ([M+H]$^+$): 315.1703; Found: 315.1705.

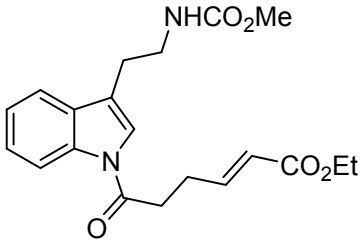

13g

13g was purified by column chromatography on silica gel (petroleum ether/EtOAc = 4/1) to give a white solid in 70% yield. ^{1}H NMR (300 MHz, $CDCl_3$) δ 8.44 (d, *J* = 8.1 Hz, 1H), 7.53 (d, *J* = 7.6 Hz, 1H), 7.44–7.23 (m, 3H), 6.42 (dt, *J* = 11.5, 7.2 Hz, 1H), 5.88 (dt, *J* = 11.3, 1.3 Hz, 1H), 5.05 (s, 1H), 4.17 (q, *J* = 7.1 Hz, 2H), 3.66 (s, 3H), 3.55 (q, *J* = 6.5 Hz, 2H), 3.20–3.00 (m, 4H), 2.93 (t, *J* = 6.8 Hz, 2H), 1.28 (t, *J* = 7.1 Hz, 3H). ^{13}C NMR (75 MHz, $CDCl_3$) δ 170.21, 166.27, 157.17, 147.56, 136.01, 130.38, 125.45, 123.63, 122.04, 121.35, 119.82, 118.81, 116.79, 60.16, 52.13, 40.31, 35.27, 25.71, 24.23, 14.28. HRMS Calcd for $C_{20}H_{24}N_2NaO_5$ ([M+Na]+): 395.1577; Found: 395.1570.

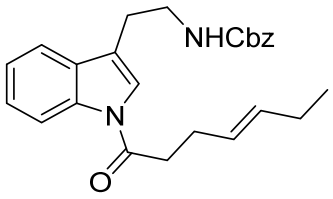

13h

13h was purified by column chromatography on silica gel (petroleum ether/EtOAc = 15/1) to give a white solid in 70% yield. ^{1}H NMR (300 MHz, $CDCl_3$) δ 8.45 (d, *J* = 8.2 Hz, 1H), 7.52 (d, *J* = 7.6 Hz, 1H), 7.43–7.27 (m, 8H), 5.68–5.40 (m, 2H), 5.11 (s, 2H), 4.96 (s, 1H), 3.55 (q, *J* = 6.7 Hz, 2H), 3.00–2.85 (m, 4H), 2.48 (q, *J* = 7.0 Hz, 2H), 2.06–1.94 (m, 2H), 0.96 (t, *J* = 7.5 Hz, 3H). ^{13}C NMR (75 MHz, $CDCl_3$) δ 170.74, 156.43, 136.53, 136.01, 133.80, 130.23, 128.55 (2C), 128.17, 128.08 (2C), 126.75, 125.38, 123.50, 122.09, 119.28, 118.75, 116.81, 66.69, 40.47, 35.90, 27.44, 25.71, 25.57, 13.77. HRMS Calcd for $C_{25}H_{28}N_2NaO_3$ ([M+Na]$^+$): 427.1992; Found: 427.1989.

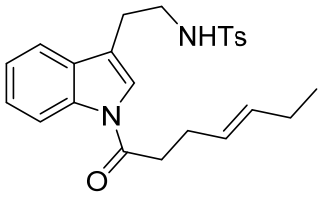

13i

13i was purified by column chromatography on silica gel (petroleum ether/EtOAc = 10/1) to give a white solid in 77% yield. ^{1}H NMR (300 MHz, $CDCl_3$) δ 8.43 (d, *J* = 8.2 Hz, 1H), 7.65 (d, *J* = 7.8 Hz, 2H), 7.35 (t, *J* = 8.5 Hz, 2H), 7.24–7.18 (m, 4H), 5.66–5.44 (m, 2H), 4.66 (d, *J* = 6.7 Hz, 1H), 3.31 (q, *J* = 6.6 Hz, 2H), 2.89 (t, *J* = 7.1 Hz, 4H), 2.45 (q, *J* = 7.2 Hz, 2H), 2.39 (s, 3H), 2.07–1.95 (m, *J* = 7.1 Hz, 2H), 1.02–0.93 (m, 3H). ^{13}C NMR (75 MHz, $CDCl_3$) δ 170.88, 143.48, 136.81, 136.01, 133.83, 129.87, 129.66 (2C), 126.94 (2C), 126.79, 125.37, 123.49, 122.73, 118.55, 118.28, 116.87, 42.40, 35.83, 27.42, 25.62, 25.56, 21.60, 13.81. HRMS Calcd for $C_{24}H_{29}N_2O_3S$ ([M+H]$^+$): 425.1893; Found: 425.1896.

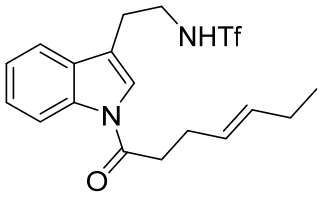

13j

13j was purified by column chromatography on silica gel (petroleum ether/EtOAc = 5/1) to give a white solid in 75% yield. ^{1}H NMR (300 MHz, $CDCl_3$) δ 8.43 (d, *J* = 8.2 Hz, 1H), 7.52–7.49 (m, 1H), 7.45–7.28 (m, 3H), 5.59–5.50 (m, 2H), 5.46–5.35 (m, 1H), 3.68 (q, *J* = 6.4 Hz, 2H), 3.03 (t, *J* = 6.5 Hz, 2H), 2.71 (dd, *J* = 8.1, 6.9 Hz, 2H), 2.32 (q, *J* = 7.1 Hz, 2H), 2.07–1.93 (m, 2H), 0.96 (t, *J* = 7.5 Hz, 3H). ^{13}C NMR (75 MHz, $CDCl_3$) δ 171.13, 135.99, 134.04, 129.84, 126.35, 125.94, 124.08, 123.19, 119.74 (q, *J* = 319 Hz), 118.74, 117.90, 117.02, 43.72, 35.47, 27.22, 26.92, 25.62, 13.80. HRMS Calcd for $C_{18}H_{22}F_3N_2O_3S$ ([M+H]$^+$): 403.1298; Found: 403.1294.

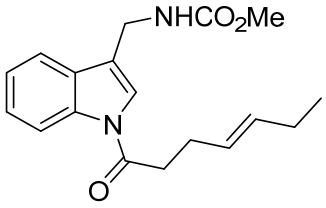

13k

13k was purified by column chromatography on silica gel (petroleum ether/EtOAc = 3/1) to give a pink solid in 60% yield. ^{1}H NMR (300 MHz, $CDCl_3$) δ 8.46 (d, *J* = 8.2 Hz, 1H), 7.57 (d, *J* = 7.7 Hz, 1H), 7.45–7.28 (m, 3H), 5.66–5.44 (m, 2H), 4.97 (s, 1H), 4.51 (d, *J* = 5.8 Hz, 2H), 3.72 (s, 3H), 2.95 (t, *J* = 7.5 Hz, 2H), 2.51 (q, *J* = 7.0 Hz, 2H), 2.07–1.96 (m, 2H), 0.97 (t, *J* = 7.5 Hz, 3H). ^{13}C NMR (75 MHz, $CDCl_3$) δ 170.95, 157.12, 136.21, 133.99, 129.10, 126.71, 125.67, 123.76, 122.80, 119.61, 118.99, 116.91, 52.43, 36.46, 35.96, 27.47, 25.64, 13.82. HRMS Calcd for $C_{18}H_{23}N_2O_3$ ([M+H]$^+$): 315.1703; Found: 315.1709.

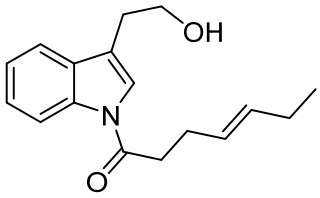

13l

13l was purified by column chromatography on silica gel (petroleum ether/EtOAc = 3/1) to give a white solid in 90% yield. ^{1}H NMR (300 MHz, $CDCl_3$) δ 8.47 (d, *J* = 8.2 Hz, 1H), 7.55 (dd, *J* = 8.0, 1.3 Hz, 1H), 7.42–7.27 (m, 3H), 5.54–5.45 (m, 2H), 3.96 (t, *J* = 6.3 Hz, 2H), 3.02–2.91 (m, 4H), 2.51 (q, *J* = 7.1 Hz, 2H), 2.08–1.96 (m, 2H), 0.97 (t, *J* = 7.5 Hz, 3H). ^{13}C NMR (75 MHz, $CDCl_3$) δ 170.89, 136.06, 133.89, 130.49, 126.81, 125.43, 123.55, 122.53, 119.20, 118.91, 116.88, 61.87, 35.96, 28.59, 27.50, 25.64, 13.83. HRMS Calcd for $C_{17}H_{22}NO_2$ ([M+H]$^+$): 272.1645; Found: 272.1642.

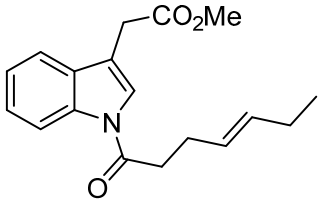

13m

13m was purified by column chromatography on silica gel (petroleum ether/EtOAc = 20/1) to give a yellow solid in 75% yield. ^{1}H NMR (300 MHz, $CDCl_3$) δ 8.49 (d, *J* = 8.2 Hz, 1H), 7.55 (d, *J* = 9.2 Hz, 2H), 7.45–7.30 (m, 2H), 5.45–5.64 (m, 2H), 3.76 (s, 5H), 2.99 (t, *J* = 7.5 Hz, 2H), 2.54 (q, *J* = 7.0 Hz, 2H), 2.14–1.94 (m, 2H), 0.99 (t, *J* = 7.5 Hz, 3H). ^{13}C NMR (75 MHz, $CDCl_3$) δ 171.03, 170.49, 135.44, 133.39, 129.69, 126.61, 125.04, 123.23, 123.07, 118.53, 116.41, 114.38, 51.84, 35.46, 30.34, 27.09, 25.32, 13.51. HRMS Calcd for $C_{18}H_{22}NO_3$ ([M+H]$^+$): 300.1594; Found: 300.1591.

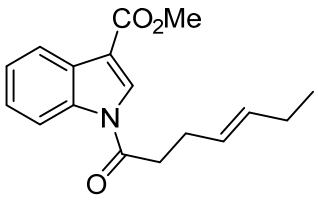

13n

13n was purified by column chromatography on silica gel (petroleum ether/EtOAc = 8/1) to give a white solid in 80% yield. ^{1}H NMR (300 MHz, $CDCl_3$) 8.49–8.46 (m, 1H), δ 8.19 (s, 1H), 8.17–8.13 (m, 1H), 7.46–7.35 (m, 2H), 5.70–5.43 (m, 2H), 3.96 (s, 3H), 3.04 (t, *J* = 7.4 Hz, 2H), 2.59–2.49 (m, 2H), 2.10–1.97 (m, 2H), 0.97 (t, *J* = 7.5 Hz, 3H). ^{13}C NMR (75 MHz, $CDCl_3$) δ 171.20, 164.50, 136.03, 134.32, 130.74, 127.26, 126.32, 125.96, 124.79, 121.55, 116.60, 113.59, 51.69, 35.90, 27.36, 25.62, 13.77. HRMS Calcd for $C_{17}H_{20}NO_3$ ([M+H]$^+$): 286.1438; Found: 286.1441.

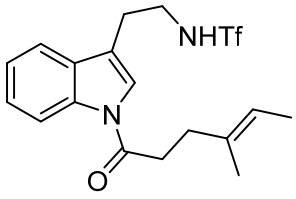

13q

13q was purified by column chromatography on silica gel (petroleum ether/EtOAc = 8/1) to give a yellow solid in 80% yield. ^{1}H NMR (300 MHz, $CDCl_3$) δ 8.42 (d, *J* = 8.2 Hz, 1H), 7.51 (d, *J* = 7.6 Hz, 1H), 7.43–7.29 (m, 3H), 5.60 (t, *J* = 6.2 Hz, 1H), 5.26 (q, *J* = 6.8 Hz, 1H), 3.68 (q, *J* = 6.4 Hz, 2H), 3.04 (t, *J* = 6.5 Hz, 2H), 2.75 (t, *J* = 7.8 Hz, 2H), 2.33 (t, *J* = 7.8 Hz, 2H), 1.64 (s, 3H), 1.59 (s, 3H). ^{13}C NMR (75 MHz, $CDCl_3$) δ 171.43, 136.06, 133.53, 129.83, 125.96, 124.10, 123.17, 119.94, 119.74 (q, *J* = 320 Hz), 118.68, 117.84, 117.05, 43.79, 34.31, 33.94, 26.92, 15.90, 13.52. HRMS Calcd for $C_{18}H_{22}F_3N_2O_3S$ ($[M+H]^+$): 403.1298; Found: 403.1291.

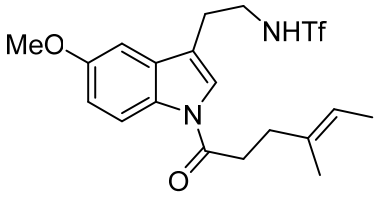

13r

13r was purified by column chromatography on silica gel (petroleum ether/EtOAc = 8/1) to give a yellow solid in 52% yield. ^{1}H NMR (300 MHz, $CDCl_3$) δ 8.26 (d, *J* = 8.9 Hz, 1H), 7.21 (s, 1H), 7.02–6.91 (m, 2H), 6.10 (s, 1H), 5.20 (q, *J* = 6.8 Hz, 1H), 3.85 (s, 3H), 3.66 (q, *J* = 6.4 Hz, 2H), 2.98 (t, *J* = 6.3 Hz, 2H), 2.57 (t, *J* = 7.9 Hz, 2H), 2.20 (t, *J* = 8.0 Hz, 2H), 1.60 (s, 3H), 1.58 (s, 3H). ^{13}C NMR (75 MHz, $CDCl_3$) δ 171.05, 156.78, 133.57, 130.95, 130.64, 123.76, 119.79, 119.74 (q, *J* = 319 Hz), 117.82, 117.76, 113.76, 101.80, 55.72, 43.83, 33.99 (2C), 26.95, 15.86, 13.51. HRMS Calcd for $C_{19}H_{24}F_3N_2O_4S$ ($[M+H]^+$): 433.1403; Found: 433.1409.

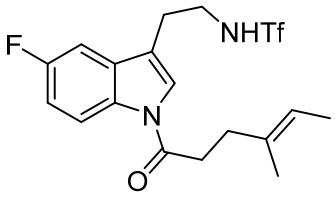

13s

13s was purified by column chromatography on silica gel (petroleum ether/EtOAc = 5/1) to give a white solid in 75% yield. ^{1}H NMR (300 MHz, $CDCl_3$) δ 8.34 (dd, *J* = 9.0, 4.7 Hz, 1H), 7.31 (s, 1H), 7.21–6.99 (m, 2H), 5.90 (s, 1H), 5.23 (q, *J* = 5.7, 1H), 3.65 (t, *J* = 6.4 Hz, 2H), 2.98 (t, *J* = 6.5 Hz, 2H), 2.73–2.57 (m, 2H), 2.24 (t, *J* = 7.9 Hz, 2H), 1.62 (s, 3H), 1.57 (d, *J* = 6.7 Hz, 3H). ^{13}C NMR (75 MHz, $CDCl_3$) δ 171.16, 159.87 (d, *J* = 242.2 Hz), 133.39, 132.43, 130.85 (d, *J* = 9.1 Hz), 124.54, 120.15, 119.74 (q, *J* = 319 Hz), 118.24 (d, *J* = 9.1 Hz), 117.42 (d, *J* = 4.0 Hz), 113.63 (d, *J* = 24.5 Hz), 104.47 (d, *J* = 23.9 Hz), 43.55, 34.28, 34.02, 26.81, 15.87, 13.54. HRMS Calcd for $C_{18}H_{20}F_4N_2NaO_3S$ ($[M+Na]^+$): 443.1023; Found: 443.1029.

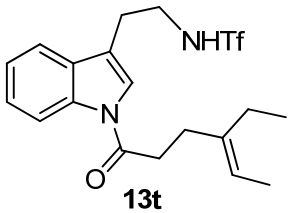

13t

13t was purified by column chromatography on silica gel (eluent: petroleum ether/EtOAc = 10/1) to give a white solid in 75% yield. ^{1}H NMR (300 MHz, $CDCl_3$) δ 8.41 (d, *J* = 8.1 Hz, 1H), 7.51 (d, *J* = 7.6 Hz, 1H), 7.40 (t, *J* = 7.6 Hz, 1H), 7.30 (d, *J* = 9.6 Hz, 2H), 5.66 (s, 1H), 5.21 (q, *J* = 6.5 Hz, 1H), 3.68 (q, *J* = 6.3 Hz, 2H), 3.03 (t, *J* = 6.4 Hz, 2H), 2.75 – 2.63 (m, 2H), 2.31 (d, *J* = 7.6 Hz, 2H), 2.06 (q, *J* = 7.5 Hz, 2H), 1.59 (d, *J* = 8.2 Hz, 3H), 0.99 (t, *J* = 7.6 Hz, 3H). ^{13}C NMR (126 MHz, $CDCl_3$) δ 171.38, 139.71, 136.16, 129.76, 125.97, 124.04, 123.09, 119.83 (q, *J* = 321 Hz), 119.28, 118.62, 117.66, 117.11, 43.82, 34.68, 30.97, 26.88, 23.13, 13.16, 12.92. HRMS Calcd for $C_{19}H_{23}F_3N_2NaO_3S$ ([M+Na]$^+$): 439.1274; Found: 439.1281.

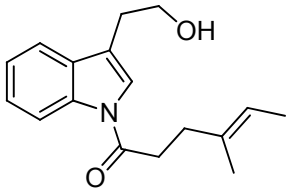

13u

13u was purified by column chromatography on silica gel (petroleum ether/EtOAc = 3/1) to give a white solid in 80% yield. ^{1}H NMR (300 MHz, $CDCl_3$) δ 8.46 (d, *J* = 8.1 Hz, 1H), 7.55 (dd, *J* = 8.0, 1.3 Hz, 1H), 7.40–7.28 (m, 3H), 5.31 (q, *J* = 6.7 Hz, 1H), 3.96 (q, *J* = 6.0 Hz, 2H), 3.05–2.95 (m, 4H), 2.50 (t, *J* = 7.9 Hz, 2H), 1.69 (s, 3H), 1.63–1.58 (d, *J* = 6.6 Hz, 3H). ^{13}C NMR (75 MHz, $CDCl_3$) δ 171.17, 136.11, 133.91, 130.48, 125.44, 123.55, 122.53, 119.78, 119.18, 118.89, 116.91, 61.90, 34.76, 34.20, 28.60, 16.00, 13.55. HRMS Calcd for $C_{17}H_{22}NO_2$ ([M+H]$^+$): 272.1645; Found: 272.1641.

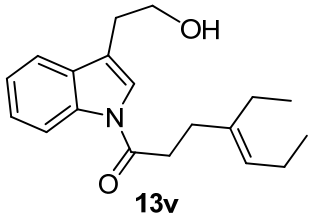

13v

13v was purified by column chromatography on silica gel (petroleum ether/EtOAc = 3/1) to give a light-yellow solid in 79% yield. ^{1}H NMR (300 MHz, $CDCl_3$) δ 8.46 (d, *J* = 8.1 Hz, 1H), 7.54 (d, *J* = 7.6 Hz, 1H), 7.42–7.27 (m, 3H), 5.17 (t, *J* = 7.1 Hz, 1H), 3.95 (t, *J* = 6.1 Hz, 2H), 3.00–2.93 (m, 4H), 2.56–2.43 (m, 2H), 2.13–1.98 (m, 4H), 1.64 (s, 1H), 1.01 (t, *J* = 7.5 Hz, 3H), 0.95 (t, *J* = 7.5 Hz, 3H). ^{13}C NMR (75 MHz, $CDCl_3$) δ 171.25, 138.62, 136.14, 130.48, 127.17, 125.46, 123.55, 122.58, 119.13, 118.90, 116.94, 61.94, 35.04, 31.08, 28.62, 23.44, 20.99, 14.72, 13.46. HRMS Calcd for $C_{19}H_{25}NNaO_2$ ([M+Na]$^+$): 322.1778; Found: 322.1781.

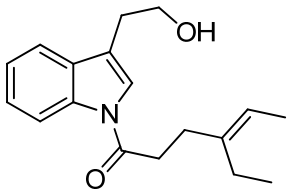

13w

13w was purified by column chromatography on silica gel (petroleum ether/EtOAc = 3/1) to give a white solid in 80% yield. ^{1}H NMR (300 MHz, $CDCl_3$) δ 8.46 (d, *J* = 8.2 Hz, 1H), 7.55 (dd, *J* = 8.1, 1.3 Hz, 1H), 7.43–7.23 (m, 3H), 5.26 (q, *J* = 6.7 Hz, 1H), 3.96 (t, *J* = 6.3 Hz, 2H), 3.10–2.91 (m, 4H), 2.52–2.48 (m, 2H), 2.11 (q, *J* = 7.6 Hz, 2H), 1.62 (d, *J* = 6.9 Hz, 3H), 1.01 (t, *J* = 7.6 Hz, 3H). ^{13}C NMR (75 MHz, $CDCl_3$) δ 171.24, 140.03, 136.17, 130.48, 125.50, 123.57, 122.55, 119.14, 118.91, 116.96, 61.96, 35.02, 31.14, 28.62, 23.19, 13.19, 12.96. HRMS Calcd for $C_{18}H_{24}NO_2$ ([M+H]$^+$): 286.1802; Found: 286.1806.

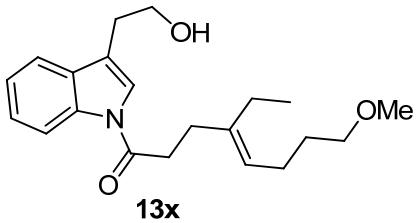

13x

13x was purified by column chromatography on silica gel (petroleum ether/EtOAc = 5/1) to give a yellow solid in 69% yield.^{1}H NMR (300 MHz, $CDCl_3$) δ 8.45 (d, *J* = 8.0 Hz, 1H), 7.54 (d, *J* = 7.6 Hz, 1H), 7.38–7.28 (m, 3H), 5.15 (t, *J* = 7.1 Hz, 1H), 3.94 (t, *J* = 6.2 Hz, 2H), 3.35–3.31 (m, 5H), 2.99–2.90 (m, 4H), 2.49 (t, *J* = 8.1 Hz, 2H), 2.13–2.04 (m, 4H), 1.93 (s, 1H), 1.67–1.54 (m, 2H), 1.01 (t, *J* = 7.6 Hz, 3H). ^{13}C NMR (75 MHz, $CDCl_3$) δ 171.18, 139.80, 136.12, 130.51, 125.44, 124.65, 123.55, 122.55, 119.24, 118.90, 116.92, 72.28, 61.88, 58.61, 34.95, 31.15, 29.85, 28.62, 24.18, 23.40, 13.32. HRMS Calcd for $C_{21}H_{29}NNaO_3$ ([M+Na]$^+$): 366.2040; Found: 366.2036.

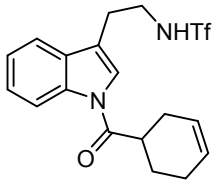

13y

13y was purified by column chromatography on silica gel (petroleum ether/EtOAc = 7/1) to give a white solid in 78% yield. ^{1}H NMR (300 MHz, $CDCl_3$) δ 8.49 (d, *J* = 8.2 Hz, 1H), 7.51 (d, *J* = 7.7 Hz, 1H), 7.46–7.27 (m, 3H), 5.77 (s, 2H), 5.14 (t, *J* = 6.2 Hz, 1H), 3.67 (q, *J* = 6.6 Hz, 2H), 3.19 (tdd, *J* = 10.7, 5.3, 2.9 Hz, 1H), 3.05 (t, *J* = 6.7 Hz, 2H), 2.54–2.37 (m, 1H), 2.35–2.17 (m, 3H), 2.04–1.76 (m, 2H). ^{13}C NMR (75 MHz, $CDCl_3$) δ 174.84, 136.09, 129.84, 126.74, 125.79, 124.86, 123.90, 122.86, 119.75 (q, *J* = 319.56 Hz), 118.55, 117.87, 117.03, 43.68, 39.69, 28.04, 26.60, 25.60, 24.57. HRMS Calcd for $C_{18}H_{19}F_3N_2NaO_3S$ ([M+Na]$^+$): 423.0961; Found: 423.0947.

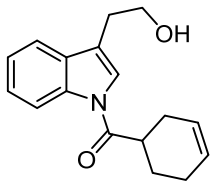

13z

13z was purified by column chromatography on silica gel (petroleum ether/EtOAc = 3/1) to give a white solid in 80% yield. ^{1}H NMR (300 MHz, $CDCl_3$) δ 8.50 (d, *J* = 8.1 Hz, 1H), 7.54 (d, *J* = 6.6, 1H), 7.39–7.25 (m, 3H), 5.77 (d, *J* = 2.6 Hz, 2H), 3.94 (t, *J* = 6.4 Hz, 2H), 3.32–3.20 (m, 1H), 2.97 (t, *J* = 6.4 Hz, 2H), 2.50–1.85 (m, 6H). ^{13}C NMR (75 MHz, $CDCl_3$) δ 174.51, 136.00, 130.48, 126.62, 125.29, 125.03, 123.46, 122.25, 119.30, 118.72, 116.90, 61.65, 39.57, 28.39, 28.07, 25.67, 24.59. HRMS Calcd for $C_{17}H_{19}NNaO_2$ ([M+Na]$^+$): 292.1308; Found: 292.1312.

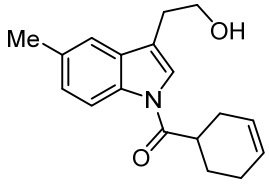

13aa

13aa was purified by column chromatography on silica gel (petroleum ether/EtOAc = 3/1) to give a white solid in 75% yield. ^{1}H NMR (300 MHz, $CDCl_3$) δ 8.38 (d, *J* = 8.5 Hz, 1H), 7.37 (d, *J* = 11.1 Hz, 2H), 7.31–7.16 (m, 2H), 5.80 (d, *J* = 2.5 Hz, 2H), 3.97 (t, *J* = 6.4 Hz, 2H), 3.32–3.20 (m, 1H), 2.99 (t, *J* = 6.3 Hz, 2H), 2.48 (s, 3H), 2.40–1.53 (m, 6H). ^{13}C NMR (75 MHz, $CDCl_3$) δ 174.34, 134.41, 133.25, 130.74, 126.79, 125.28, 122.51, 119.04, 118.98, 118.81, 116.77, 61.94, 39.70, 28.61, 28.25, 25.88, 24.80, 21.56. HRMS Calcd for $C_{18}H_{21}NNaO_2$ ([M+Na]$^+$): 306.1465; Found: 306.1469.

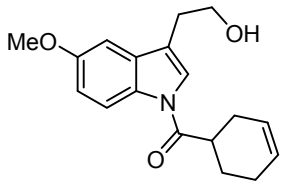

13ab

13ab was purified by column chromatography on silica gel (petroleum ether/EtOAc = 3/1) to give a white solid in 60% yield. ^{1}H NMR (300 MHz, $CDCl_3$) δ 8.39 (d, *J* = 8.8 Hz, 1H), 7.38 (s, 1H), 6.99 (s, 1H), 6.95(d, *J* = 3.2 Hz, 1H), 5.77 (d, *J* = 2.5 Hz, 2H), 3.87 (s, 5H), 3.23 (ddq, *J* = 13.5, 7.9, 2.8 Hz, 1H), 2.95 (td, *J* = 6.3, 0.9 Hz, 2H), 2.58–1.50 (m, 6H).^{13}C NMR (75 MHz, $CDCl_3$) δ 174.14, 156.47, 131.56, 130.84, 126.74, 125.21, 123.03, 119.08, 117.87, 113.39, 101.95, 61.81, 55.78, 39.50, 28.56, 28.26, 25.86, 24.74. HRMS Calcd for $C_{18}H_{21}NNaO_3$ ([M+Na]$^+$): 322.1414; Found: 322.1419.

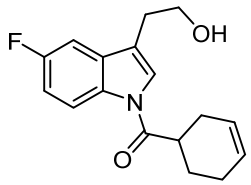

13ac

13ac was purified by column chromatography on silica gel (petroleum ether/EtOAc = 3/1) to give a white solid in 75% yield. ^{1}H NMR (300 MHz, $CDCl_3$) δ 8.46 (dd, *J* = 9.1, 4.7 Hz, 1H), 7.44 (s, 1H), 7.19 (dd, *J* = 8.7, 2.6 Hz, 1H), 7.07 (td, *J* = 9.1, 2.6 Hz, 1H), 5.77 (d, *J* = 2.6 Hz, 2H), 3.94 (t, *J* = 6.3 Hz, 2H), 3.29–3.10 (m, 1H), 2.93 (t, *J* = 6.3, 2H), 2.56–2.02 (m, 6H). ^{13}C NMR (75 MHz, $CDCl_3$) δ 174.34, 159.72 (d, *J* = 240.7 Hz), 132.54, 131.70 (d, *J* = 9.2 Hz), 126.79, 125.13, 123.86, 119.10 (d, *J* = 4.0 Hz), 118.21 (d, *J* = 8.8 Hz), 113.04 (d, *J* = 24.6 Hz), 104.64 (d, *J* = 23.8 Hz), 61.77, 39.59, 28.46, 28.26, 25.87, 24.72. HRMS Calcd for $C_{17}H_{18}FNNaO_2$ ([M+Na]$^+$): 310.1214; Found: 310.1201.

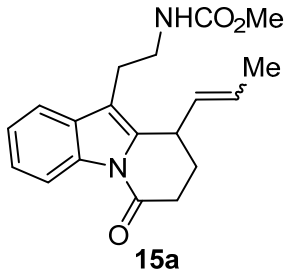

15a

15a was purified by column chromatography on silica gel (petroleum ether/EtOAc = 8/1) to give a yellow solid in 76% yield with a *E/Z* ratio of ca. 5:1. ^{1}H NMR (300 MHz, $CDCl_3$) δ 8.51 (d, *J* =9 Hz, 1H), 7.56–7.43 (m, 1H), 7.30 (ddd, *J* = 6.3, 3.8, 1.8 Hz, 2H), 5.63–5.53 (m, 1H), 5.37–5.24 (m, 1H), 4.81 (s, 1H), 4.22–4.08 (m, 0.17H), 3.86 (s, 0.83H), 3.66 (s, 3H), 3.49–3.34 (m, 2H), 2.94–2.62 (m, 4H), 2.29–2.12 (m, 1H), 2.09–1.97 (m, 1H), 1.80 (d, *J* = 5.7 Hz, 0.5H), 1.66 (d, *J* = 6.4 Hz, 2.5H). ^{13}C NMR (101 MHz, $CDCl_3$) δ 169.13, 157.09, 137.54, 133.16, 131.53, 130.05, 129.67, 129.21 (minor isomer), 128.43, 126.27 (minor isomer), 124.72, 117.96, 117.75, 114.13, 52.22, 40.65, 34.38, 31.13 (minor isomer), 30.28 (minor isomer), 29.82, 27.83 (minor isomer), 27.06, 24.52, 17.85, 13.03 (minor isomer). HRMS Calcd for $C_{19}H_{22}KN_2O_3$ ([M+K]$^+$): 365.1262; Found: 365.1272.

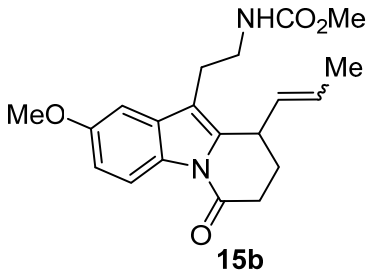

15b

15b was purified by column chromatography on silica gel (petroleum ether/EtOAc = 8/1) to give a yellow solid in 62% yield with a *E*/*Z* ratio of *ca.* 5:1. ^{1}H NMR (300 MHz, $CDCl_3$) δ 8.36 (d, *J* = 8.9 Hz, 1H), 7.01–6.86 (m, 2H), 5.57–5.29 (m, 2H), 4.76 (s, 1H), 4.22–4.08 (m, 0.17 H), 3.87 (s, 3.83H), 3.66 (s, 3H), 3.50–3.31 (m, 2H), 2.82–2.03 (m, 6H), 1.81 (d, *J* = 6.0 Hz, 0.5H), 1.67 (d, *J* = 6.3 Hz, 2.5H). ^{13}C NMR (151 MHz, $CDCl_3$) δ 168.87, 157.10,

156.99, 136.84, 131.20, 130.39, 129.51, 128.24, 117.58, 114.53, 112.50, 101.68, 55.90, 52.19, 40.65, 34.43, 31.08 (minor isomer), 30.25, 27.99 (minor isomer), 27.24, 24.70, 17.86. HRMS Calcd for $C_{20}H_{24}N_2NaO_4$ ([M+Na]$^+$): 379.1628; Found: 379.1624.

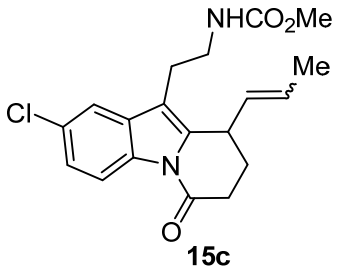

15c

15c was purified by column chromatography on silica gel (petroleum ether/EtOAc = 7/1) to give a yellow solid in 70% yield with a *E/Z* ratio of *ca.* 5:1. ^{1}H NMR (300 MHz, $CDCl_3$) δ 8.39 (dd, *J* = 8.7, 2.1 Hz, 1H), 7.45 (s, 1H), 7.28–7.14 (m, 1H), 5.61–5.53 (m, 1H), 5.32–5.23 (m, 1H), 4.75 (s, 1H), 4.16 (s, 0.17H), 3.86 (s, 0.83H), 3.67 (s, 3H), 3.47–3.32 (m, 2H), 2.95–2.61 (m, 4H), 2.21–2.00 (m, 2H), 1.81 (dd, *J* = 6.7, 1.5 Hz, 0.5H), 1.68 (d, *J* = 6.3, 2.5H). ^{13}C NMR (126 MHz, $CDCl_3$) δ169.29, 157.10, 136.00, 134.87, 130.37, 130.05, 129.60 (minor isomer), 128.23, 125.89 (minor isomer), 124.73, 124.03, 118.16, 116.79, 114.61, 52.15, 40.68, 34.32, 31.23 (minor isomer), 30.38, 30.26 (minor isomer), 29.81 (minor isomer), 27.88 (minor isomer), 27.11, 24.69, 17.82, 13.02 (minor isomer). HRMS Calcd for $C_{19}H_{21}ClN_2NaO_3$ ([M+Na]$^+$): 383.1133; Found: 383.1143.

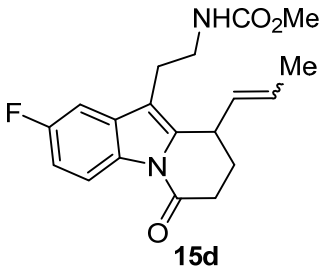

15d

15d was purified by column chromatography on silica gel (petroleum ether/EtOAc = 7/1) to give a yellow solid in 71% yield with a *E/Z* ratio of *ca.* 5:1. ^{1}H NMR (300 MHz, $CDCl_3$) δ 8.41 (dd, *J* = 8.9, 4.7 Hz, 1H), 7.17 (d, *J* = 8.8 Hz, 1H), 7.01 (td, *J* = 9.1, 2.6 Hz, 1H), 5.67–5.54 (m, 1H), 5.41–5.22 (m, 1H), 4.87 (s, 1H), 4.18–4.11 (m, 0.17H), 3.86 (s, 0.83H), 3.67 (s, 3H), 3.40–2.04 (m, 8H), 1.81 (d, *J* = 6.3 Hz, 0.5H), 1.68(d, *J* = 5.7 Hz, 2.5H). ^{13}C NMR (126 MHz, $CDCl_3$) δ 169.00, 160.09 (d, *J* = 240.6 Hz), 157.08, 138.54 (minor isomer), 137.75, 131.36 (minor isomer), 131.11, 130.08, 129.28 (minor isomer), 128.33, 126.14, 117.74 (d, *J* = 9.0 Hz), 114.46, 112.02 (d, *J* = 24.4 Hz), 104.09 (d, *J* = 24.0 Hz), 52.16, 40.56, 34.42, 31.06 (minor isomer), 30.36 (minor isomer), 30.20, 29.79 (minor isomer), 27.86 (minor isomer), 27.24, 27.10 (minor isomer), 24.61, 17.82, 14.30 (minor isomer), 12.99 (minor isomer). HRMS Calcd for $C_{19}H_{21}FN_2NaO_3$ ([M+Na]$^+$): 367.1428; Found: 367.1422.

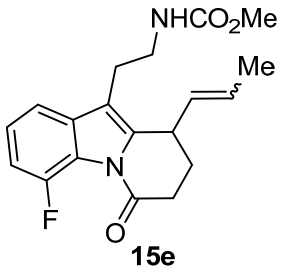

15e

15e was purified by column chromatography on silica gel (petroleum ether/EtOAc = 5/1) to give a yellow solid in 69% yield with a *E/Z* ratio of *ca.* 5:1. ^{1}H NMR (300 MHz, $CDCl_3$) δ 7.26 (m, 2H), 7.10–6.99 (m, 1H), 5.58 (m, 1H), 5.40–5.18 (m, 1H), 4.88 (t, *J* = 6.3 Hz, 1H), 4.20–4.09 (m, 0.17H), 3.90 (s, 0.83H), 3.67 (s, 3H), 3.45–3.34 (m, 2H), 2.89–2.06 (m, 6H), 1.83 (d, *J* = 6.0 Hz, 0.5H), 1.68 (d, *J* = 6.4 Hz, 2.5H). ^{13}C NMR (75 MHz, $CDCl_3$) δ 167.09, 157.13, 150.58 (d, *J* = 254.8 Hz), 138.13, 134.32 (d, *J* = 4.2 Hz), 130.18 ,129.43, 126.13 (minor isomer), 125.11 (d, *J* = 7.0 Hz), 121.39 (minor isomer), 121.28 (d, *J* = 11.7 Hz), 114.98, 113.95, 112.23 (d, *J* = 22.9 Hz), 52.20, 40.53, 34.58, 31.38 (minor isomer), 30.62, 29.81 (minor isomer), 27.62 (minor isomer), 26.98, 24.75, 17.86, 13.03 (minor isomer). HRMS Calcd for $C_{19}H_{21}FN_2NaO_3$ ([M+Na]$^+$): 367.1428; Found: 367.1438.

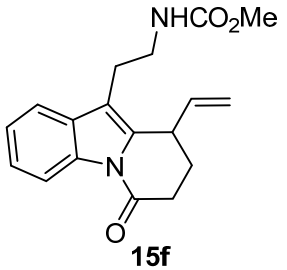

15f

15f was purified by column chromatography on silica gel (petroleum ether/acetone = 17/1) to give a yellow solid in 66% yield. ^{1}H NMR (300 MHz, $CDCl_3$) δ 8.54–8.38 (m, 1H), 7.53 (d, *J* = 6.8 Hz, 1H), 7.35–7.26 (m, 2H), 5.96 (ddd, *J* = 17.1, 10.2, 5.4 Hz, 1H), 5.21 (d, *J* = 10.2 Hz, 1H), 4.95–4.58 (m, 2H), 3.93 (s, 1H), 3.66 (s, 3H), 3.52–3.32 (m, 2H), 2.95–2.65 (m, 4H), 2.32–2.05 (m, 2H). ^{13}C NMR (75 MHz, $CDCl_3$) δ 169.13, 157.15, 137.55, 134.93, 129.99, 124.86, 124.09, 118.26, 117.60 (2C), 116.83, 115.15, 52.22, 40.67, 35.21, 30.29, 26.60, 24.75. HRMS Calcd for $C_{18}H_{20}N_2NaO_3$ ([M+Na]$^+$): 335.1366; Found: 335.1370.

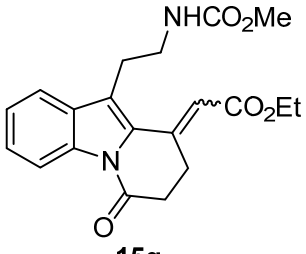

15g

15g was purified by column chromatography on silica gel (petroleum ether/EtOAc = 5/1) to give a white solid in 56% yield. ^{1}H NMR (300 MHz, $CDCl_3$) δ 8.50 (d, *J* = 8.1 Hz, 1H), 7.68 (d, *J* = 7.7 Hz, 1H), 7.36 (dtd, *J* = 23.4, 7.4, 1.2 Hz, 2H), 6.06 (s, 1H), 4.69 (s, 1H), 4.18 (q, *J* = 7.2 Hz, 2H), 3.63 (s, 3H), 3.54–3.38 (m, 2H), 2.95 (t, *J* = 6.6 Hz, 2H), 2.89 (t, *J* = 7.2 Hz, 2H), 2.76 (t, *J* = 6.6 Hz, 2H), 1.26 (t, *J* = 7.1 Hz, 3H). ^{13}C NMR (75 MHz, $CDCl_3$) δ 168.43, 165.41,

157.01, 141.34, 135.16, 130.42, 129.84, 126.71, 124.45, 120.77, 119.99, 118.19, 116.70, 60.79, 52.21, 39.98, 34.99, 34.64, 26.90, 14.40. HRMS Calcd for $C_{20}H_{22}N_2NaO_5$ ([M+Na]+): 393.1426; Found: 393.1429.

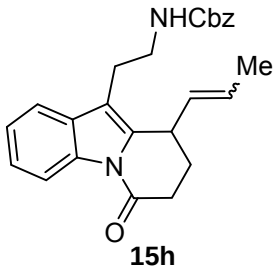

15h

15h was purified by column chromatography on silica gel (petroleum ether/EtOAc = 16/1) to give a white solid in 57% yield with a *E/Z* ratio of *ca.* 5:1. ^{1}H NMR (300 MHz, $CDCl_3$) δ 8.48 (d, *J* = 7.8 Hz, 1H), 7.51 (d, *J* = 7.2 Hz, 1H), 7.40–7.22 (m, 7H), 5.62–5.21 (m, 1H), 5.27 (m, 1H), 5.16–5.03 (m, 2H), 4.88 (s, 1H), 4.12–4.08 (m, 0.17), 3.83 (s, 0.83H), 3.53–3.37 (m, 2H), 2.87–1.94 (m, 6H), 1.75 (d, *J* = 5.4 Hz, 0.5H), 1.63 (d, *J* = 6.5 Hz, 2.5H). ^{13}C NMR (101 MHz, $CDCl_3$) δ 169.26, 156.42, 136.67, 136.01, 134.84, 130.32, 130.04, 129.55 (minor isomer), 128.62 (2C), 128.27 (2C), 128.16, 125.87, 124.70, 124.02, 118.16, 116.78, 114.59, 66.72, 40.68, 34.30, 31.20 (minor isomer), 30.35, 29.81 (minor isomer), 27.82 (minor isomer), 27.04, 24.64, 17.81, 14.32 (minor isomer), 13.01 (minor isomer). HRMS Calcd for $C_{25}H_{26}N_2NaO_3$ ($[M+Na]^+$): 425.1836; Found: 425.1839.

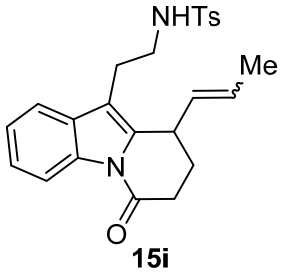

15i

15i was purified by column chromatography on silica gel (petroleum ether/EtOAc = 10/1) to give a yellow solid in 47% yield with a *E/Z* ratio of *ca.* 5:1. ^{1}H NMR (300 MHz, $CDCl_3$) δ 8.43 (d, *J* = 8.0 Hz, 1H), 7.69–7.19 (m, 3H), 7.31–7.19 (m, 4H), 5.66–5.46 (m, 1H), 5.35–5.18 (m, 1H), 4.72–4.66 (m, 1H), 4.11 (m, 0.17H) 3.80 (s, 0.83H), 3.21 (q, *J* = 6.8 Hz, 2H), 2.91–2.60 (m, 4H), 2.38 (s, 3H), 2.18–1.93 (m, 2H), 1.78 (d, *J* = 6.8 Hz, 0.5H), 1.63 (d, *J* = 6.5 Hz, 2.5H). ^{13}C NMR (75 MHz, $CDCl_3$) δ 169.27, 143.59 (minor isomer),143.44, 136.96, 136.34, 134.79 (minor isomer), 130.35, 129.77, 129.65 (2C), 129.42 (minor isomer), 128.28, 126.97 (2C), 126.51, 126.29 (minor isomer), 124.70, 124.01, 117.90, 116.78, 113.70, 42.56, 34.31, 31.23 (minor isomer), 30.34, 30.26 (minor isomer), 29.80 (minor isomer), 27.76 (minor isomer), 27.04, 24.77, 24.65 (minor isomer), 21.60, 17.80, 14.30 (minor isomer), 13.09 (minor isomer). HRMS Calcd for $C_{24}H_{26}N_2NaO_3S$ ($[M+Na]^+$): 445.1556; Found: 445.1564.

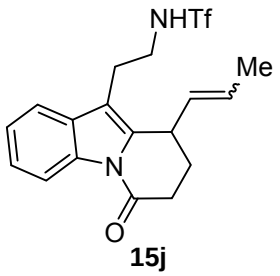

15j

15j was purified by column chromatography on silica gel (petroleum ether/EtOAc = 6/1) to give a yellow solid in 78% yield with a *E/Z* ratio of *ca.* 5:1. ^{1}H NMR (300 MHz, $CDCl_3$) δ 8.54–8.44 (m, 1H), 7.49–7.29 (m, 3H), 5.73–5.54 (m, 1H), 5.39–5.25 (m, 1H), 5.37–5.27 (m, 1H), 4.25–4.10 (m, 0.13H), 3.88 (s, 0.87H), 3.57–2.05(m, 8H), 1.84 (dd, *J* = 6.3, 1.5 Hz, 0.5H), 1.69 (d, *J* = 6.5, 2.5H). ^{13}C NMR (126 MHz, $CDCl_3$) δ 169.33, 136.83, 134.91, 130.78, 129.43 (minor isomer), 129.41, 128.79, 126.83 (minor isomer), 125.20, 124.71 (minor isomer), 124.40 (minor isomer), 124.36, 119.71 (q, *J* = 321 Hz), 117.75, 117.07, 112.69, 43.77, 34.53, 31.74 (minor isomer), 31.17 (minor isomer), 30.40 (minor isomer), 30.31, 27.86 (minor isomer), 27.11, 25.60, 22.81 (minor isomer), 17.80, 14.28 (minor isomer), 13.10 (minor isomer). HRMS Calcd for $C_{18}H_{19}F_3N_2NaO_3S$ ([M+Na]$^+$): 423.0961; Found: 423.0965.

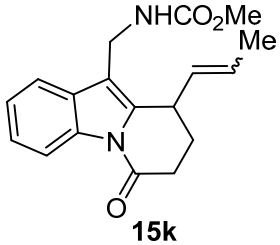

15k

15k was purified by column chromatography on silica gel (petroleum ether/EtOAc = 4/1) to give a yellow solid in 79% yield with a *E/Z* ratio of *ca.* 5:1. ^{1}H NMR (300 MHz, $CDCl_3$) δ 8.53–8.42 (m, 1H), 7.56 (s, 1H), 7.31 (ddd, *J* = 6.5, 4.2, 1.7 Hz, 2H), 5.71–5.49 (m, 1H), 5.39–5.20 (m, 1H), 4.80 (s, 1H), 4.51 (dd, *J* = 14.7, 6.1 Hz, 1H), 4.35 (dd, *J* = 14.6, 5.1 Hz, 1H), 4.02 (s, 1H), 3.68 (s, 3H), 2.91–2.65 (m, 2H), 2.29–2.01 (m, 2H), 1.83 (dd, *J* = 6 Hz, 0.5H), 1.67 (d, *J* = 6.5 Hz, 2.5H). ^{13}C NMR (151 MHz, $CDCl_3$) δ 169.36, 157.03, 137.10, 134.85, 130.43, 129.62 (minor isomer), 129.17, 128.31, 126.22 (minor isomer), 125.00, 124.25, 118.33, 116.83, 114.47, 52.37, 34.95, 34.32, 31.43 (minor isomer), 30.45, 27.75 (minor isomer), 26.99, 17.88. HRMS Calcd for $C_{18}H_{20}N_2NaO_3$ ([M+Na]$^+$): 335.1366; Found: 335.1361.

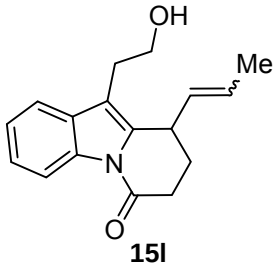

15l

15l was purified by column chromatography on silica gel (petroleum ether/EtOAc = 4/1) to give a yellow solid in 72% yield with a *E/Z* ratio of *ca.* 5:1. ^{1}H NMR (300 MHz, $CDCl_3$) δ 8.55–8.43 (m, 1H), 7.61–7.46 (m, 1H), 7.43–7.28 (m, 2H), 5.71–5.52 (m, 1H), 5.45–5.17 (m, 1H),

4.02–3.78 (m, 3H), 2.99–2.63 (m, 4H), 2.27–1.97 (m, 2H), 1.82 (d, *J* = 6.0 Hz, 0.5H), 1.68 (d, *J* = 6.3 Hz, 2.5H). ^{13}C NMR (75 MHz, $CDCl_3$) δ 169.40, 136.26, 134.86, 130.46, 130.27, 128.09, 124.71, 123.98, 118.24, 116.79, 114.24, 62.19, 34.22, 30.34, 27.68, 27.03, 17.86. HRMS Calcd for $C_{17}H_{19}NNaO_2$ ([M+Na]$^+$): 292.1308; Found: 292.1308.

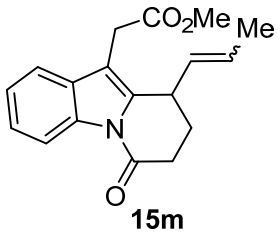

15m

15m was purified by column chromatography on silica gel (petroleum ether/EtOAc = 20/1) to give a yellow solid in 80% yield with a *E/Z* ratio *ca.* of 5:1. ^{1}H NMR (300 MHz, $CDCl_3$) δ 8.53–8.42 (m, 1H), 7.54–7.44 (m, 1H), 7.36–7.27 (m, 2H), 5.75–5.28 (m, 2H), 4.24–4.17 (m, 0.17H), 3.91 (s, 0.83H), 3.69–3.63 (m, 5H), 2.87–2.64 (m, 2H), 2.29–1.99 (m, 2H), 1.80 (dd, *J* = 6.8, 1.7 Hz, 0.5 H), 1.66 (dt, *J* = 6.3, 1.5 Hz, 2.5H). ^{13}C NMR (75 MHz, $CDCl_3$) δ 171.35, 169.28, 136.62, 134.69, 129.96 (minor isomer), 129.63, 129.31 (minor isomer), 128.34, 126.22, 124.80, 124.08, 118.26, 118.08 (minor isomer), 116.71, 110.93, 52.21, 34.67, 31.89 (minor isomer), 30.98 (minor isomer), 30.69, 29.95, 29.84 (minor isomer), 29.77 (minor isomer), 27.93 (minor isomer), 27.16, 17.87, 13.03 (minor isomer). HRMS Calcd for $C_{18}H_{19}NNaO_3$ ([M+Na]$^+$): 320.1257; Found: 320.1260.

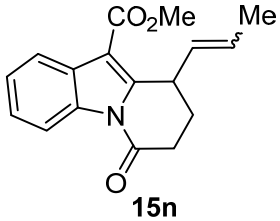

15n

15n was purified by column chromatography on silica gel (petroleum ether/EtOAc = 8/1) to give a yellow solid in 64% yield with a *E/Z* ratio of *ca.* 5:1. ^{1}H NMR (300 MHz, $CDCl_3$) δ 8.51 (dd, *J* = 6.1, 3.3 Hz, 1H), 8.11 (dd, *J* = 6.1, 3.2 Hz, 1H), 7.37 (dt, *J* = 6.1, 3.7 Hz, 2H), 5.73–5.46 (m, 1H), 5.37–5.15 (m, 1H), 5.03 (s, 0.13H), 4.75 (s, 0.87H), 3.95 (s, 3H), 3.05–2.72 (m, 2H), 2.34–2.07 (m, 2H), 1.85 (dd, *J* = 6.9 Hz, 0.5H), 1.65 (dt, *J* = 6.5, 1.7 Hz, 2.5H). ^{13}C NMR (126 MHz, $CDCl_3$) δ 169.75, 165.04, 147.83, 134.74, 128.97, 127.99, 127.75 (minor isomer), 127.29, 127.17, 125.39, 125.02, 121.49, 116.52, 109.34 (minor isomer), 51.46, 34.73, 30.81 (minor isomer), 30.57 (minor isomer), 30.21, 29.83 (minor isomer), 27.38, 26.09, 18.03 (minor isomer), 13.13 (minor isomer). HRMS Calcd for $C_{17}H_{17}NNaO_3$ ([M+Na]$^+$): 306.1101; Found: 306.1102.

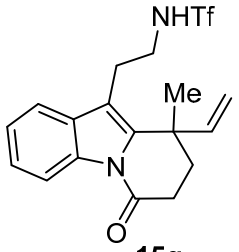

15q

15q was purified by column chromatography on silica gel (petroleum ether/EtOAc = 8/1) to give a yellow solid in 69% yield. ^{1}H NMR (300 MHz, $CDCl_3$) δ 8.59–8.46 (m, 1H), 7.48 (dd, *J* = 6.5, 2.4 Hz, 1H), 7.33 (ddd, *J* = 6.9, 5.0, 1.7 Hz, 2H), 6.01 (dd, *J* = 17.3, 10.5 Hz, 1H), 5.39 (t, *J* = 6.1 Hz, 1H), 5.26 (d, *J* = 10.4 Hz, 1H), 5.02 (d, *J* = 17.4 Hz, 1H), 3.65–3.41 (m, 2H), 3.13 (t, *J* = 7.7 Hz, 2H), 2.77 (t, *J* = 6.5 Hz, 2H), 1.99 (qt, *J* = 13.5, 5.6 Hz, 2H), 1.64 (s, 3H). ^{13}C NMR (126 MHz, $CDCl_3$) δ 169.37, 143.70, 138.95, 134.61, 130.05, 125.44, 124.38, 119.74 (q, *J* = 321 Hz), 117.77, 117.13, 114.94, 113.73, 43.88, 39.34, 35.52, 30.76, 26.25, 25.26. HRMS Calcd for $C_{18}H_{19}F_3N_2NaO_3S$ ([M+Na]$^+$): 423.0961; Found: 423.0963.

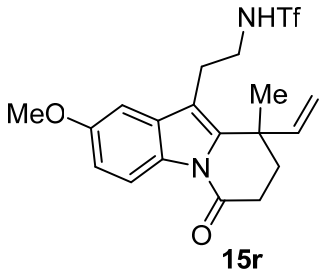

15r

15r was purified by column chromatography on silica gel (petroleum ether/EtOAc = 8/1) to give a yellow solid in 53% yield. ^{1}H NMR (300 MHz, $CDCl_3$) δ 8.34 (d, *J* = 8.9 Hz, 1H), 7.07–6.88 (m, 2H), 5.98 (dd, *J* = 17.3, 10.4 Hz, 1H), 5.86 (s, 1H), 5.24 (d, *J* = 10.4 Hz, 1H), 5.00 (d, *J* = 17.3 Hz, 1H), 3.86 (s, 3H), 3.52 (dt, *J* = 9.5, 4.3 Hz, 2H), 3.08 (t, *J* = 7.8 Hz, 2H), 2.72 (t, *J* = 6.5 Hz, 2H), 1.97 (qd, *J* = 13.7, 12.8, 5.9 Hz, 2H), 1.60 (s, 3H). ^{13}C NMR (75 MHz, $CDCl_3$) δ 169.32, 157.05, 143.54, 139.51, 131.33, 129.07, 119.9 (q, *J* = 321 Hz), 117.84, 114.85, 113.94, 113.23, 101.15, 55.82, 43.73, 39.30, 35.48, 30.51, 26.39, 25.14. HRMS Calcd for $C_{19}H_{21}F_3N_2NaO_4S$ ([M+Na]$^+$): 453.1066; Found: 453.1072.

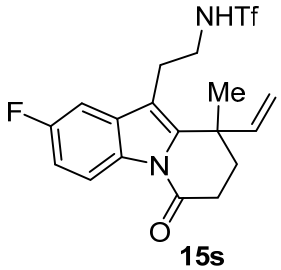

15s

15s was purified by column chromatography on silica gel (petroleum ether/EtOAc = 5/1) to give a yellow solid in 66% yield. ^{1}H NMR (300 MHz, $CDCl_3$) δ 8.47 (dd, *J* = 9.0, 4.8 Hz, 1H), 7.18–6.97 (m, 2H), 6.00 (dd, *J* = 17.3, 10.4 Hz, 1H), 5.27 (d, *J* = 10.5 Hz, 1H), 5.01 (d, *J* = 17.3 Hz, 1H), 3.52 (td, *J* = 7.4, 2.1 Hz, 2H), 3.07 (t, *J* = 7.8 Hz, 2H), 2.79 (t, *J* = 6.5 Hz, 2H), 2.01 (qt, *J* = 13.5, 6.4 Hz, 2H), 1.62 (s, 3H). ^{13}C NMR (126 MHz, $CDCl_3$) δ 168.99, 160.19 (d, *J* = 241.7 Hz), 143.45, 140.70, 131.30 (d, *J* = 9.3 Hz), 130.91, 119.74 (q, *J* = 321 Hz)，118.29 (d, *J* = 9.0 Hz), 115.12, 113.41, 112.90 (d, *J* = 24.3 Hz), 103.70 (d, *J* = 24.0 Hz), 43.66, 39.43, 35.53, 30.64, 26.32, 25.17. HRMS Calcd for $C_{18}H_{18}F_4N_2NaO_3S$ ([M+Na]$^+$): 441.0866; Found: 441.0872.

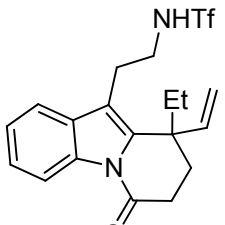

15t

15t was purified by column chromatography on silica gel (petroleum ether/EtOAc = 15/1) to give a yellow solid in 78% yield. ^{1}H NMR (300 MHz, $CDCl_3$) δ 8.52 (d, *J* = 9.0 Hz, 1H), 7.50 (d, *J* = 8.7 Hz, 1H), 7.35 (q, *J* = 6.4, 6.0 Hz, 2H), 6.01 (dd, *J* = 17.4, 10.5 Hz, 1H), 5.32 (t, *J* = 6.0 Hz, 1H), 5.27 (d, *J* = 10.6 Hz, 1H), 4.89 (d, *J* = 17.4 Hz, 1H), 3.56 (q, *J* = 6.3 Hz, 2H), 3.16–3.05 (m, 2H), 2.78–2.72 (m, 2H), 2.24–2.08 (m, 2H), 1.98–1.83 (m, 2H), 0.97 (t, *J* = 7.4 Hz, 3H). ^{13}C NMR (75 MHz, $CDCl_3$) δ 169.92, 142.48, 137.63, 134.74, 130.20, 125.29, 124.35, 119.77 (q, *J* = 318 Hz), 117.82, 117.02, 115.83, 114.08, 43.61, 43.49, 30.56, 30.51, 30.32, 26.77, 8.69. HRMS Calcd for $C_{19}H_{21}F_3N_2NaO_3S$ ([M+Na]$^+$): 437.1117; Found: 437.1121.

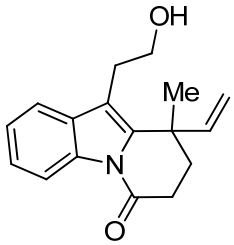

15u

15u was purified by column chromatography on silica gel (petroleum ether/EtOAc = 3/1) to give a yellow solid in 69% yield. ^{1}H NMR (300 MHz, $CDCl_3$) δ 8.63–8.44 (m, 1H), 7.53 (dd, *J* = 7.6, 1.5 Hz, 1H), 7.31 (qd, *J* = 7.0, 1.5 Hz, 2H), 5.99 (dd, *J* = 17.3, 10.4 Hz, 1H), 5.20 (d, 1H), 4.98 (d, *J* = 17.4 Hz, 1H), 3.87 (td, *J* = 7.4, 1.1 Hz, 2H), 3.06 (t, *J* = 7.2 Hz, 2H), 2.77 (t, *J* = 6.5 Hz, 2H), 2.01–1.90 (m, 2H), 1.62 (s, 3H). ^{13}C NMR (75 MHz, $CDCl_3$) δ 169.33, 143.72, 138.18, 134.51, 130.85, 124.94, 123.91, 118.27, 116.81, 115.20, 114.48, 62.22, 39.33, 35.53, 30.79, 28.06, 25.51. HRMS Calcd for $C_{17}H_{19}NNaO_2$ ([M+Na]$^+$): 292.1308; Found: 292.1316.

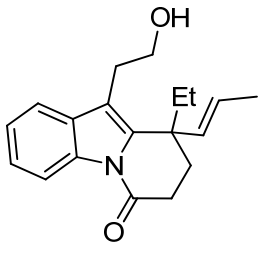

15v

15v was purified by column chromatography on silica gel (petroleum ether/EtOAc = 5/1) to give a yellow solid in 70% yield. ^{1}H NMR (300 MHz, $CDCl_3$) δ 8.51 (d, *J* = 7.5 Hz, 1H), 7.54 (d, *J* = 7.9 Hz, 1H), 7.35–7.28 (m, 2H), 5.58 (d, *J* = 15.6 Hz, 1H), 5.34–5.19 (m, 1H), 3.87 (t, *J* = 7.2 Hz, 2H), 3.12–2.95 (m, 2H), 2.78–2.71 (m, 2H), 2.23–2.09 (m, 2H), 1.92–1.76 (m, 2H), 1.70–1.68 (m, 4H), 0.94 (t, *J* = 7.4 Hz, 3H). ^{13}C NMR (75 MHz, $CDCl_3$) δ 169.78, 137.70, 135.44, 134.54, 130.96, 125.85, 124.64, 123.75, 118.11, 116.66, 114.81, 61.85, 42.73, 30.98,

30.74, 30.43, 28.48, 17.85, 8.61. HRMS Calcd for $C_{19}H_{23}NNaO_2$ ([M+Na]$^+$): 320.1621; Found: 320.1626.

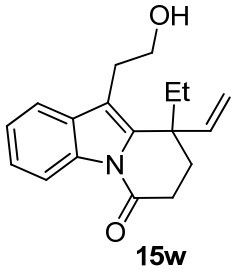

15w

15w was purified by column chromatography on silica gel (petroleum ether/EtOAc = 3/1) to give a yellow solid in 80% yield. ^{1}H NMR (300 MHz, $CDCl_3$) δ 8.52 (d, *J* = 7.7 Hz, 1H), 7.59–7.50 (m, 1H), 7.40–7.23 (m, 2H), 5.99 (dd, *J* = 17.4, 10.5 Hz, 1H), 5.21 (d, *J* = 10.5 Hz, 1H), 4.86 (d, *J* = 17.4 Hz, 1H), 4.01–3.83 (m, 2H), 3.03 (dd, *J* = 13.8, 6.9 Hz, 2H), 2.75 (q, *J* = 5.2 Hz, 2H), 2.18 (tt, *J* = 15.2, 6.7 Hz, 2H), 2.00–1.78 (m, 2H), 0.95 (t, *J* = 7.4 Hz, 3H). ^{13}C NMR (75 MHz, $CDCl_3$) δ 169.54, 142.68, 136.96, 134.78, 130.95, 124.93, 123.91, 118.29, 116.87, 115.47, 115.23, 62.12, 43.74, 30.66 (2C), 30.49, 28.57, 8.72. HRMS Calcd for $C_{18}H_{21}NNaO_2$ ([M+Na]$^+$): 306.1465; Found: 306.1469.

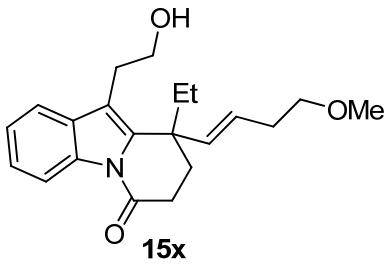

15x

15x was purified by column chromatography on silica gel (petroleum ether/EtOAc = 6/1) to give a yellow solid in 73% yield. ^{1}H NMR (300 MHz, $CDCl_3$) δ 8.51 (d, *J* = 7.3 Hz, 1H), 7.52 (d, *J* = 7.9 Hz, 1H), 7.30 (t, *J* = 5.4 Hz, 2H), 5.68 (d, *J* = 15.7 Hz, 1H), 5.37–5.27 (m, 1H), 3.94–3.78 (m, 2H), 3.43 (q, *J* = 6.0 Hz, 2H), 3.32 (s, 3H), 3.03 (t, *J* = 7.3 Hz, 2H), 2.78–2.73 (m, 2H), 2.78–2.28 (m, 3H), 2.17–2.06 (m, 2H), 1.96–1.80 (m, 2H), 0.94 (t, *J* = 7.4 Hz, 3H). ^{13}C NMR (75 MHz, $CDCl_3$) δ 169.52, 137.51, 136.67, 134.71, 131.04, 127.63, 124.77, 123.84, 118.26, 116.82, 115.32, 72.12, 62.14, 58.59, 42.64, 33.01, 31.31, 30.48, 30.26, 28.54, 8.81. HRMS Calcd for $C_{21}H_{27}NNaO_3$ ([M+Na]$^+$): 364.1883; Found: 364.1879.

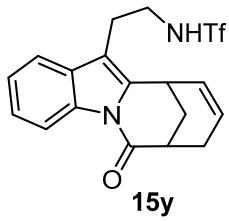

15y

15y was purified by column chromatography on silica gel (petroleum ether/EtOAc = 8/1) to give a yellow solid in 21% yield. ^{1}H NMR (300 MHz, $CDCl_3$) δ 8.41 (d, *J* = 8.6 Hz, 1H), 7.41 (d, *J* = 8.0 Hz, 1H), 7.33–7.27 (m, 2H), 5.95–5.84 (m, 1H), 5.70–5.67 (m, 1H), 5.35 (t, *J* = 5.4 Hz, 1H), 3.66 (s, 1H), 3.59 (q, *J* = 6.8 Hz, 2H), 3.14 (s, 1H), 3.08–2.97 (m, 2H), 2.67–2.59 (m, 1H), 2.48–2.24 (m, 2H), 2.18–2.14 (m, 1H). ^{13}C NMR (75 MHz, $CDCl_3$) δ 173.01, 139.68, 135.34,

129.60, 128.15, 126.22, 125.09, 124.37, 119.71 (q, J = 316.56 Hz), 117.98, 116.84, 110.09, 43.99, 38.05, 29.37, 28.39, 27.13, 25.97. HRMS Calcd for $C_{18}H_{17}F_3N_2NaO_3S$ ([M+Na]$^+$): 421.0804; Found: 421.0788.

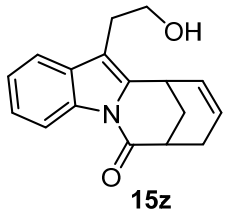

15z

15z was purified by column chromatography on silica gel (petroleum ether/EtOAc = 3/1) to give a white solid in 72% yield. ^{1}H NMR (300 MHz, $CDCl_3$) δ 8.51–8.37 (m, 1H), 7.53–7.39 (m, 1H), 7.36–7.20 (m, 2H), 6.03–5.79 (m, 1H), 5.66 (ddd, J = 9.8, 4.5, 2.5 Hz, 1H), 3.88 (q, J = 6.0 Hz, 2H), 3.69 (s, 1H), 3.19 (ddd, J = 6.6, 3.9, 1.9 Hz, 1H), 2.96 (td, J = 6.4, 3.0 Hz, 2H), 2.72–2.56 (m, 1H), 2.52–2.38 (m, 1H), 2.32 (dt, J = 12.8, 3.3 Hz, 1H), 2.16 (dt, J = 12.3, 3.0 Hz, 1H), 1.55 (t, J = 5.9 Hz, 1H). ^{13}C NMR (75 MHz, $CDCl_3$) δ 172.77, 139.12, 135.29, 130.36, 128.67, 125.62, 124.66, 123.99, 118.34, 116.62, 111.50, 62.04, 38.14, 29.41, 28.45, 27.63, 27.15. HRMS Calcd for $C_{17}H_{17}NNaO_2$ ([M+Na]$^+$): 290.1151; Found: 290.1156.

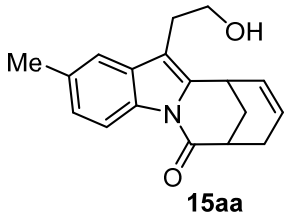

15aa

15aa was purified by column chromatography on silica gel (petroleum ether/EtOAc = 3/1) to give a yellow solid in 71% yield. ^{1}H NMR (300 MHz, $CDCl_3$) δ 8.29 (d, J = 8.2 Hz, 1H), 7.24 (s, 1H), 7.11 (d, J = 8.4, 1H), 5.90 (t, J = 7.7 Hz, 1H), 5.74–5.60 (m, 1H), 3.97–3.83 (m, 2H), 3.67 (s, 1H), 3.18 (s, 1H), 2.93 (td, J = 6.4, 2.8 Hz, 2H), 2.69–2.56 (m, 1H), 2.50–2.41 (m, 4H), 2.33–2.29 (m, 1H), 2.15 (dt, J = 12.6, 2.7 Hz, 1H), 1.48 (s, 1H). ^{13}C NMR (75 MHz, $CDCl_3$) δ 172.52, 139.26, 133.63, 133.46, 130.57, 128.70, 125.80, 125.63, 118.46, 116.27, 111.24, 62.09, 38.11, 29.41, 28.53, 27.66, 27.19, 21.65. HRMS Calcd for $C_{18}H_{19}NNaO_2$ ([M+Na]$^+$): 304.1308; Found: 304.1312.

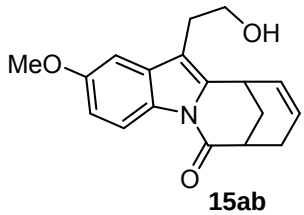

15ab

15ab was purified by column chromatography on silica gel (petroleum ether/EtOAc = 3/1) to give a yellow solid in 68% yield. ^{1}H NMR (300 MHz, $CDCl_3$) δ 8.30 (d, J = 8.7 Hz, 1H), 6.96–6.85 (m, 2H), 5.89 (t, J = 7.8 Hz, 1H), 5.66–5.63 (m, 1H), 3.84–3.88 (m, 5H), 3.65 (dd, J = 6.7, 3.4 Hz, 1H), 3.14 (s, 1H), 2.91 (td, J = 6.5, 2.1 Hz, 2H), 2.66–2.38 (m, 1H), 2.49–2.34 (m, 1H), 2.29 (d, J = 11.3 Hz, 1H), 2.16 (dt, J = 12.6, 2.7 Hz, 1H), 1.82 (s, 1H). ^{13}C NMR (75 MHz, $CDCl_3$) δ 172.26, 156.88, 140.00, 131.51, 129.89, 128.62, 125.69, 117.31, 111.94, 111.38,

102.22, 61.99, 55.87, 37.99, 29.32, 28.55, 27.64, 27.22. HRMS Calcd for $C_{18}H_{19}NNaO_3$ ([M+Na]$^+$): 320.1257; Found: 320.1251.

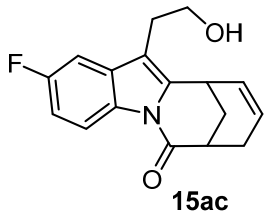

15ac

15ac was purified by column chromatography on silica gel (petroleum ether/EtOAc = 3/1) to give a yellow solid in 68% yield. ^{1}H NMR (300 MHz, $CDCl_3$) δ 8.38 (dd, *J* = 8.9, 4.8 Hz, 1H), 7.11 (dd, *J* = 8.9, 2.6 Hz, 1H), 7.00 (td, *J* = 9.1, 2.6 Hz, 1H), 5.92 (t, *J* = 7.8 Hz, 1H), 5.68 (dt, *J* = 9.7, 3.9 Hz, 1H), 3.87 (d, *J* = 5.2 Hz, 2H), 3.69 (s, 1H), 3.20 (s, 1H), 2.92 (t, *J* = 6.1 Hz, 2H), 2.65 (dd, *J* = 18.1, 6.7 Hz, 1H), 2.52–2.30 (m, 2H), 2.17 (dt, *J* = 12.7, 2.7 Hz, 1H), 1.46 (s, 1H). ^{13}C NMR (75 MHz, $CDCl_3$) δ 172.49, 160.13 (d, *J* = 240.0 Hz), 140.91, 131.84 (d, *J* = 9.9 Hz), 131.63 (d, *J* = 4.0 Hz), 128.50, 125.90, 117.60 (d, *J* = 8.8 Hz), 111.93 (d, *J* = 24.3 Hz), 111.41 (d, *J* = 3.4 Hz), 104.48 (d, *J* = 23.9 Hz), 61.96, 38.01, 29.36, 28.50, 27.57, 27.26. HRMS Calcd for $C_{17}H_{16}FNNaO_2$ ([M+Na]$^+$): 308.1057; Found: 308.1061.

5. Mechanistic study

5.1 Isotopic effect

The *t*BuCO$_2$D (*ca.* 90% D incorporation) and 2-deuterated tryptamine (*ca.* 92% D incorporation) for the synthesis of **13a-D** were prepared according to the reported literature, respectively (Liu et al., 2013; Pan et al., 2012).

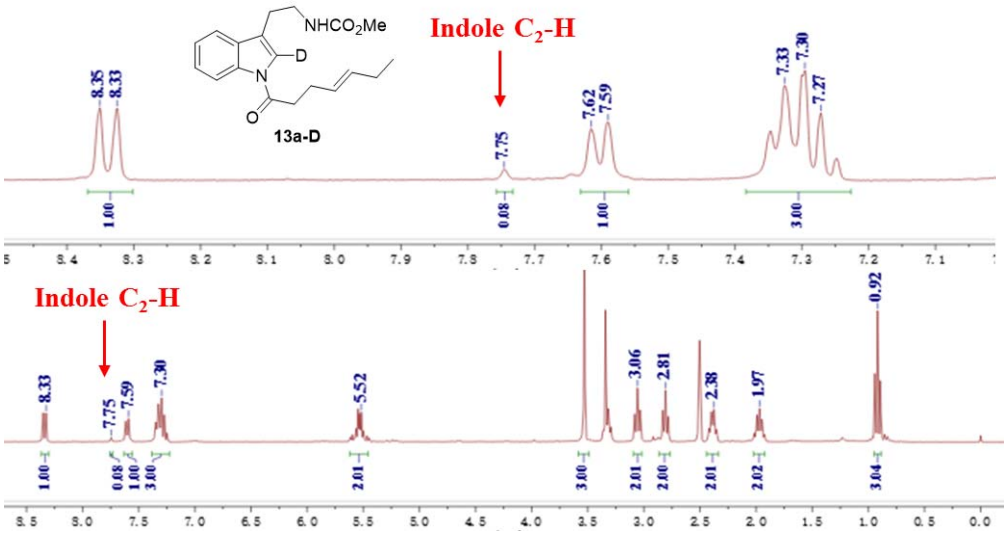

Figure S2. The ^{1}H NMR spectrum of **13a-D** (*ca.* 92% D incorporation), related to **Figure 4** and **eq 1**

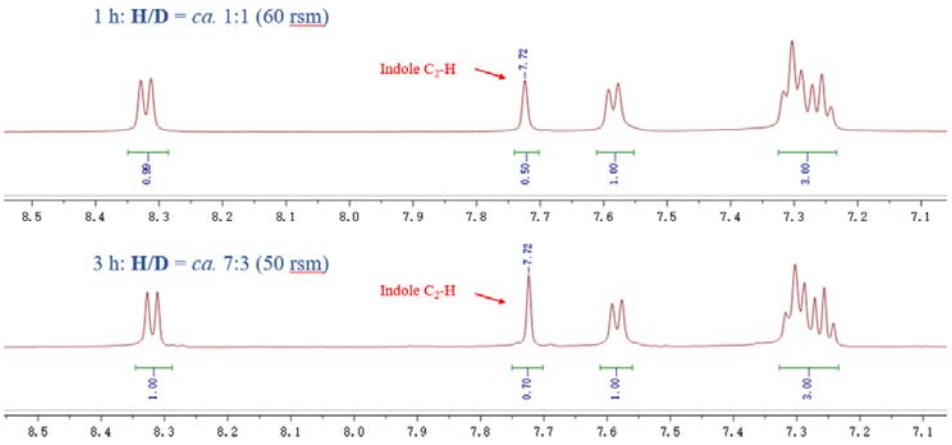

Figure S3. The quantitative ^{1}H NMR spectra of H/D ratio for the recovered **13a-D** under standard reaction conditions after 1h (upper) and 3h (lower), related to **Figure 4** and **eq. 1**.

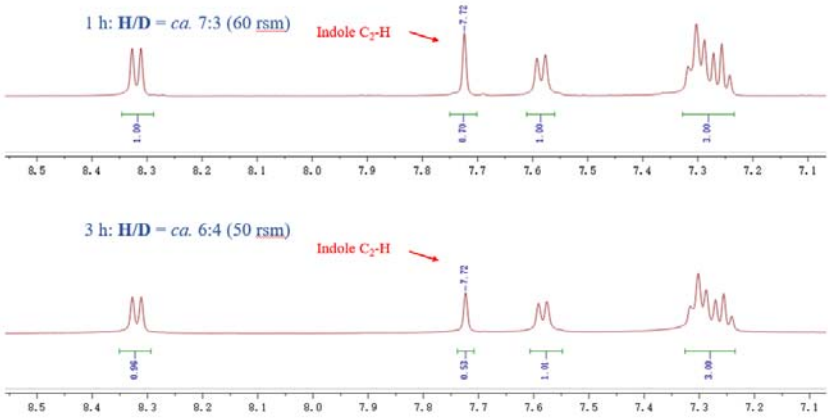

Figure S4. The quantitative ^{1}H NMR spectra of H/D ratio for the recovered **13a** by replacing *t*BuCO$_2$H with *t*BuCO$_2$D after 1h (upper) and 3h (lower), related to **Figure 4** and **eq. 2**.

Table S1. The time-dependent conversion of substrates as monitored by HPLC, related to **Figure 3**.

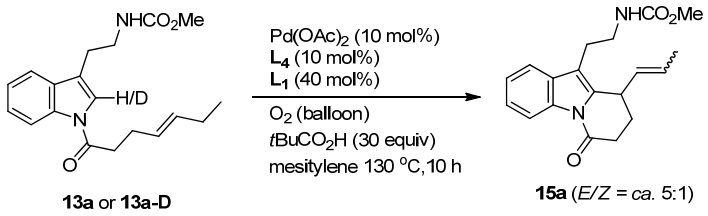

13a or **13a-D**

15a (*E*/*Z* = *ca.* 5:1)

(*t*BuCO$_2$H was replaced by *t*BuCO$_2$D in the case of **13a-D**)

Entry	Time (h)	Con. (%) **13a**	Con. (%) **13a**-D
1	1	22	7
2	2	31	14
3	3	47	16
4	4	54	16.8
5	5	61	17.3
6	6	70	21.7
7	7	75	22.4
8	8	76	25
9	9	78	26
10	10	79	31

5.2 HRMS analysis of the reaction mixture

LTQ-Orbitrap mass spectrometer (Thermo Fisher Scientific, USA) connected to the UHPLC instrument via ESI interface. Data acquisition and processing were carried out using Xcalibur 2.1 software (Thermo Fisher Scientific, USA). Unless otherwise noted, the operating conditions were set as follow: spray voltage 3.2 kV, heated capillary temperature 200 °C, sheath gas flow rate 35 arbitrary units, auxiliary gas flow rate 10 arbitrary units. Mobile phase is CH_3CN (100%), flow rate 0.2 mL/min.

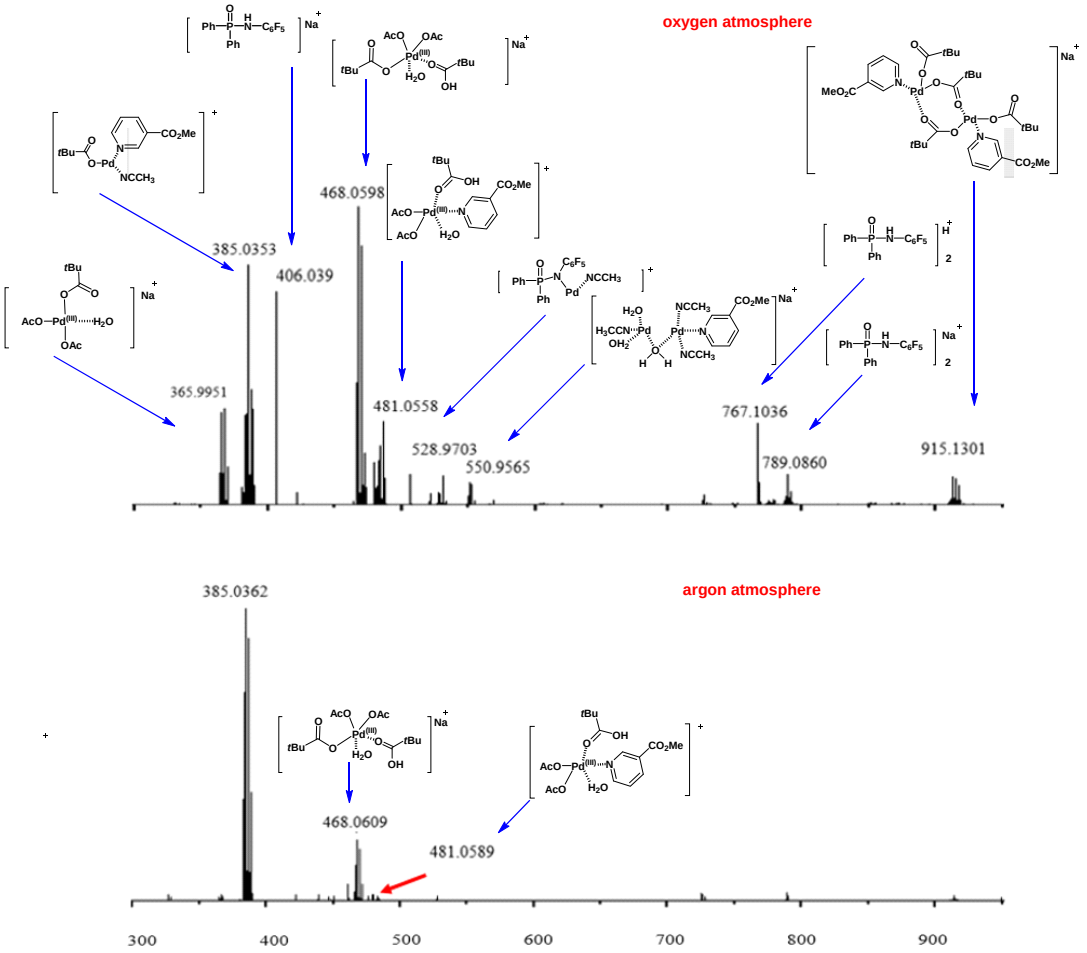

Figure S5. HRMS spectra for the reaction mixture under oxygen atmosphere (upper) and argon atmosphere (lower) after reacted at 130 °C for 1 h, related to **Figure 4**

(The detailed comparison on the theoretical and experimental isotopic distribution of the peaks was showed in following).

(The values are reported for ^{106}Pd for monomeric Pd complexes and ^{106}Pd and ^{108}Pd for bimetallic Pd complexes)

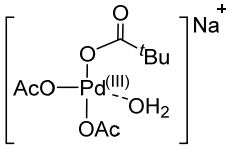

Chemical Formula: $C_9H_{17}NaO_7Pd^+$
Calcd: 365.99013
Found: 365.99512
Rel error(ppm): 13.6

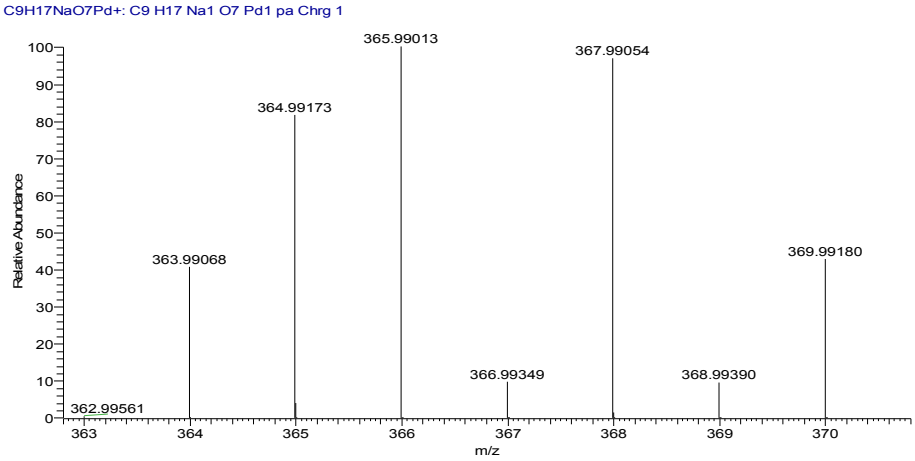

Figure S6. Theoretical isotopic distribution, related to **Figure 4**

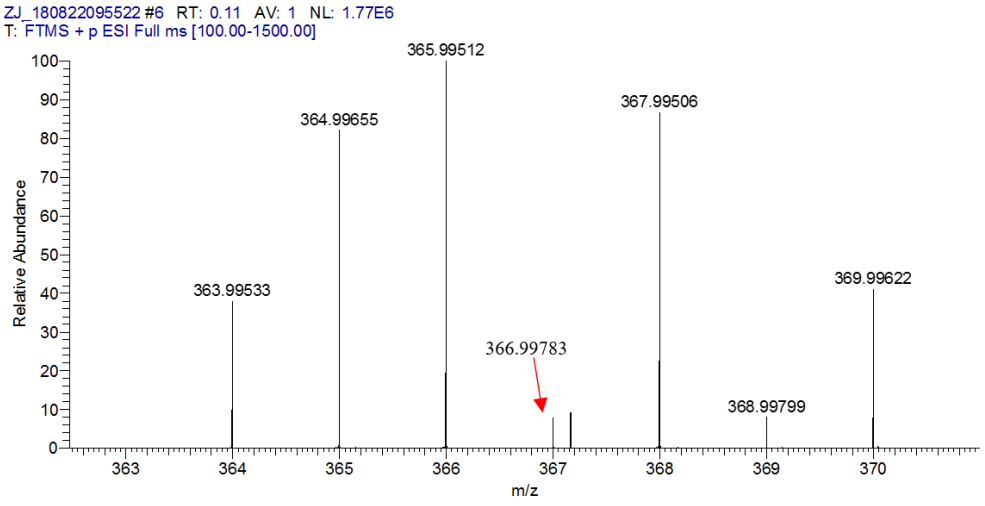

Figure S7. Experimental isotopic distribution, related to **Figure 4**

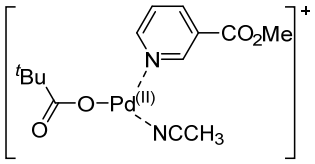

Chemical Formula: $C_{14}H_{19}N_2O_4Pd^+$
Calcd: 385.0374
Found: 385.0353
Rel error(ppm): -5.4

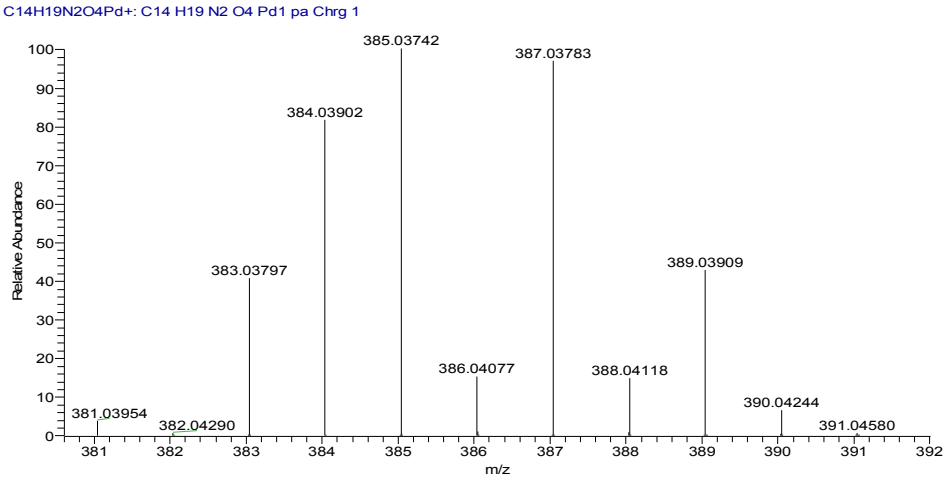

Figure S8. Theoretical isotopic distribution, related to **Figure 4**

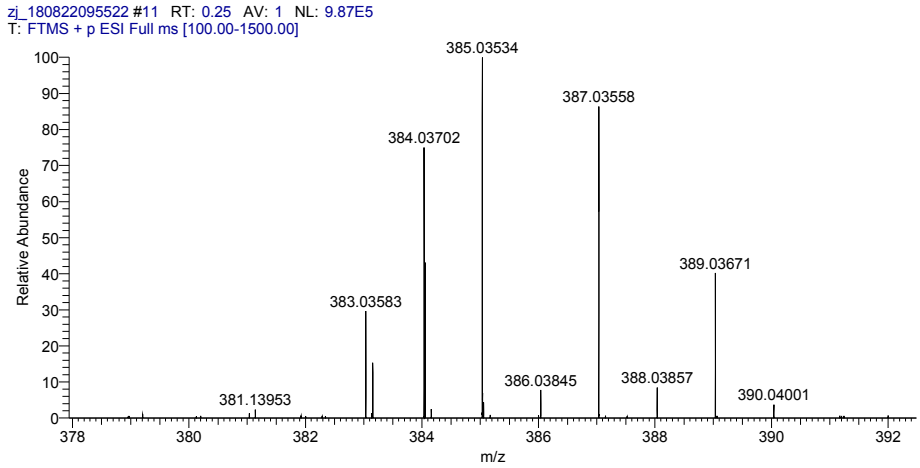

Figure S9. Experimental isotopic distribution, related to **Figure 4**

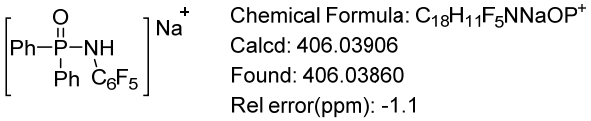

Chemical Formula: $C_{18}H_{11}F_5NNaOP^+$
Calcd: 406.03906
Found: 406.03860
Rel error(ppm): -1.1

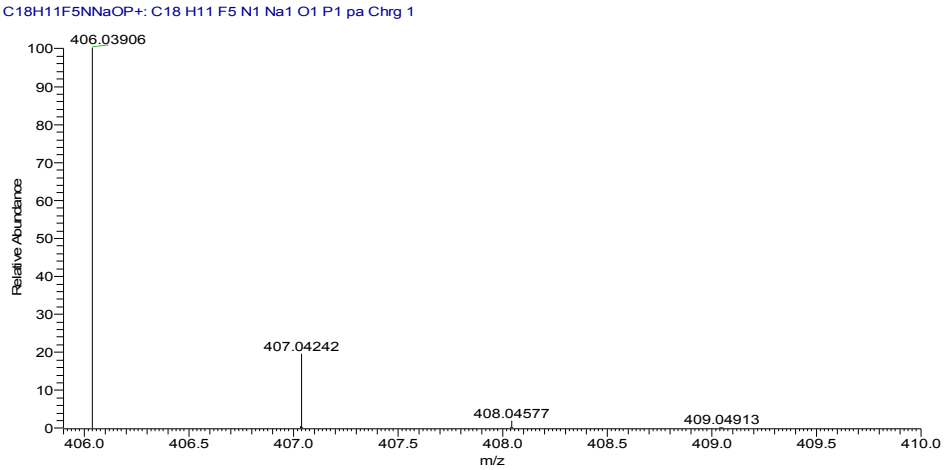

Figure S10. Theoretical isotopic distribution, related to **Figure 4**

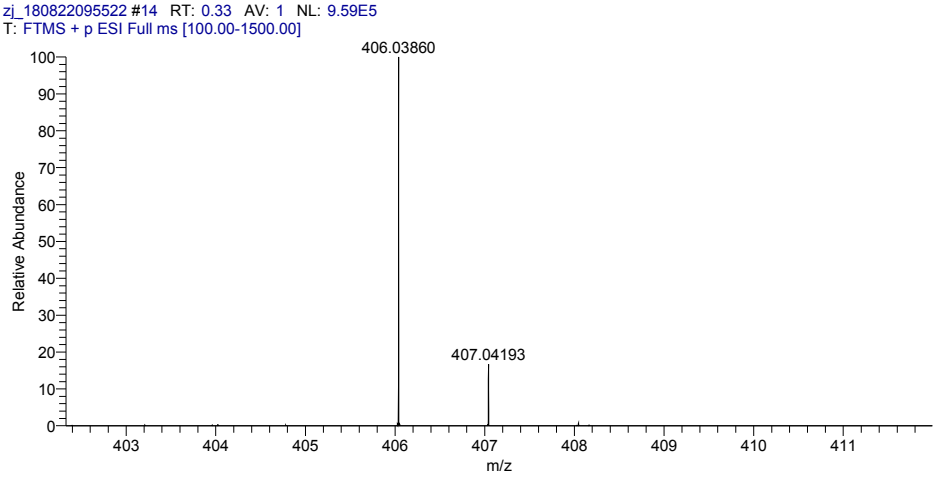

Figure S11. Experimental isotopic distribution, related to **Figure 4**

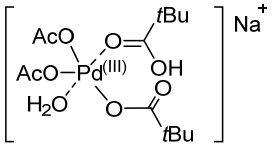

Chemical Formula: $C_{14}H_{27}NaO_9Pd^+$
Calcd: 468.05821
Found: 468.05981
Rel error(ppm): 3.4

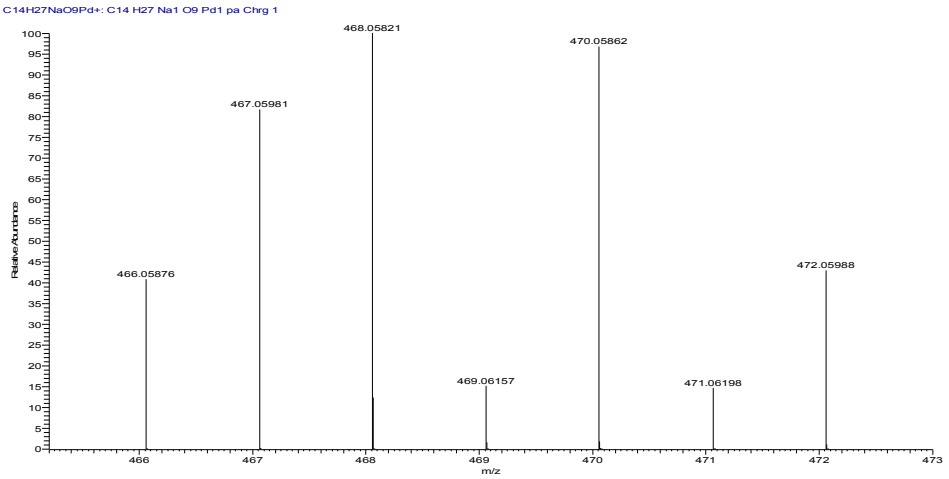

Figure S12. Theoretical isotopic distribution, related to **Figure 4**

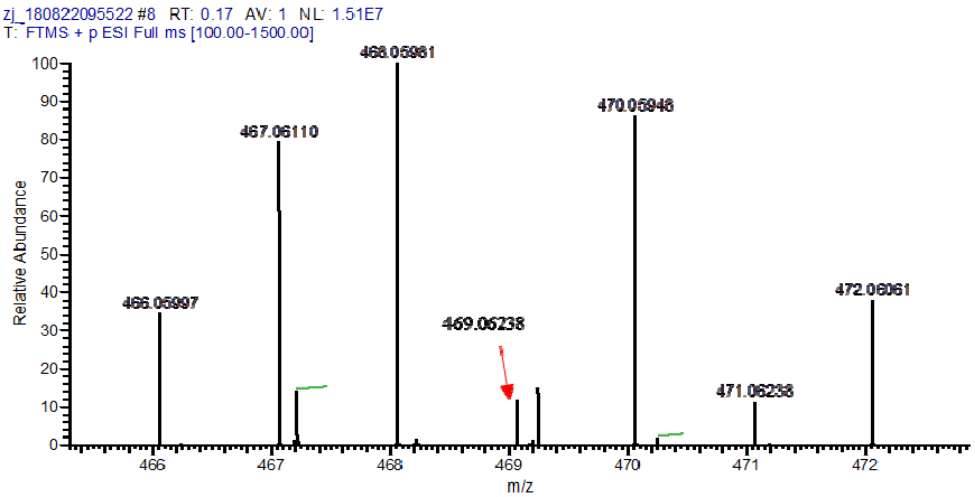

Figure S13. Experimental isotopic distribution, related to **Figure 4**

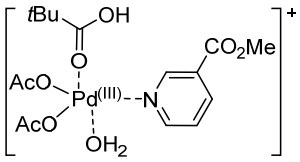

Chemical Formula: $C_{16}H_{25}NO_9Pd^+$
Calcd: 481.05587
Found: 481.05581
Rel error(ppm): -0.1

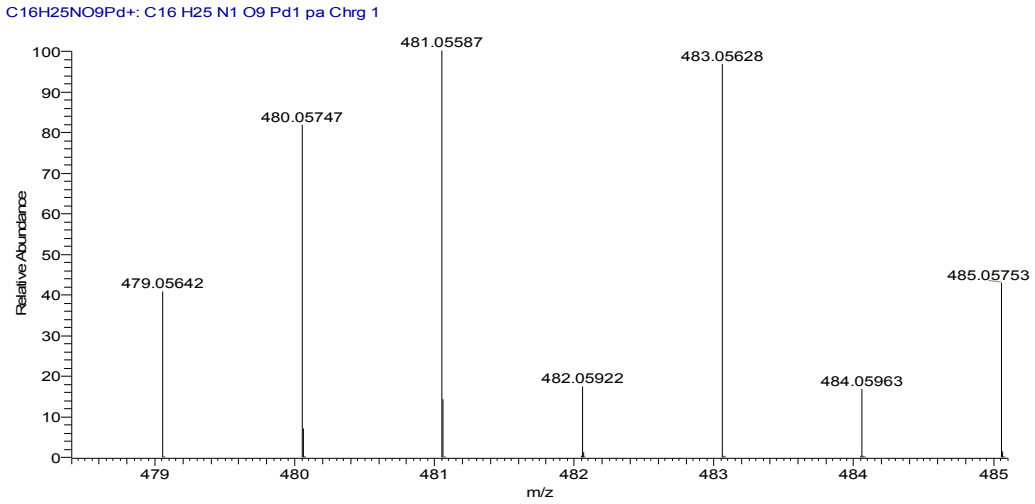

Figure S14. Theoretical isotopic distribution, related to **Figure 4**

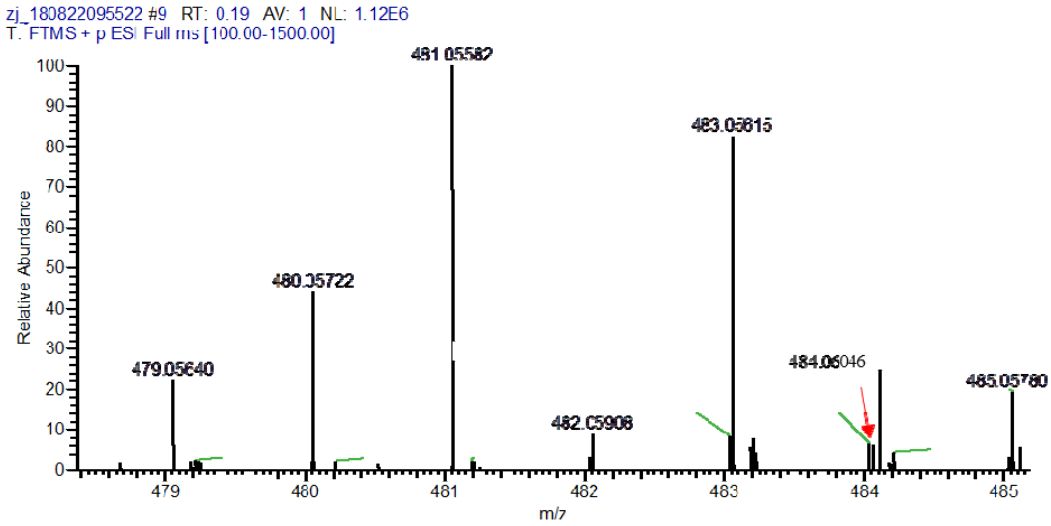

Figure S15. Experimental isotopic distribution, related to **Figure 4**

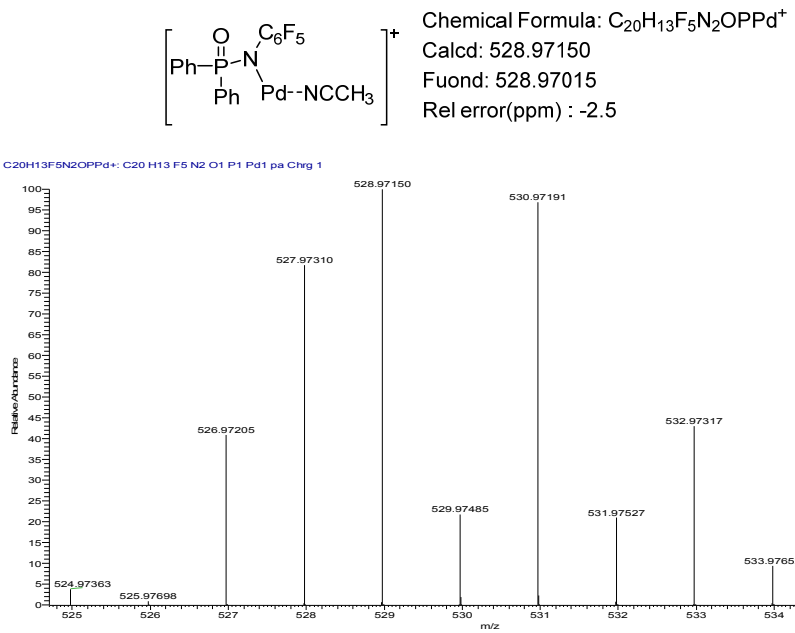

Figure S16. Theoretical isotopic distribution, related to **Figure 4**

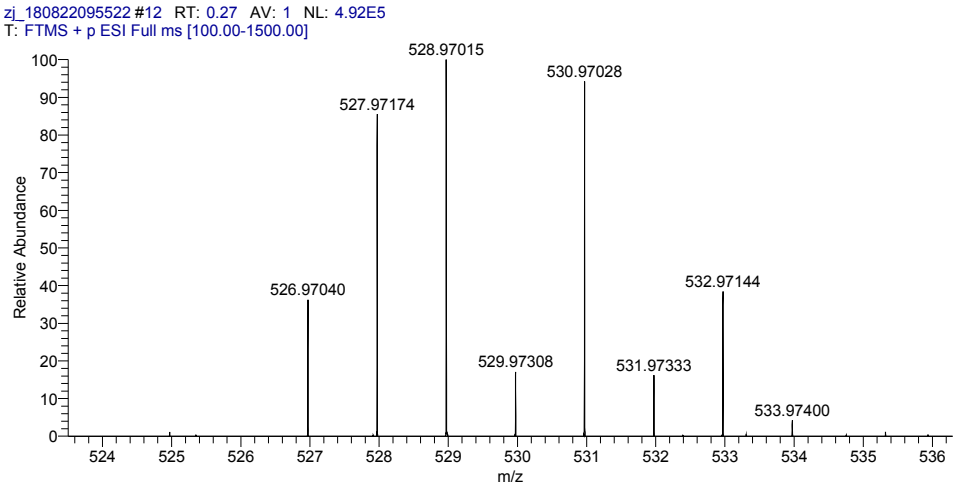

Figure S17. Experimental isotopic distribution, related to **Figure 4**

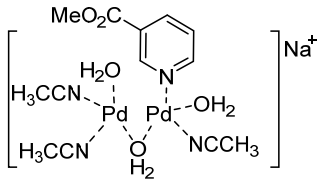

Chemical Formula: $C_{13}H_{22}N_4NaO_5Pd_2^+$
Calcd:550.95562
Found: 550.95648
Rel error(ppm) :1.5

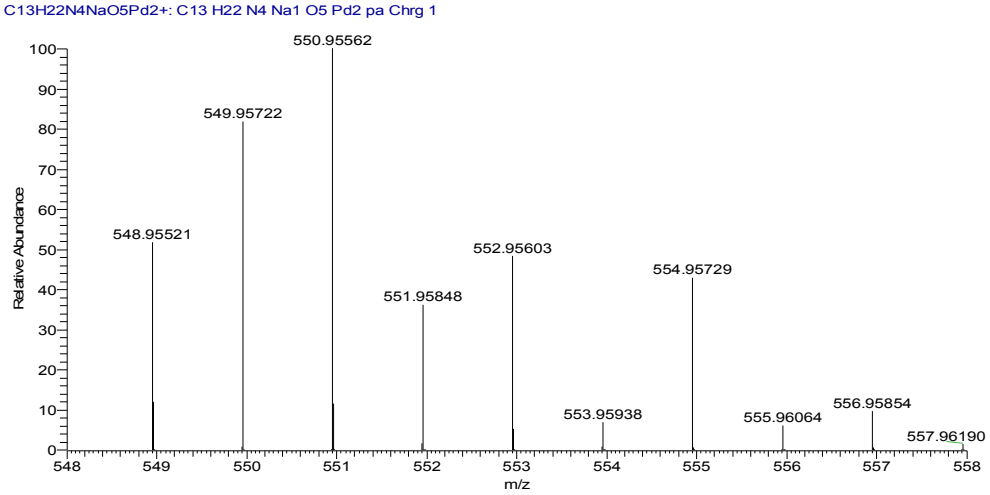

Figure S18. Theoretical isotopic distribution, related to **Figure 4**

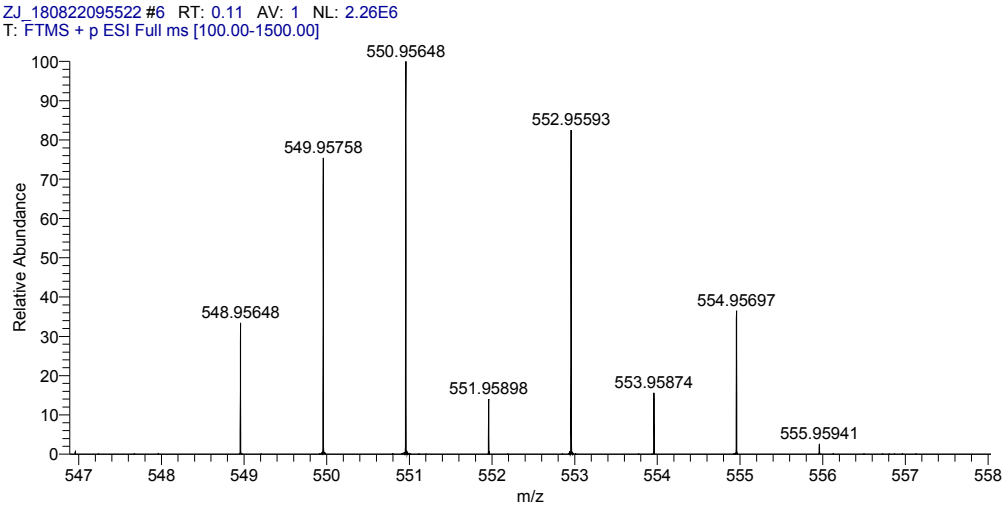

Figure S19. Experimental isotopic distribution, related to **Figure 4**

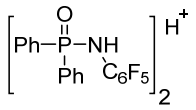

Chemical Formula: $C_{36}H_{23}F_{10}N_2O_2P_2^+$
Calcd: 767.10696
Found: 767.10364
Rel error(ppm): -4.32

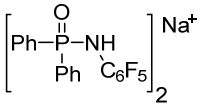

Chemical Formula: $C_{36}H_{22}F_{10}N_2NaO_2P_2^+$
Calcd: 789.08890
Found: 789.08521
Rel error(ppm): -4.67

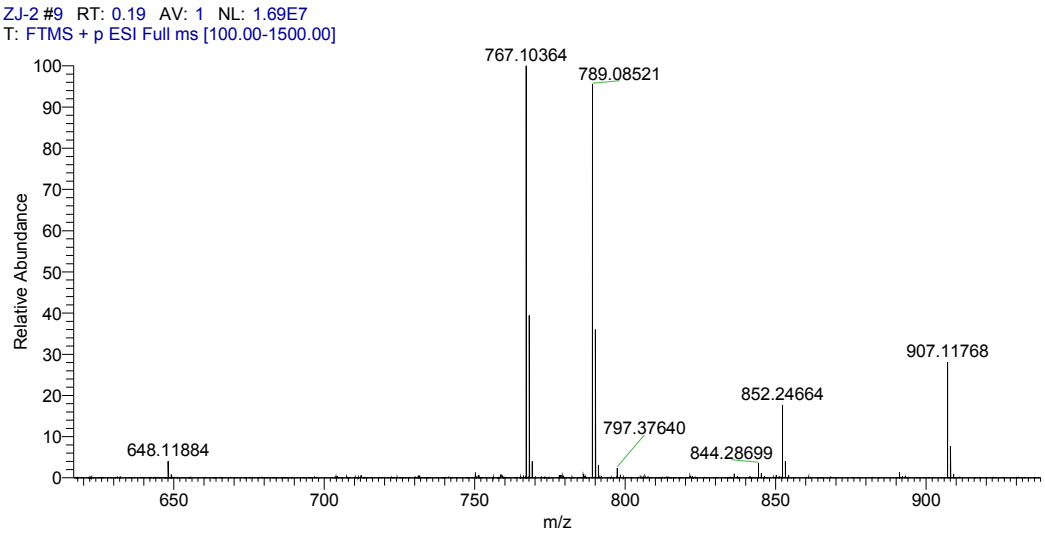

Figure S20. Experimental isotopic distribution, related to **Figure 4**

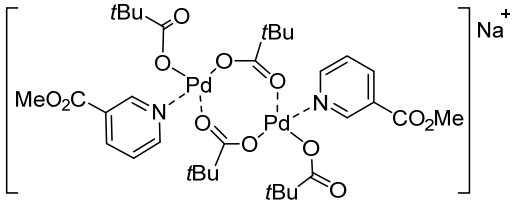

Chemical Formula: $C_{34}H_{50}N_2NaO_{12}Pd_2^+$
Calcd: 915.13297
Found: 915.13806
Rel error(ppm): 5.6

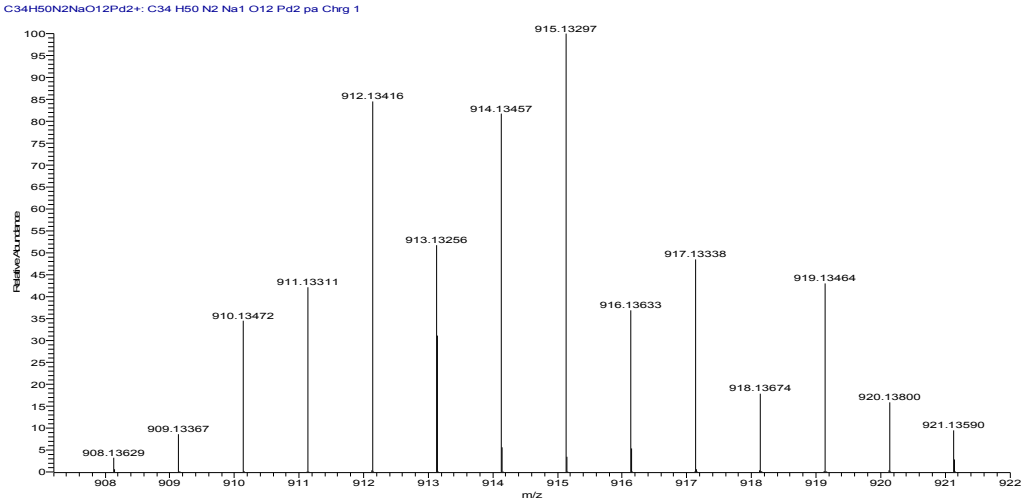

Figure S21. Theoretical isotopic distribution, related to **Figure 4**

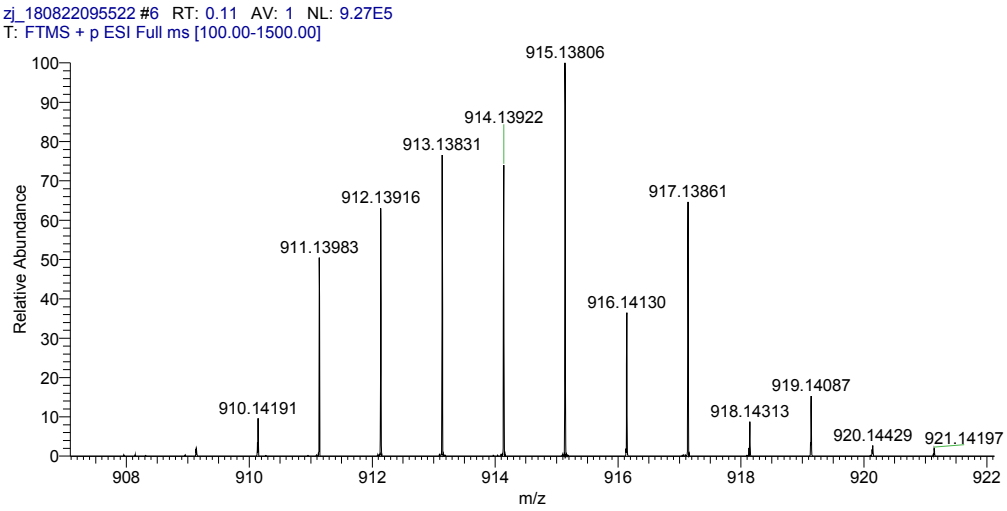

Figure S22. Experimental isotopic distribution, related to **Figure 4**

5.3 The color changes under oxygen and argon atmosphere

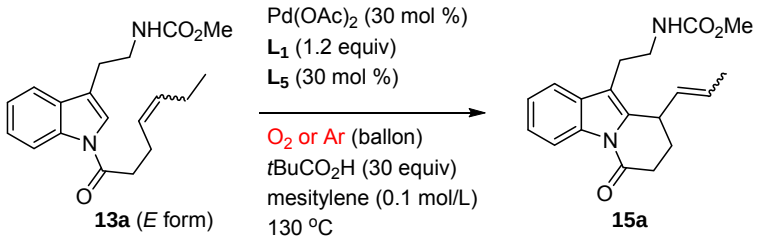

Figure S23. Oxidative Heck coupling of **13a**, related to **Figure 4**

As shown in **Figure S24**, under oxygen atmosphere, the color of the reaction mixture changed from pale yellow to deep red-brown and the solution maintained almost transparent. In contrast, palladium black precipitated out rapidly for the reaction mixture under argon atmosphere and a palladium mirror was observed after 2 h. A clearer observation on the color change could be observed from the filtrates as shown **Figure S25**. These results indicate the generation of $Pd^{(III)}$ species under oxygen atmosphere according to the reported literature (Powers et al., 2009).

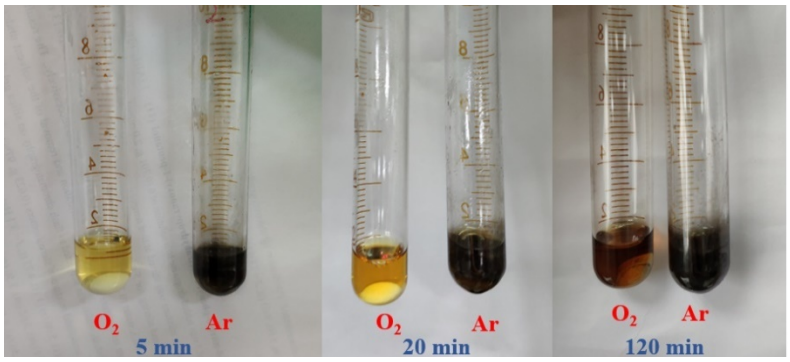

Figure S24. The color change of the reaction mixture under O_2 and Ar atmosphere, related to **Figure 4**

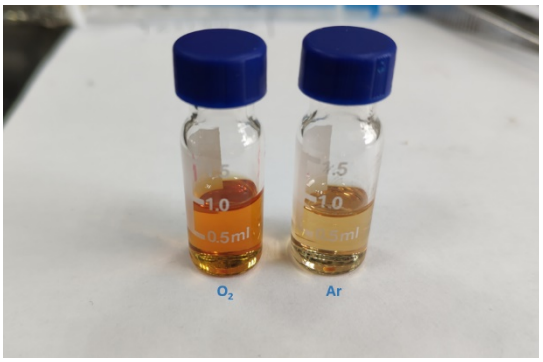

Figure S25. The color change of the filtrates under O_2 and Ar atmosphere, related to **Figure 4**

6. X-Ray data of 15q and 15ac

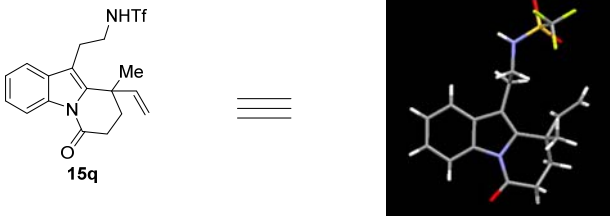

Table S2. Crystal data and structure refinement for **15q** (CCDC 1866425), related to **Table 3**

formula	C18 H19 F3 N2 O3 S
Formula weight	400.41
Temperature/K	273(2)
Crystal system	monoclinic
Space group	$P2_1/n$
Unit cell dimensions	a= 9.3981(6) Å alpha=90°
	b= 18.3270(12) Å beta= 105.0480(10) °
	c= 11.3035(7) Å gamma=90°
Volume/Å3	1880.1(2)
Z	4
Computing data collection	Bruker SMART
Crystal description	block
Crystal colour	colorless
Crystal size max	0.21
Crystal size mid	0.2
Crystal size mix	0.18
ρcalcg/cm3	1.415
μ/mm□1	0.222
F(000)	832.0
Radiation	MoKα (λ = 0.71073)
2Θ range for data collection/°	4.344 to 52.802
Index ranges	-11 ⩽ h ⩽ 11, -22 ⩽ k ⩽ 17, -14 ⩽ l ⩽ 13
Reflections collected	10631
Independent reflections	3840 [Rint = 0.0277, Rsigma = 0.0352]
Data/restraints/parameters	3840/0/245
Goodness-of-fit on F2	1.033
Final R indexes [I>=2σ (I)]	R1 = 0.0825, wR2 = 0.2235
Final R indexes [all data]	R1 = 0.0982, wR2 = 0.2386
Largest diff. peak/hole / e Å-3	1.55/-0.49

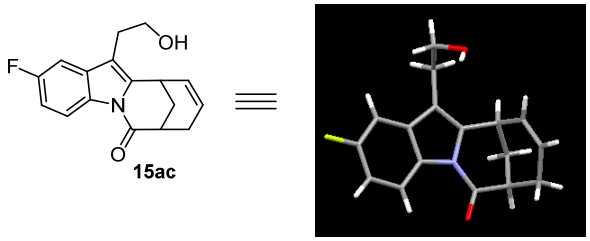

Table S3. Crystal data and structure refinement for **15ac** (CCDC 1866424), related to **Table 3**

Formula	C17 H16 F N O2
Formula weight	316.42
Temperature/K	273(2)
Crystal system	monoclinic
Space group	$P2_1/n$
Unit cell dimensions	a= 15.720(3) Å alpha=90°
	b= 8.9379(16) Å beta= 107.152(4)°
	c= 9.8722(19) Å gamma=90°
Volume/Å3	1880.1(2)
Z	4
Computing data collection	Bruker SMART
Crystal description	block
Crystal colour	colorless
Crystal size max	0.5
Crystal size mid	0.4
Crystal size mix	0.2
Radiation	MoKα (λ = 0.71073)
2Θ range for data collection/°	2.72 to 49.58
Index ranges	$-17 \leq h \leq 18$, $-10 \leq k \leq 9$, $-11 \leq l \leq 9$
Reflections collected	7099
Independent reflections	2266 [Rint = 0.0515, Rsigma = 0.0527]
Data/restraints/parameters	2266/0/191
Goodness-of-fit on F2	1.079
Final R indexes [I>=2σ (I)]	R1 = 0.0442, wR2 = 0.1167
Final R indexes [all data]	R1 = 0.0580, wR2 = 0.1333
Largest diff. peak/hole / e Å-3	0.21/-0.25

7. Copies of NMR spectra of substrates and products

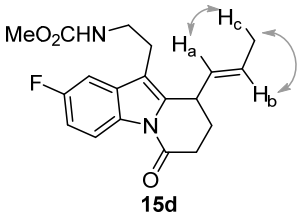

15d

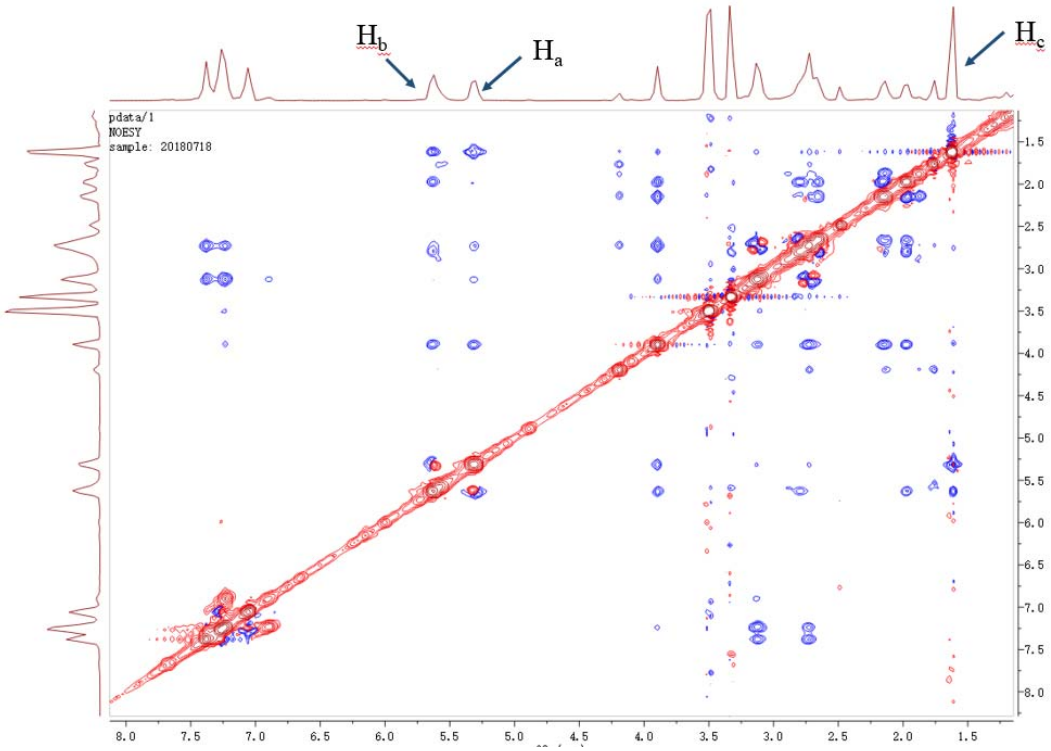

Figure S26. NOESY spectrum of **15d**, related to **Table 2**

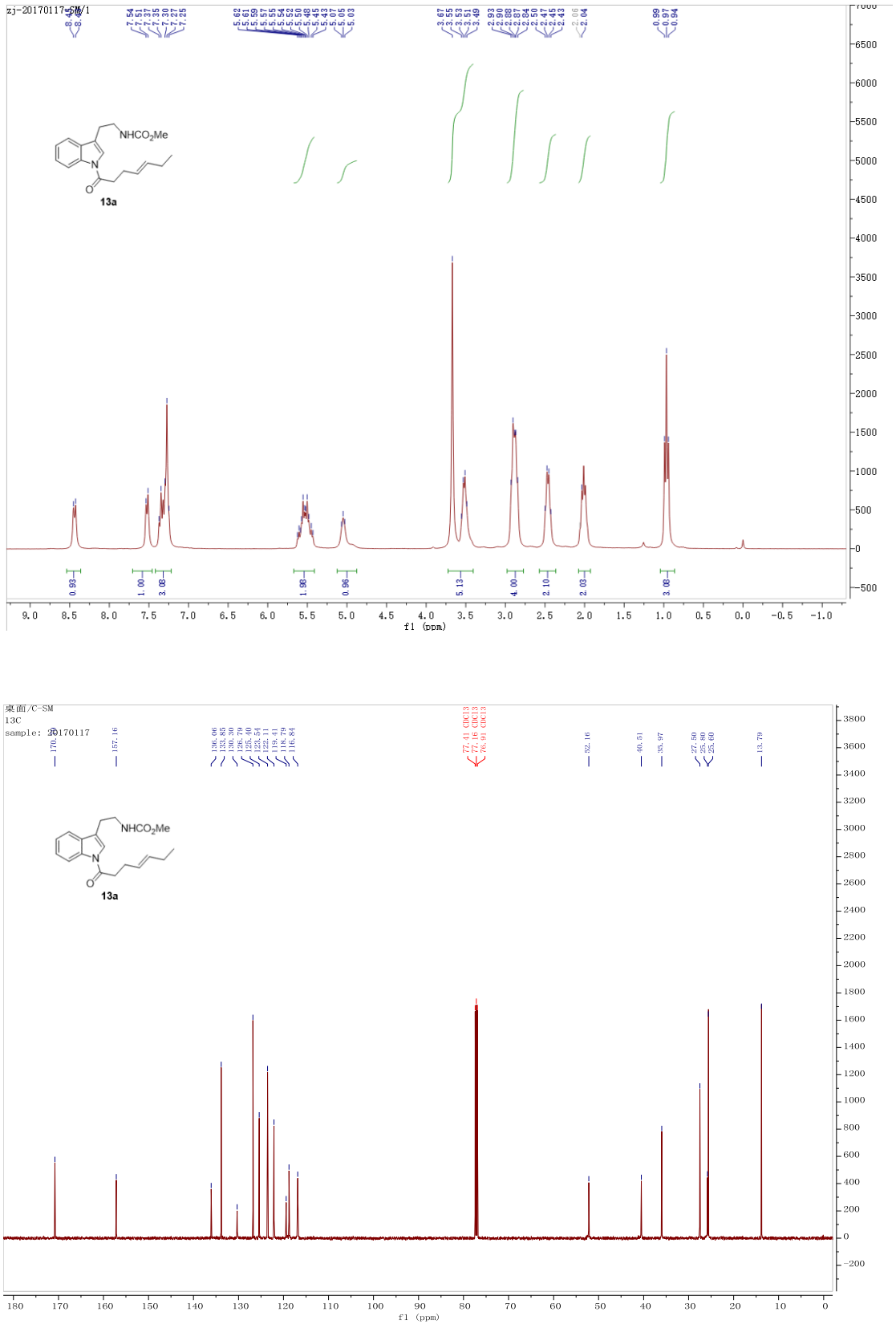

Figure S27. ^{1}H (upper) and ^{13}C-NMR (lower) of compound **13a**, related to **Table 1**

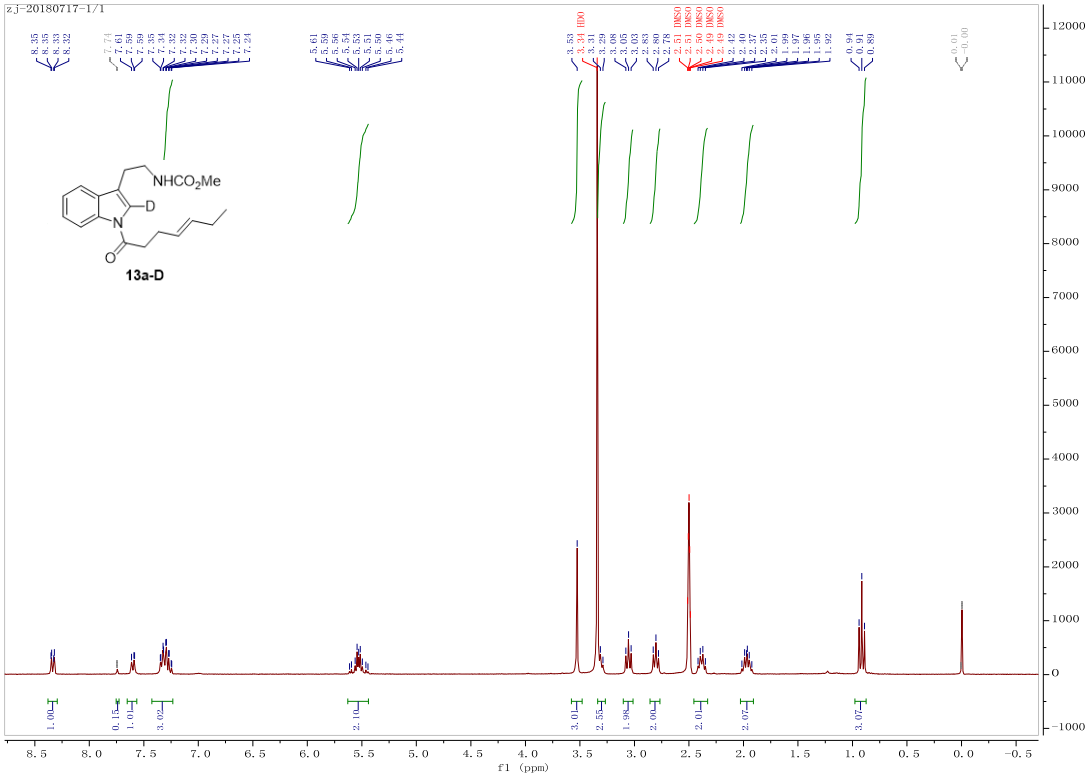

Figure S28. ^{1}H-NMR of compound **13a-D**, related to **Figure 4** and **eq. 1**

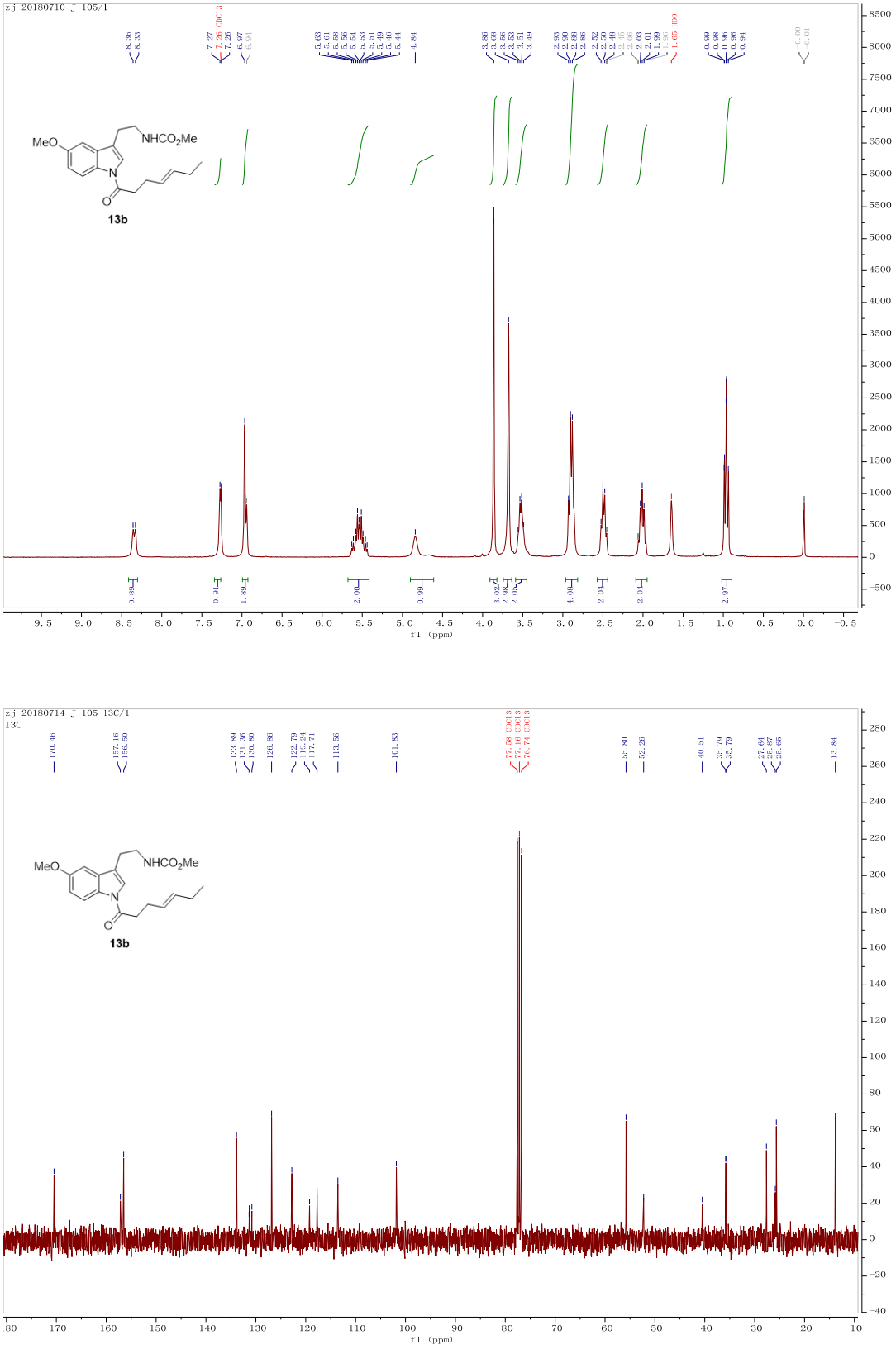

Figure S29. ^{1}H (upper) and ^{13}C-NMR (lower) of compound **13b**, related to **Table 2**

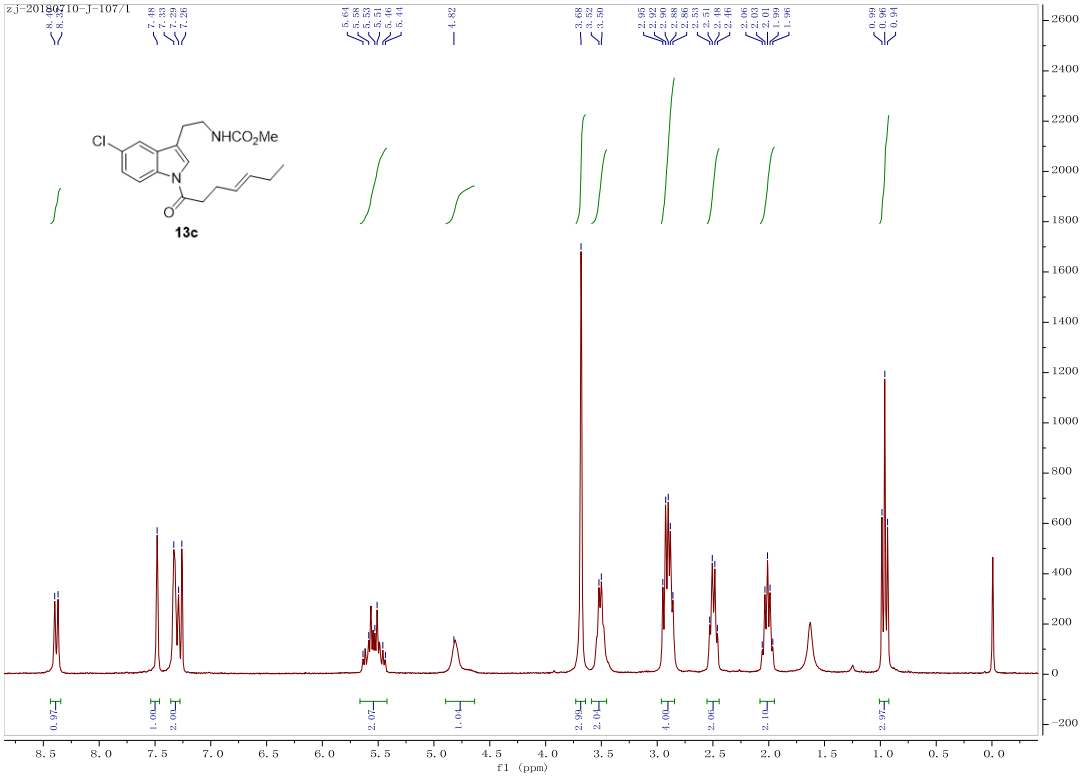

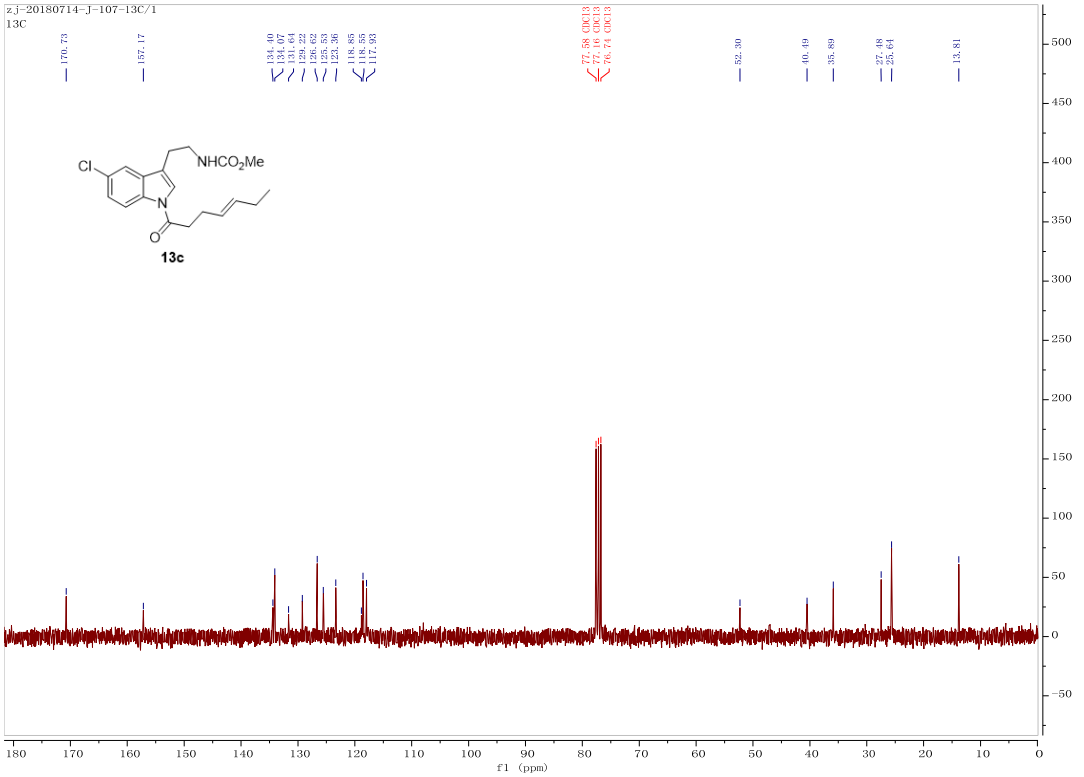

Figure S30. ^{1}H (upper) and ^{13}C-NMR (lower) of compound **13c**, related to **Table 2**

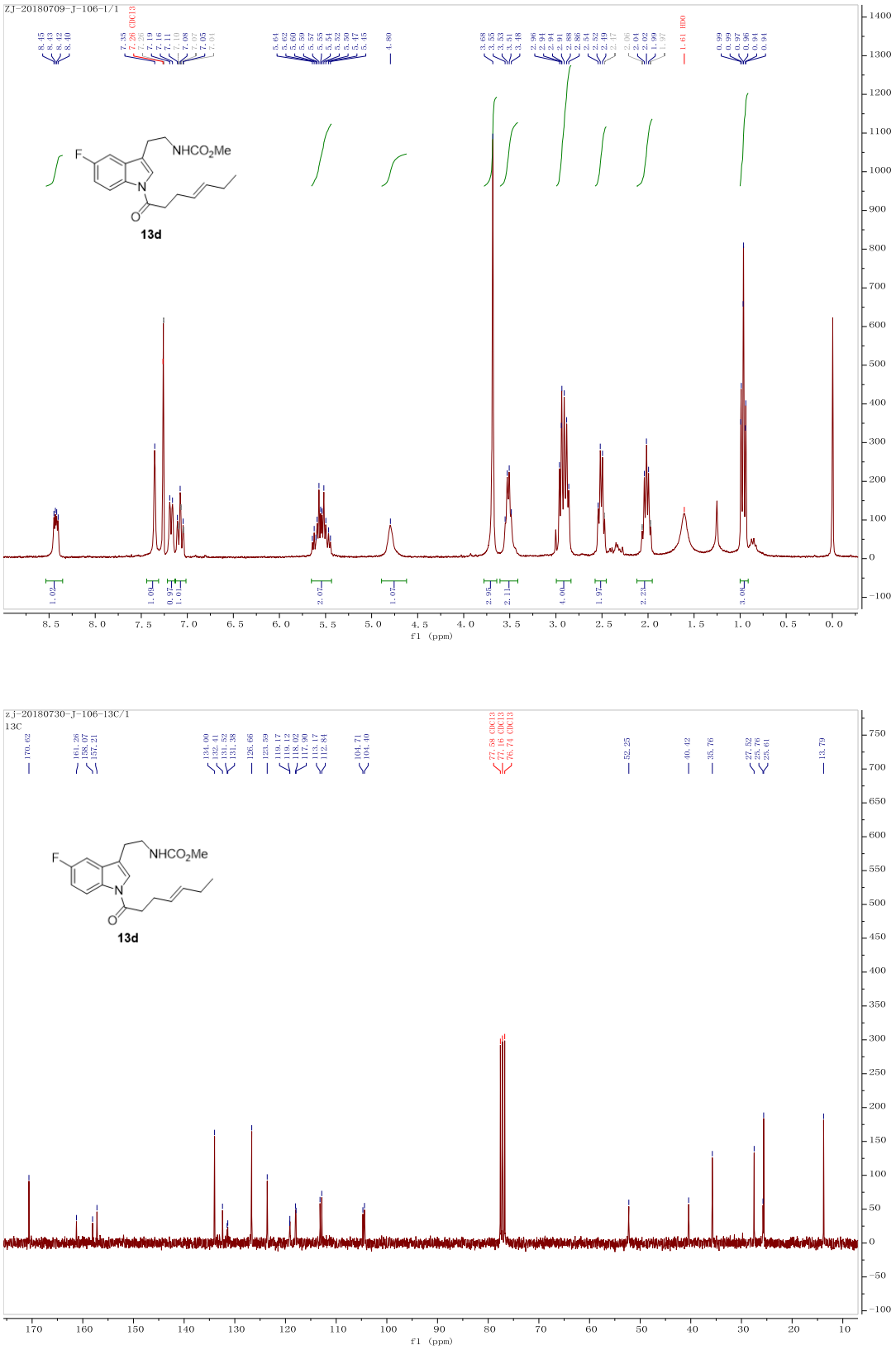

Figure S31. ^{1}H (upper) and ^{13}C-NMR (lower) of compound **13d**, related to **Table 2**

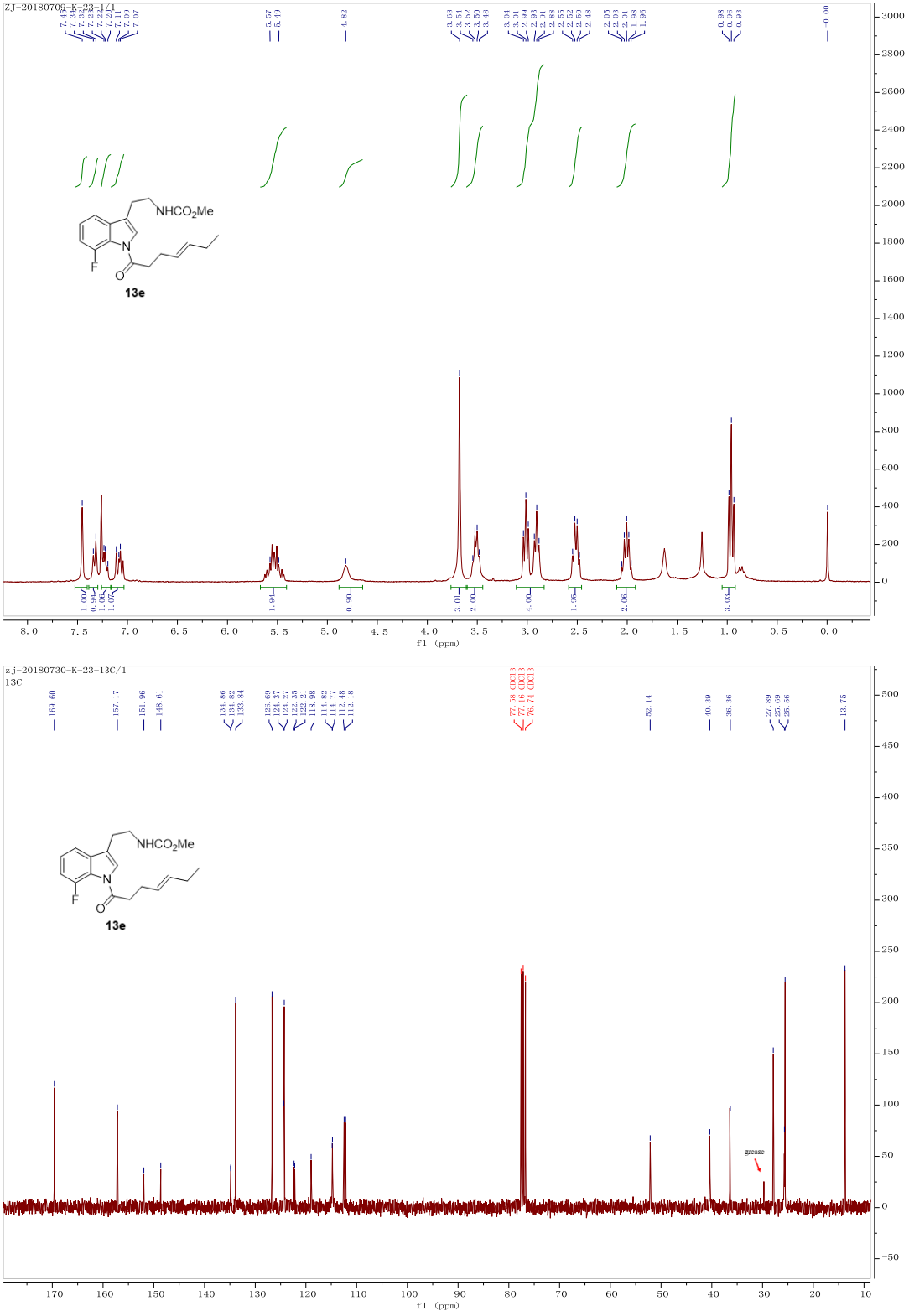

Figure S32. ^{1}H (upper) and ^{13}C-NMR (lower) of compound **13e**, related to **Table 2**

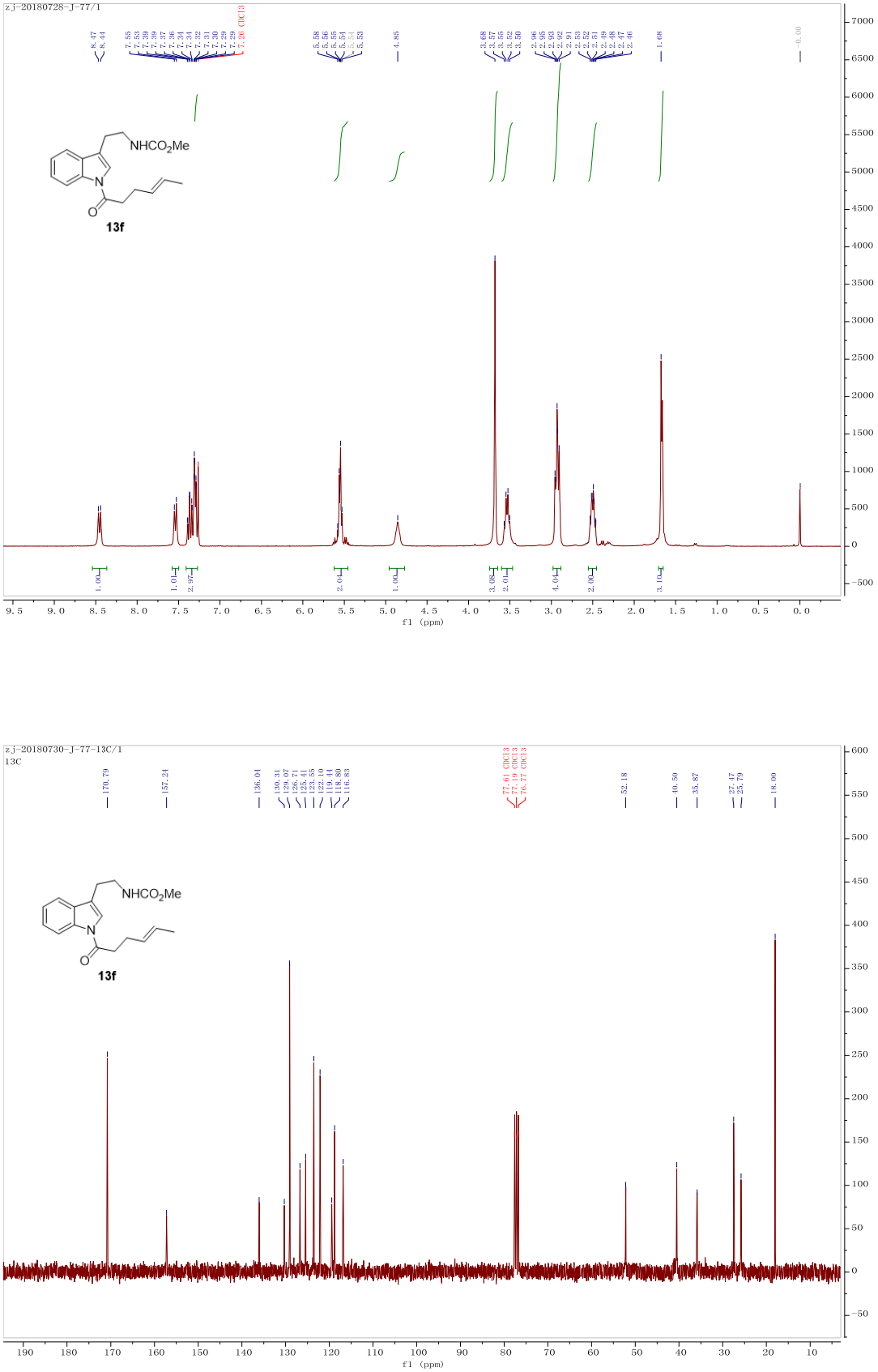

Figure S33. ^{1}H (upper) and ^{13}C-NMR (lower) of compound **13f**, related to **Table 2**

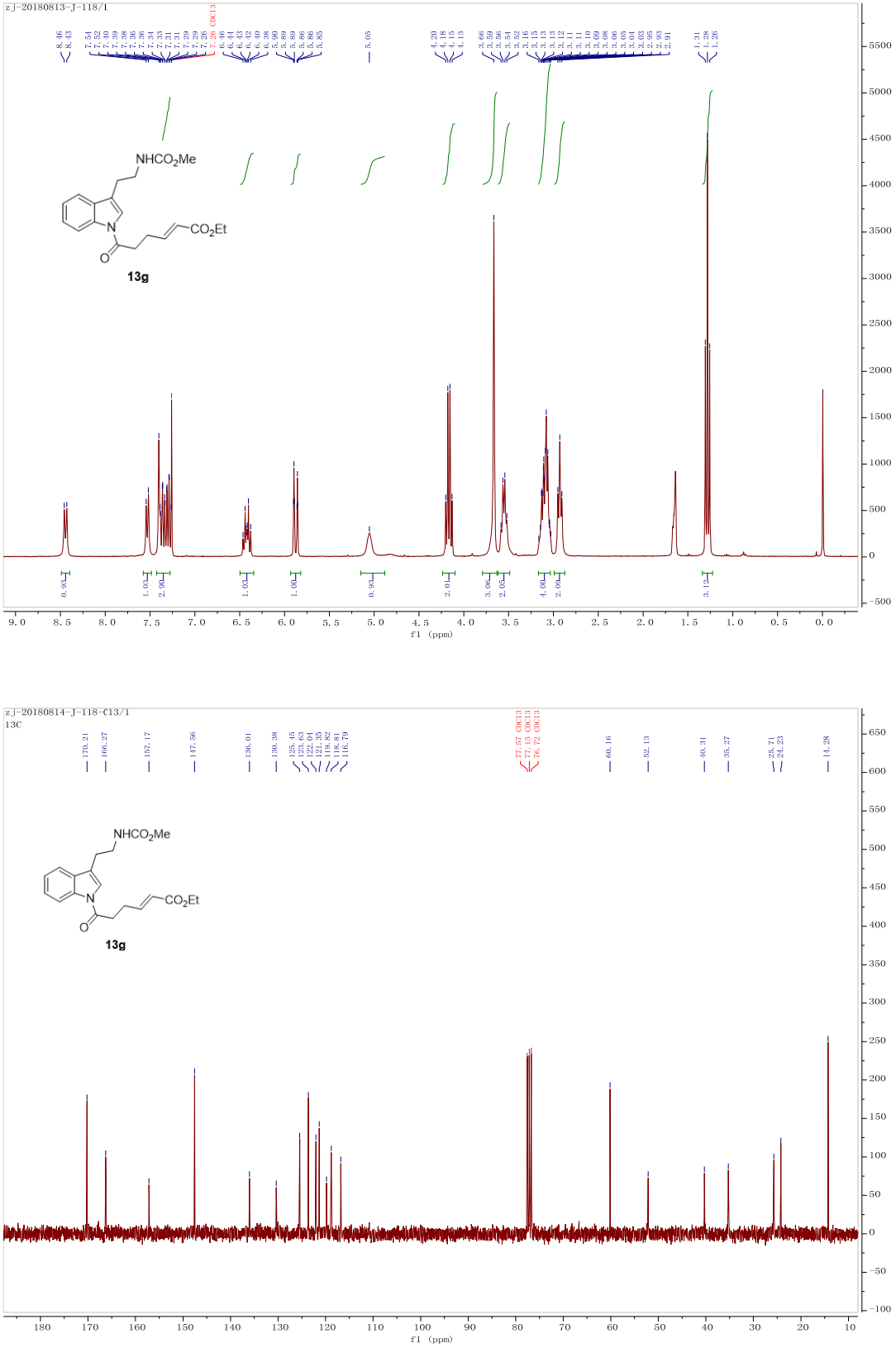

Figure S34. ^{1}H (upper) and ^{13}C-NMR (lower) of compound **13g**, related to **Table 2**

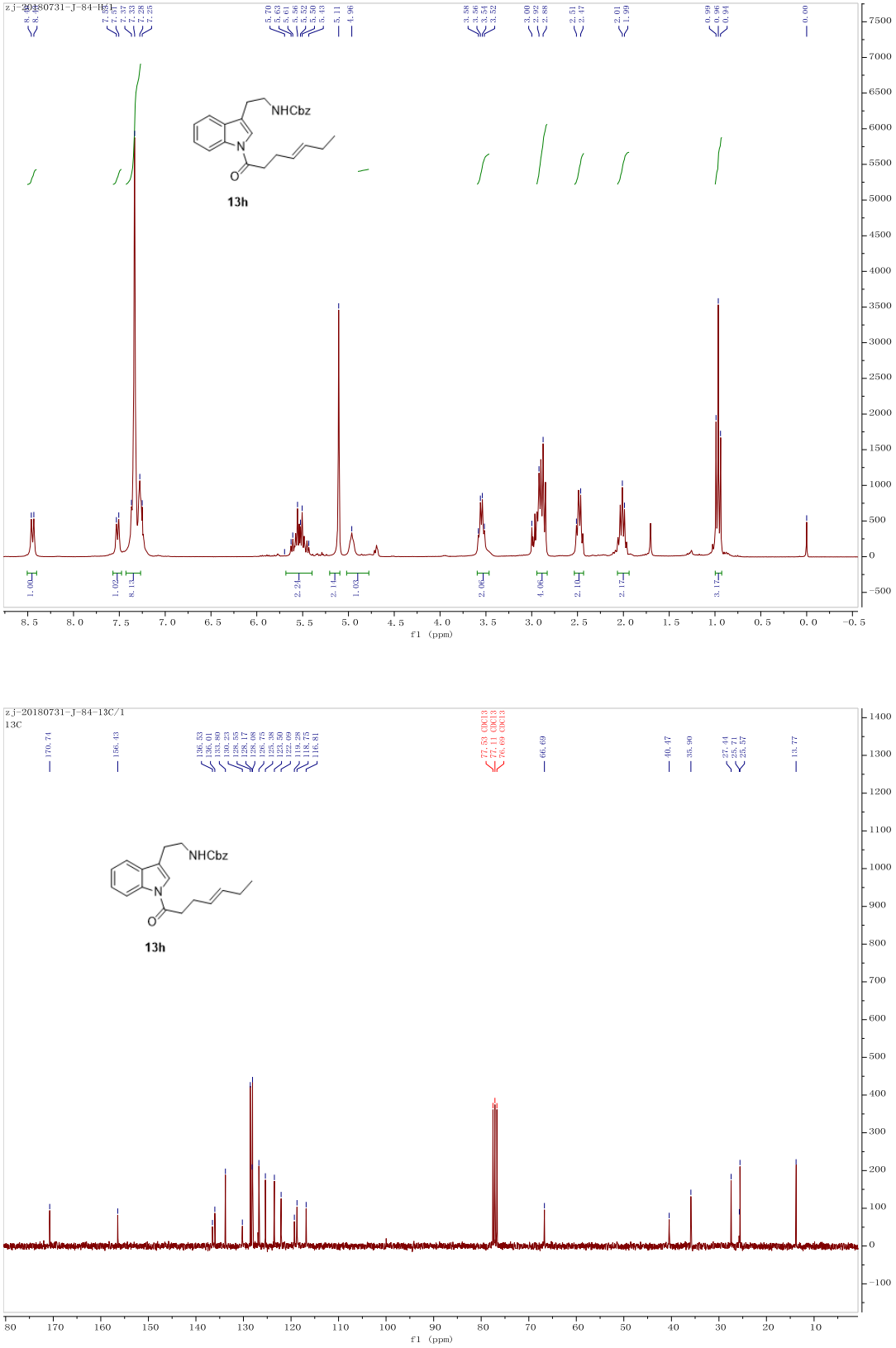

Figure S35. ^{1}H (upper) and ^{13}C-NMR (lower) of compound **13h**, related to **Table 2**

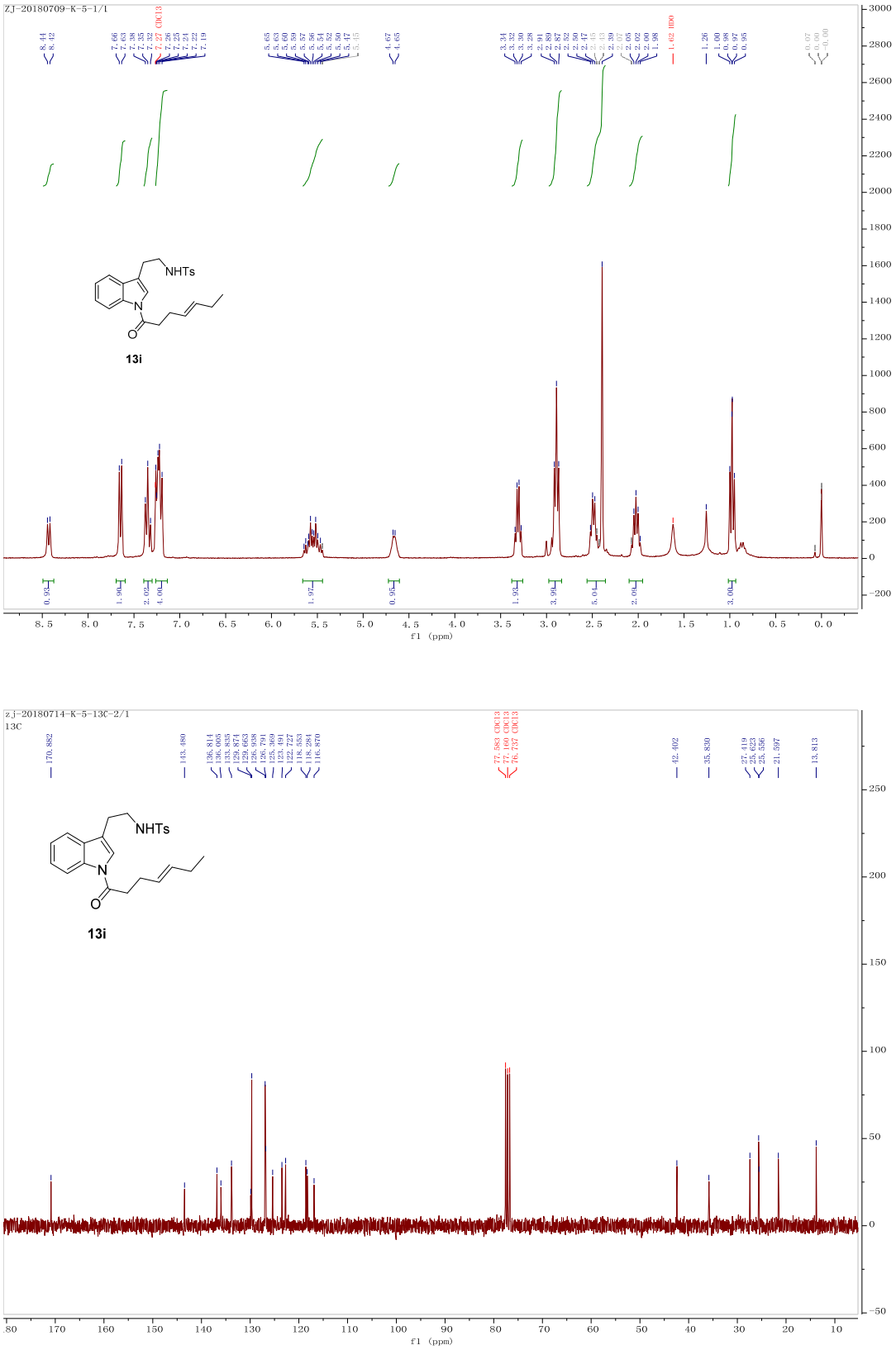

Figure S36. ^{1}H (upper) and ^{13}C-NMR (lower) of compound **13i**, related to **Table 2**

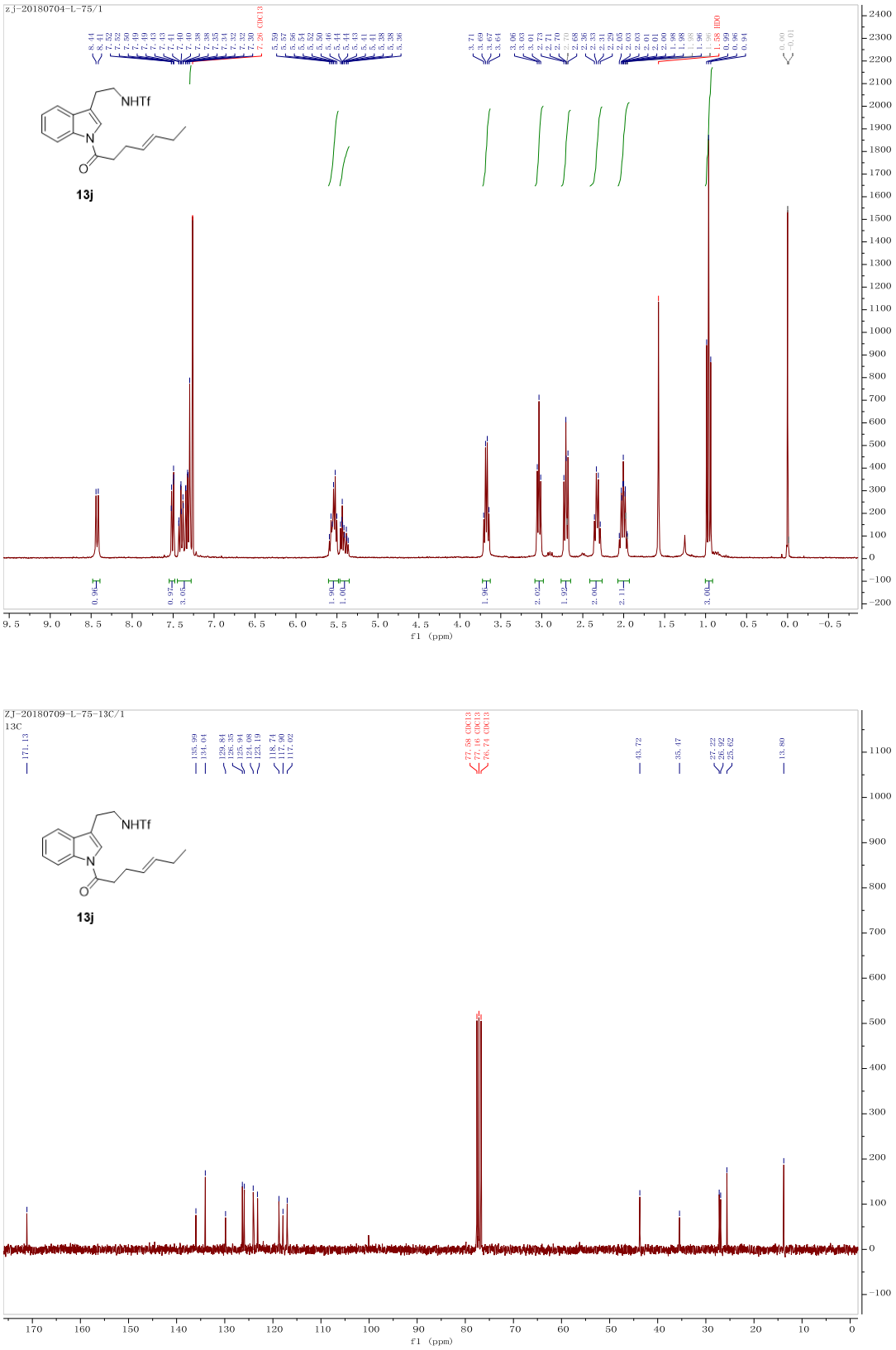

Figure S37. ^{1}H (upper) and ^{13}C-NMR (lower) of compound **13j**, related to **Table 2**

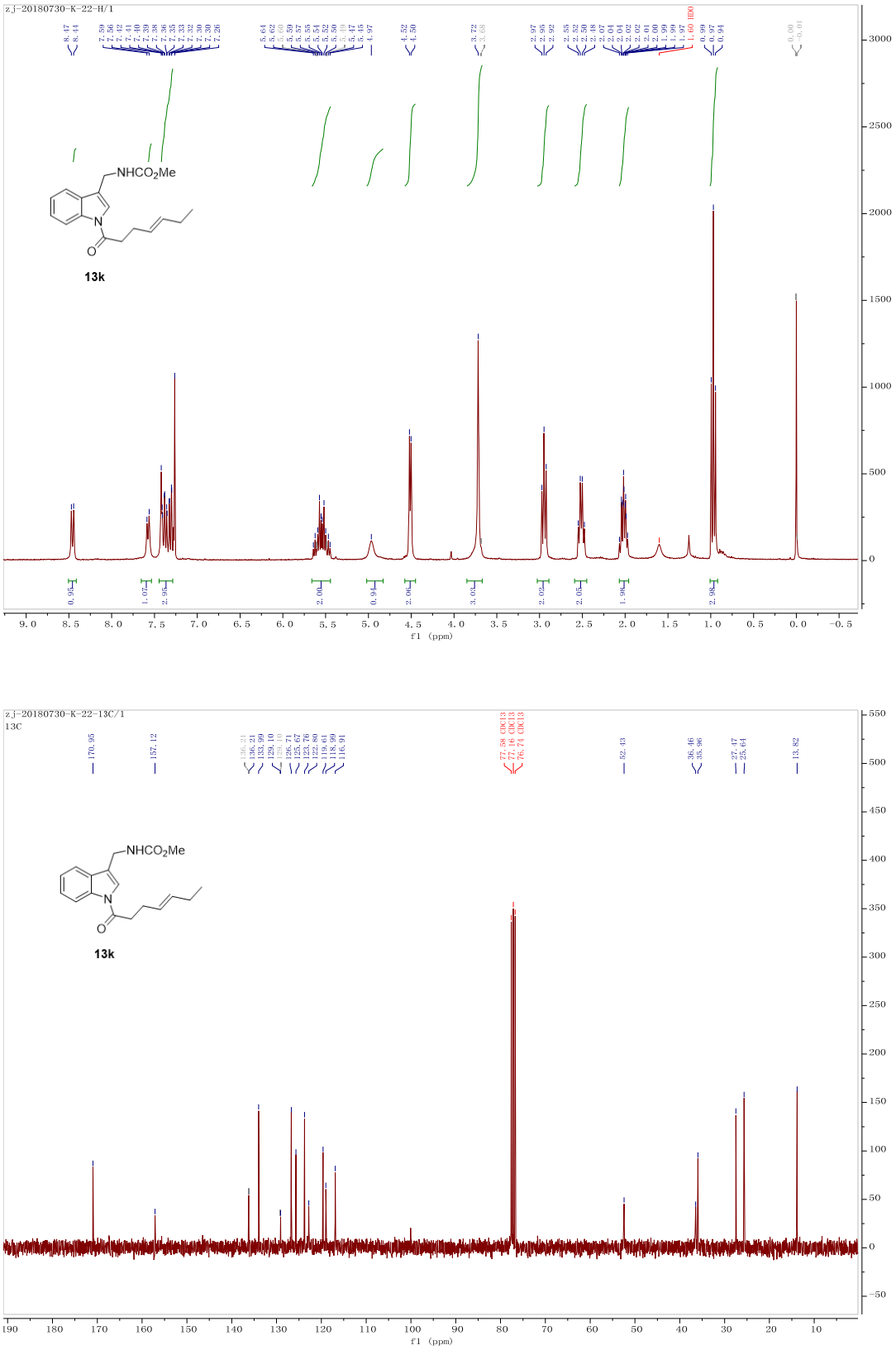

Figure S38. ^{1}H (upper) and ^{13}C-NMR (lower) of compound **13k**, related to **Table 2**

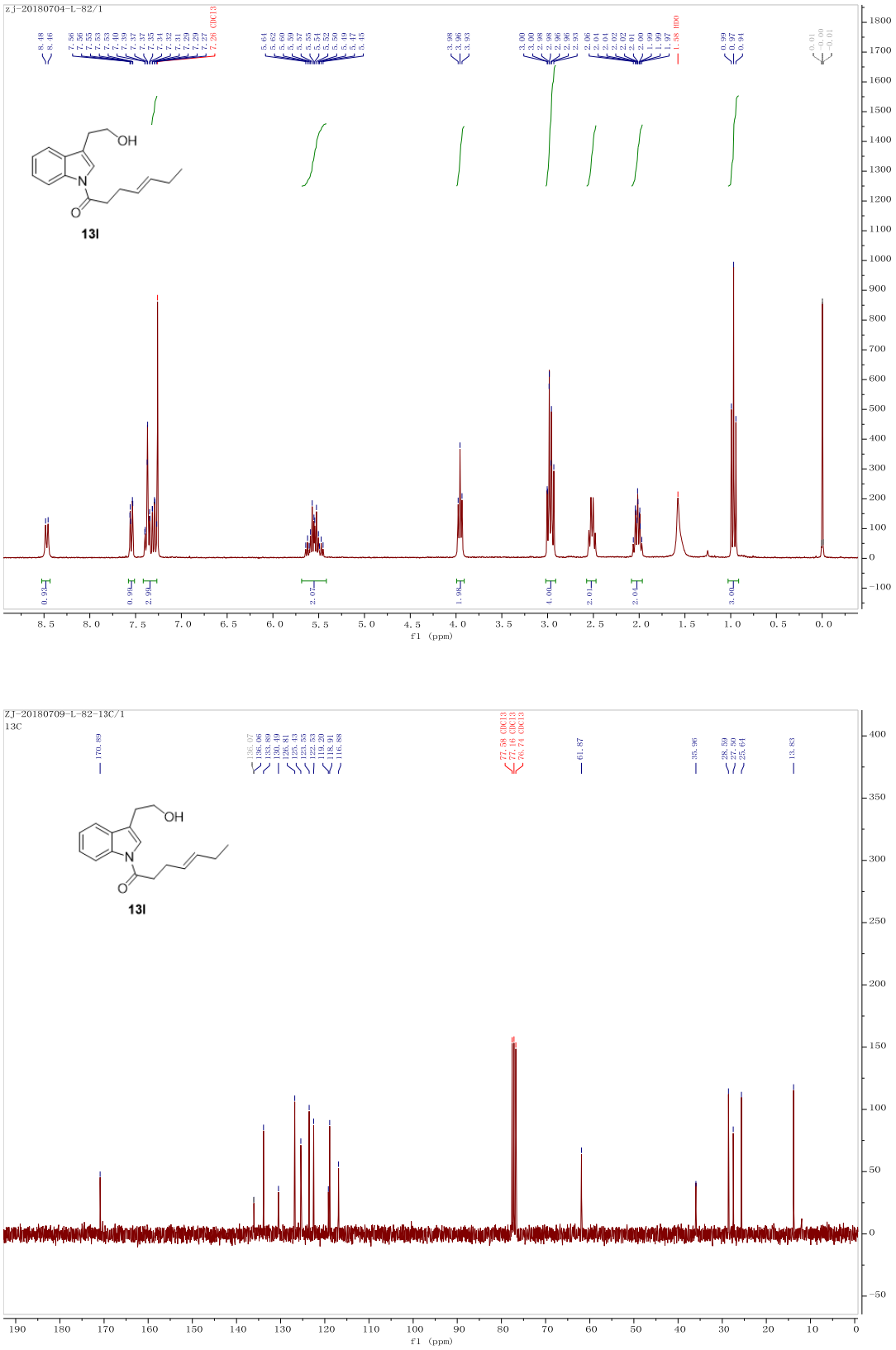

Figure S39. ^{1}H (upper) and ^{13}C-NMR (lower) of compound **13l**, related to **Table 2**

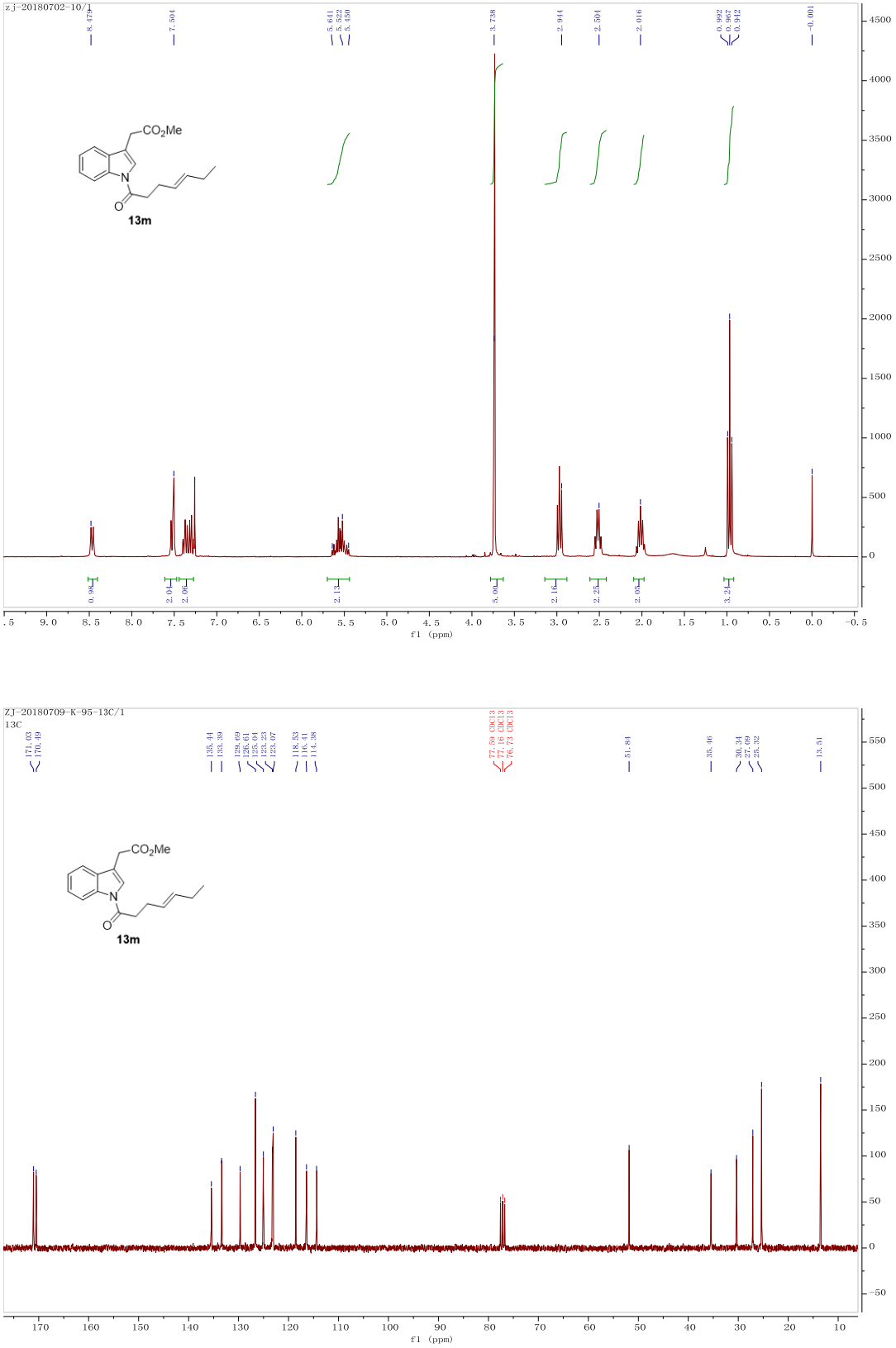

Figure S40. ^{1}H (upper) and ^{13}C-NMR (lower) of compound **13m**, related to **Table 2**

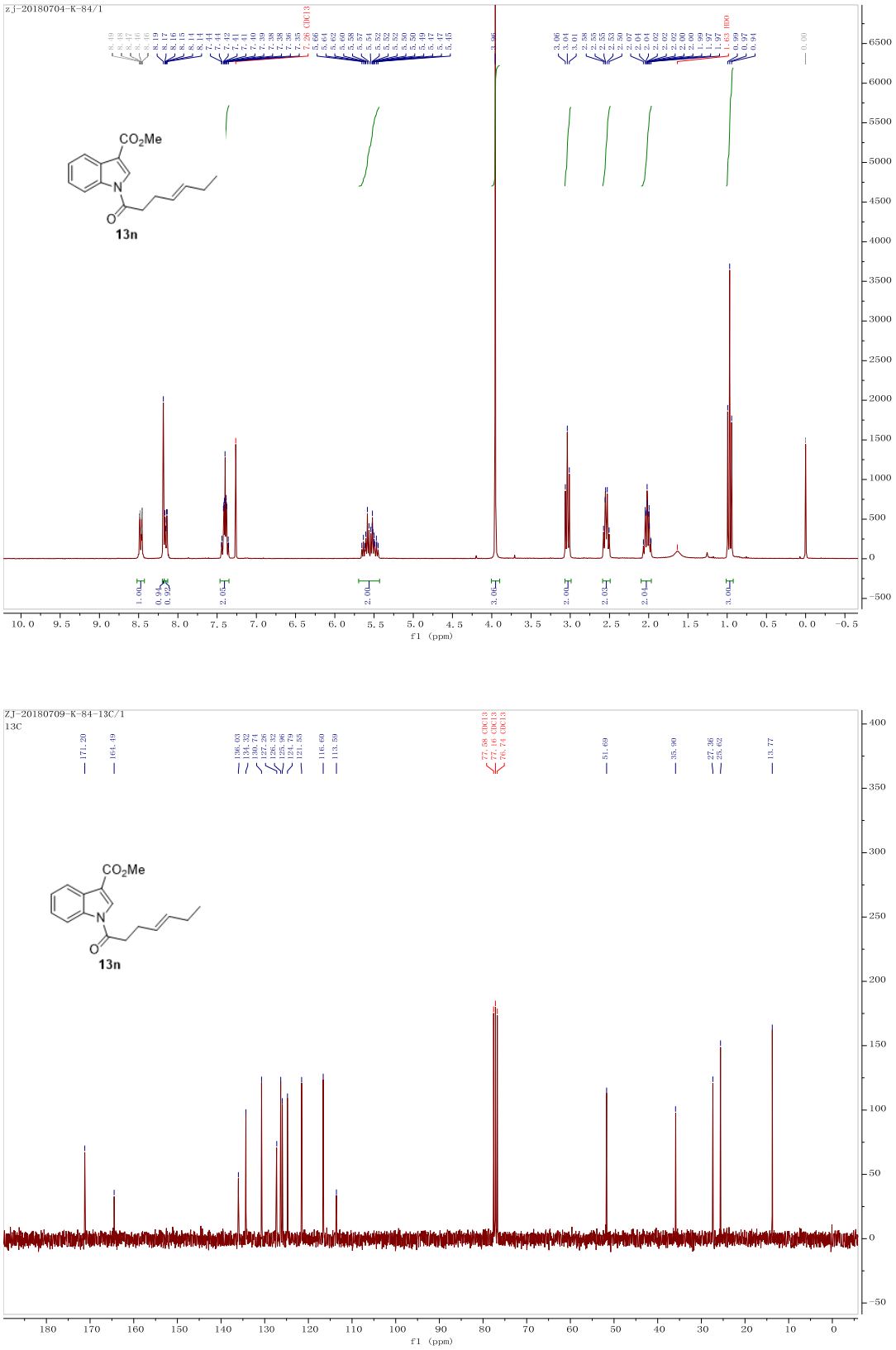

Figure S41. ^{1}H (upper) and ^{13}C-NMR (lower) of compound **13n**, related to **Table 2**

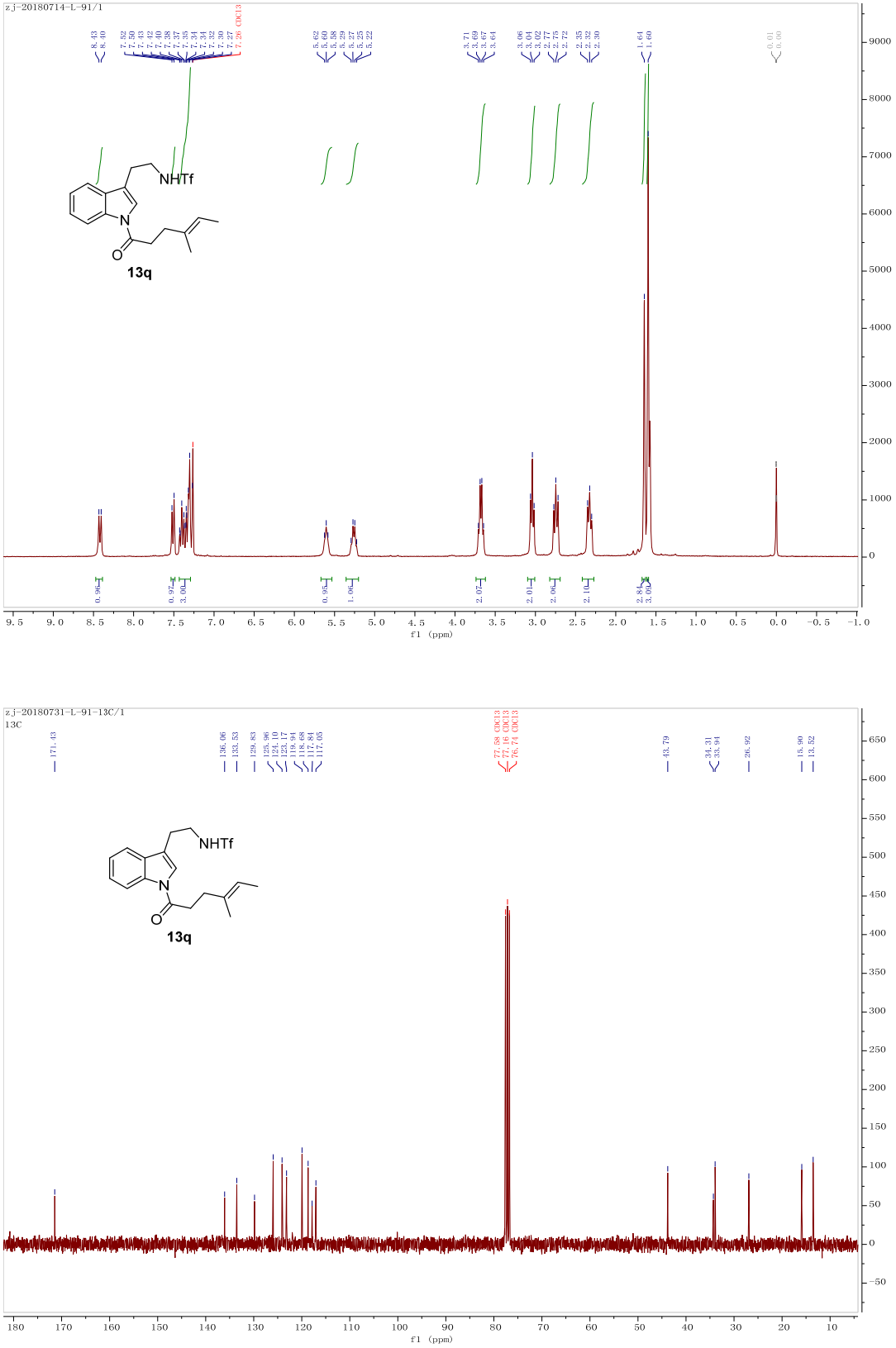

Figure S42. ^{1}H (upper) and ^{13}C-NMR (lower) of compound **13q**, related to **Table 3**

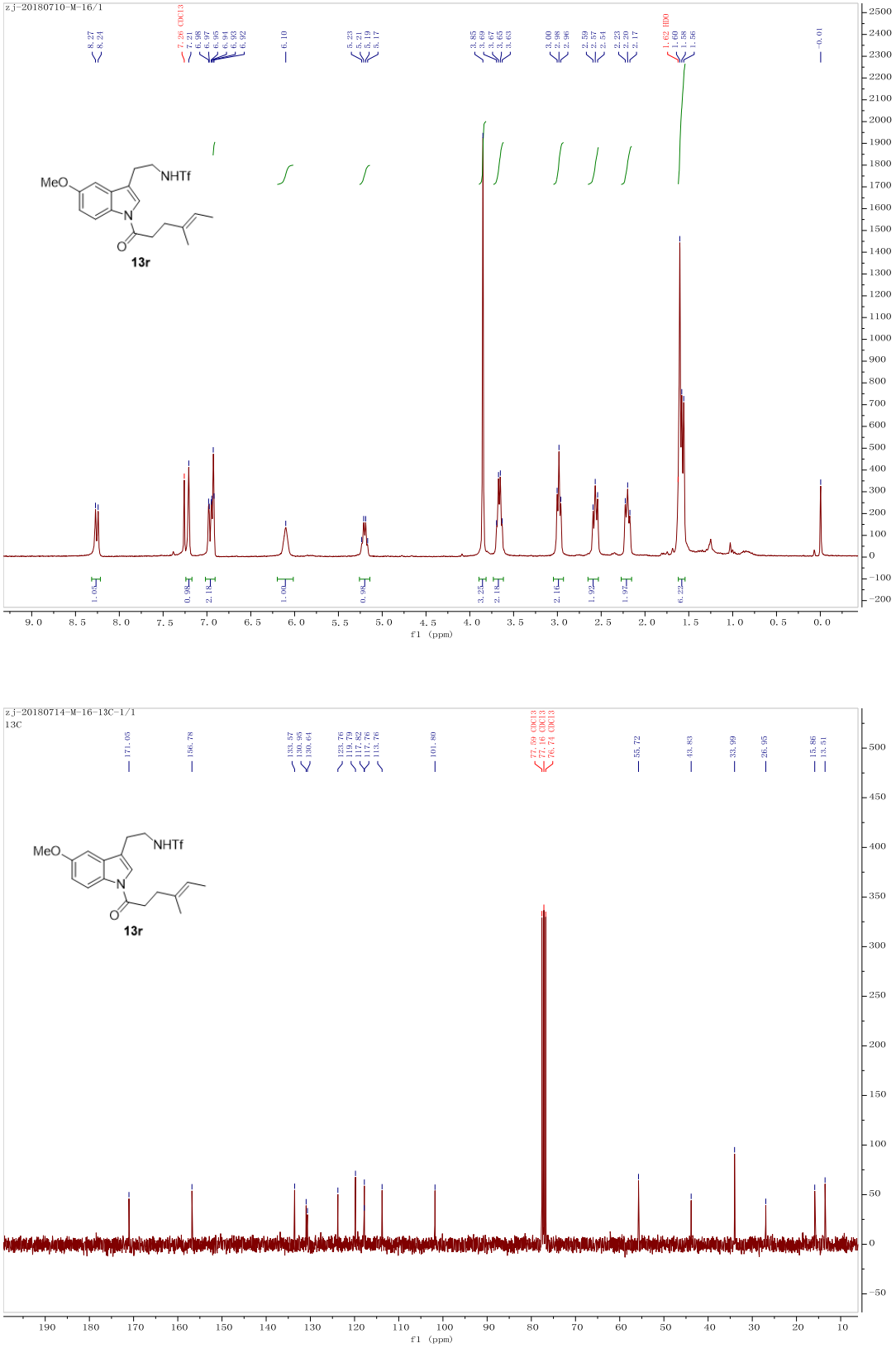

Figure S43. ^{1}H (upper) and ^{13}C-NMR (lower) of compound **13r**, related to **Table 3**

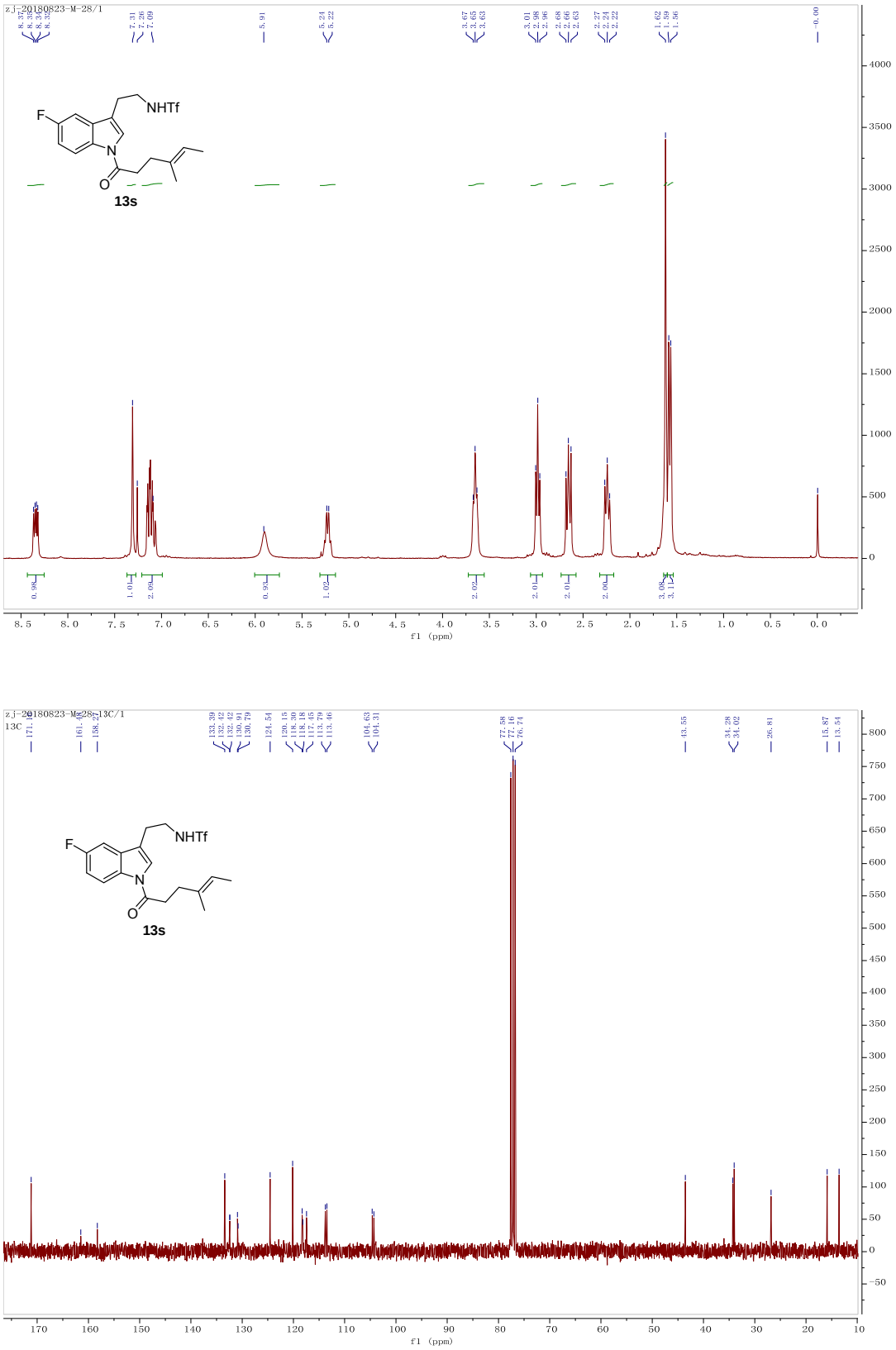

Figure S44. ^{1}H (upper) and ^{13}C-NMR (lower) of compound **13s**, related to **Table 3**

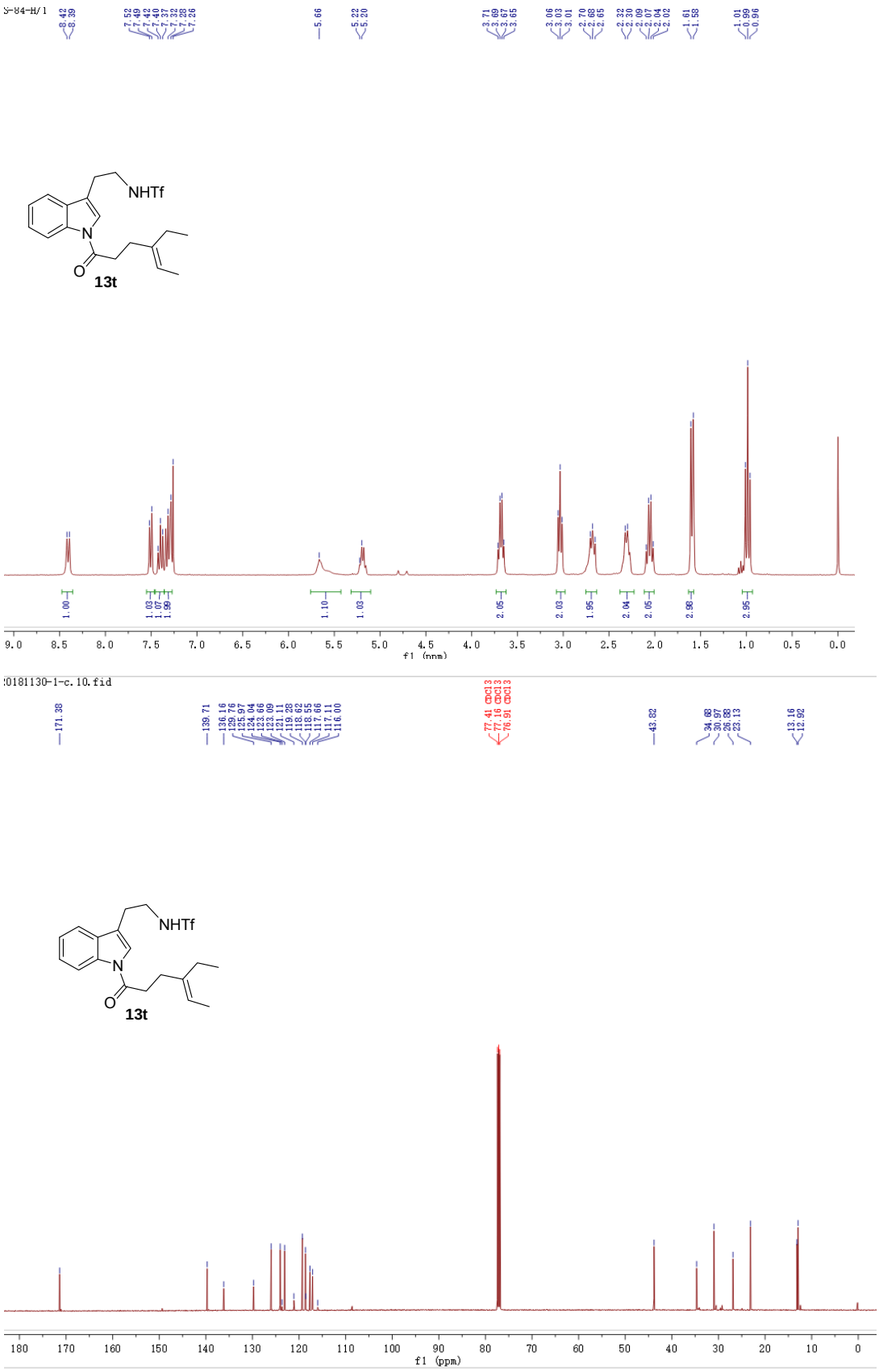

Figure S45. ^{1}H (upper) and ^{13}C-NMR (lower) of compound **13t**, related to **Table 3**

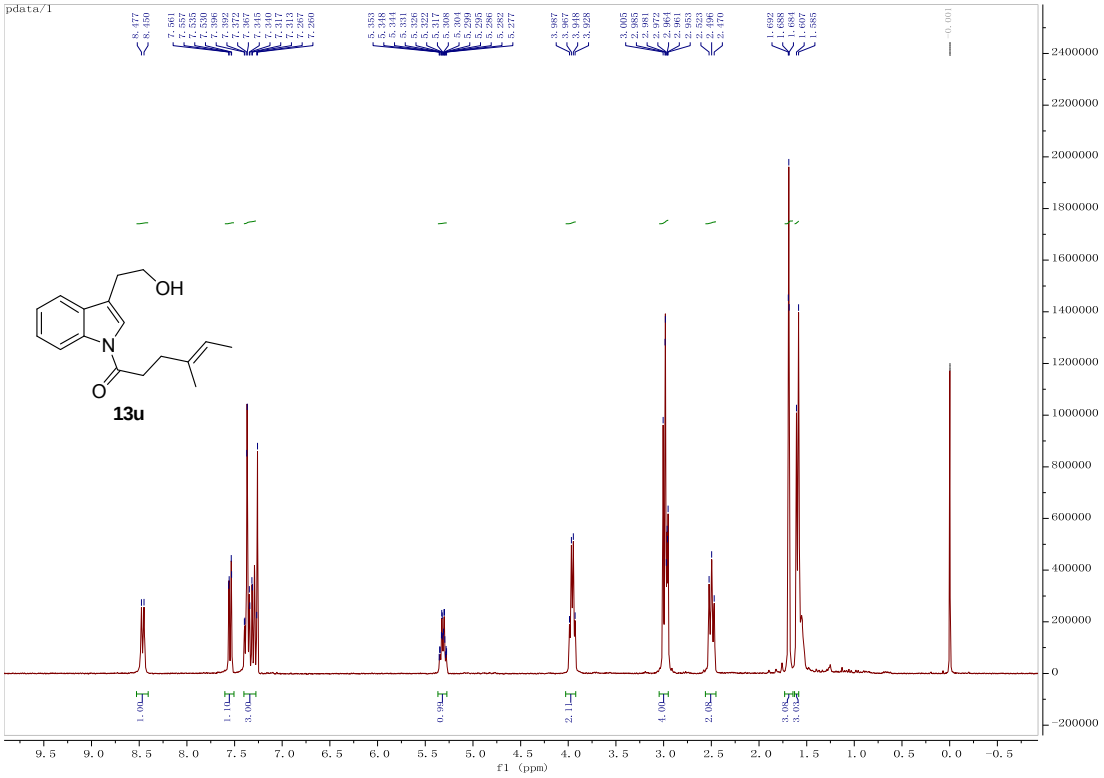

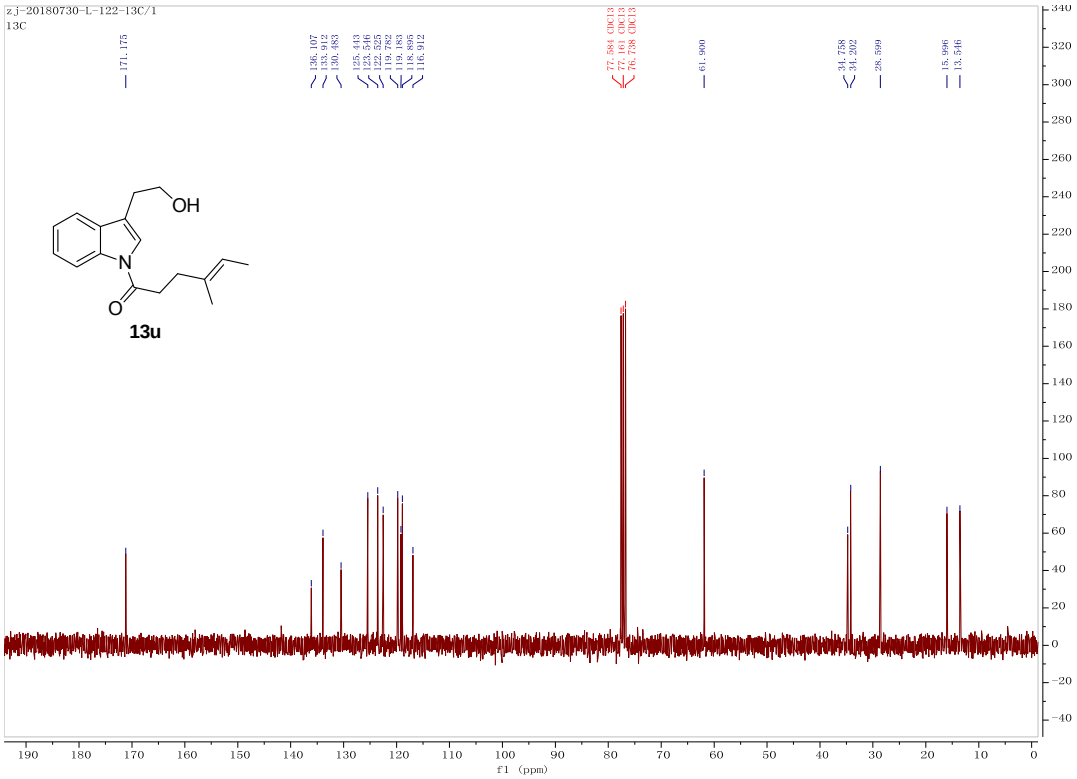

Figure S46. ^{1}H (upper) and ^{13}C-NMR (lower) of compound **13u**, related to **Table 3**

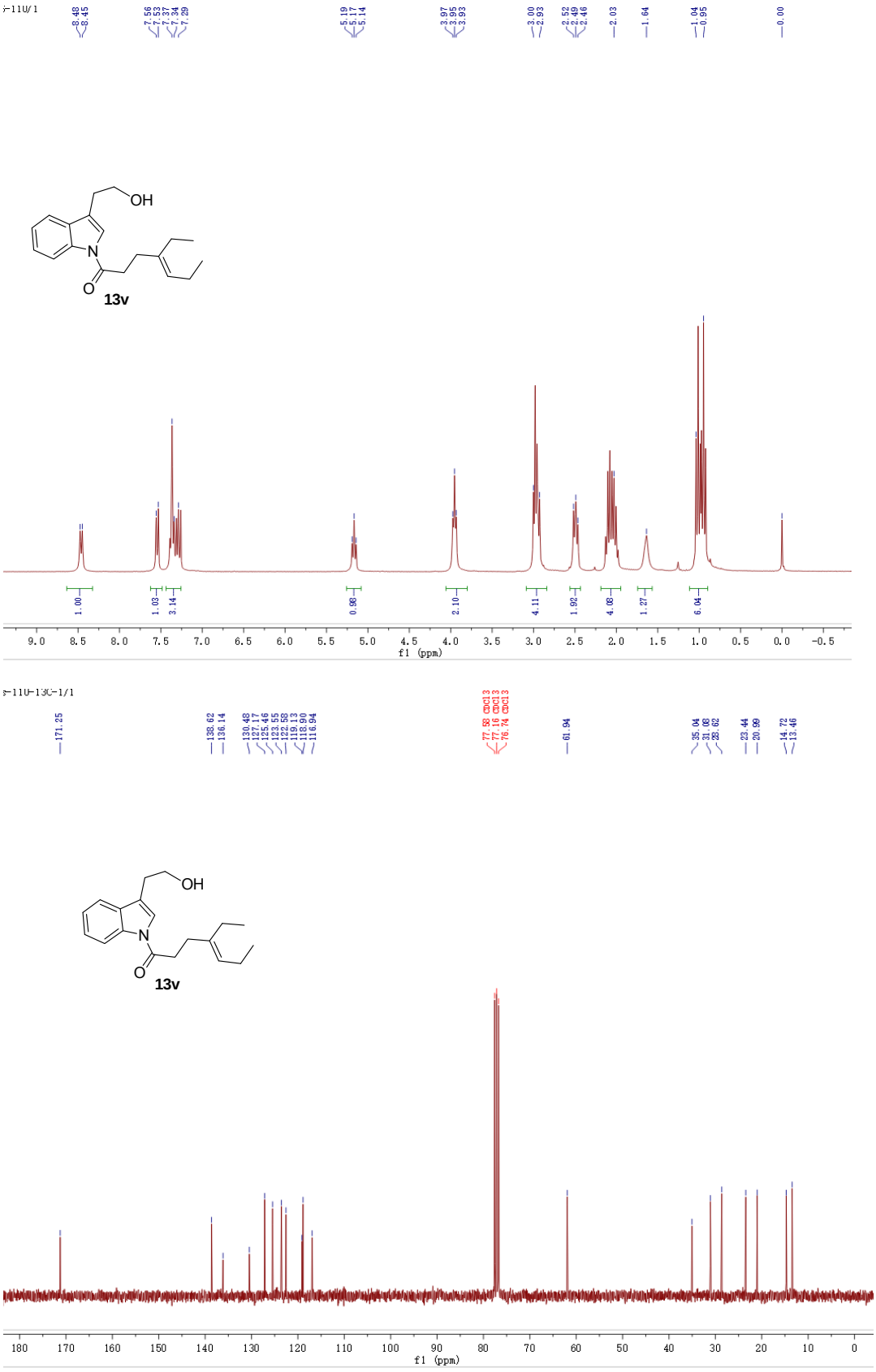

Figure S47. ^{1}H (upper) and ^{13}C-NMR (lower) of compound **13v**, related to **Table 3**

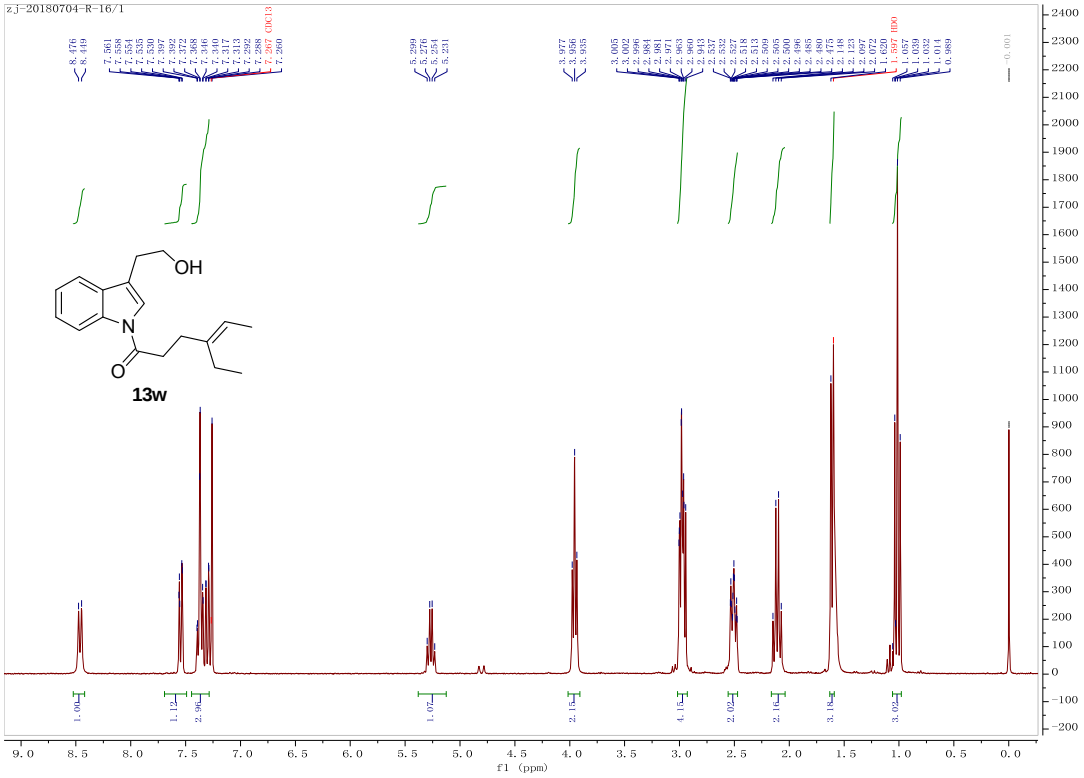

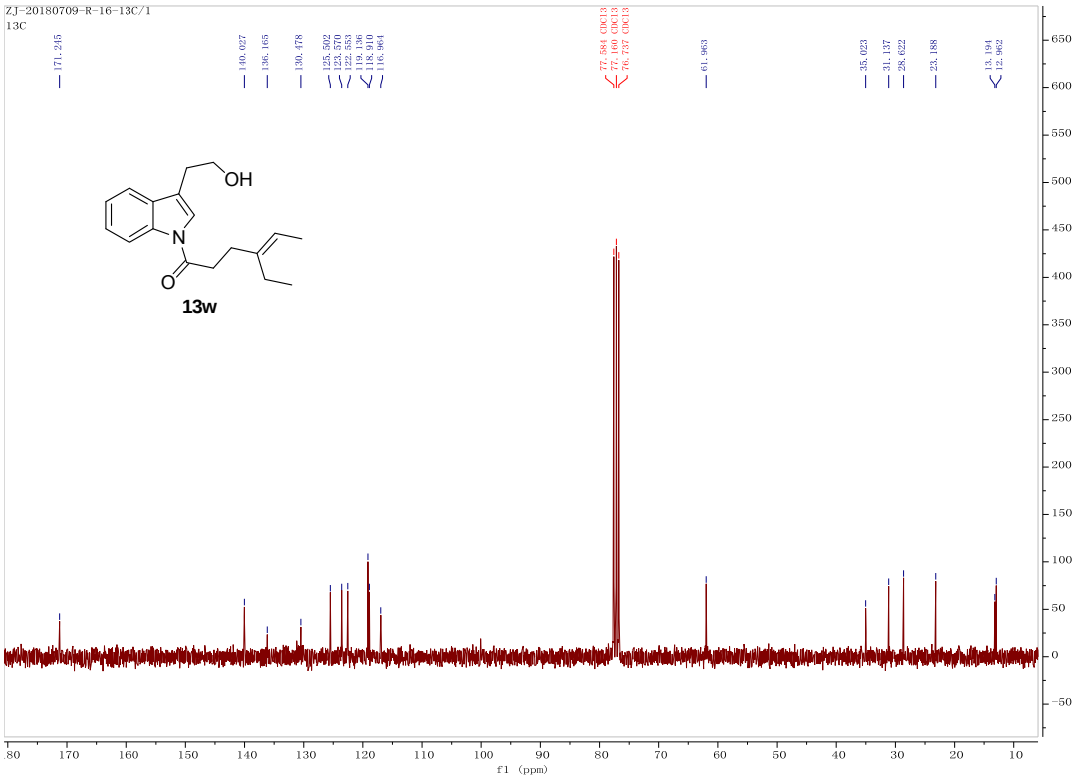

Figure S48. ^{1}H (upper) and ^{13}C-NMR (lower) of compound **13w**, related to **Table 3**

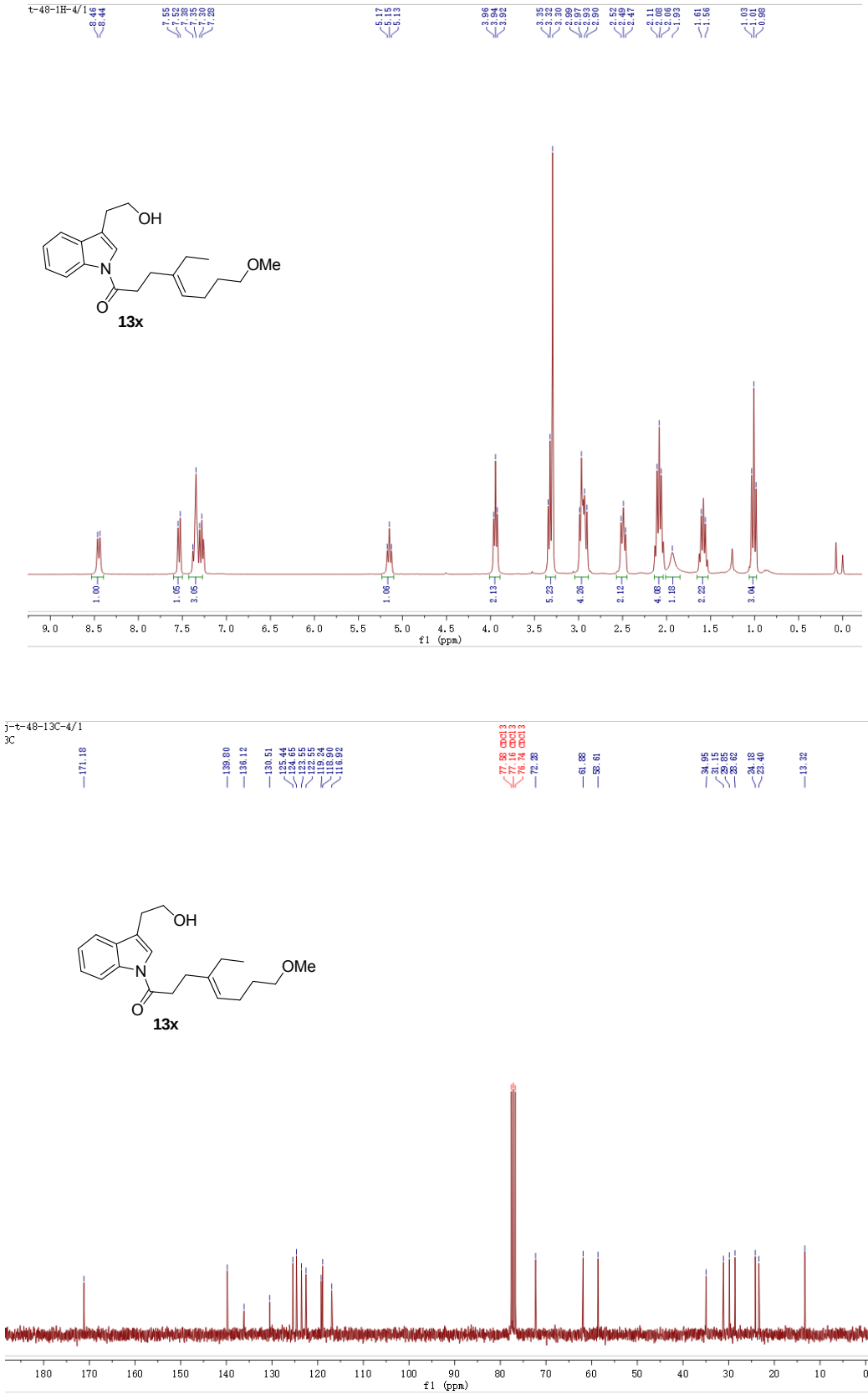

Figure S49. ^{1}H (upper) and ^{13}C-NMR (lower) of compound **13x**, related to **Table 3**

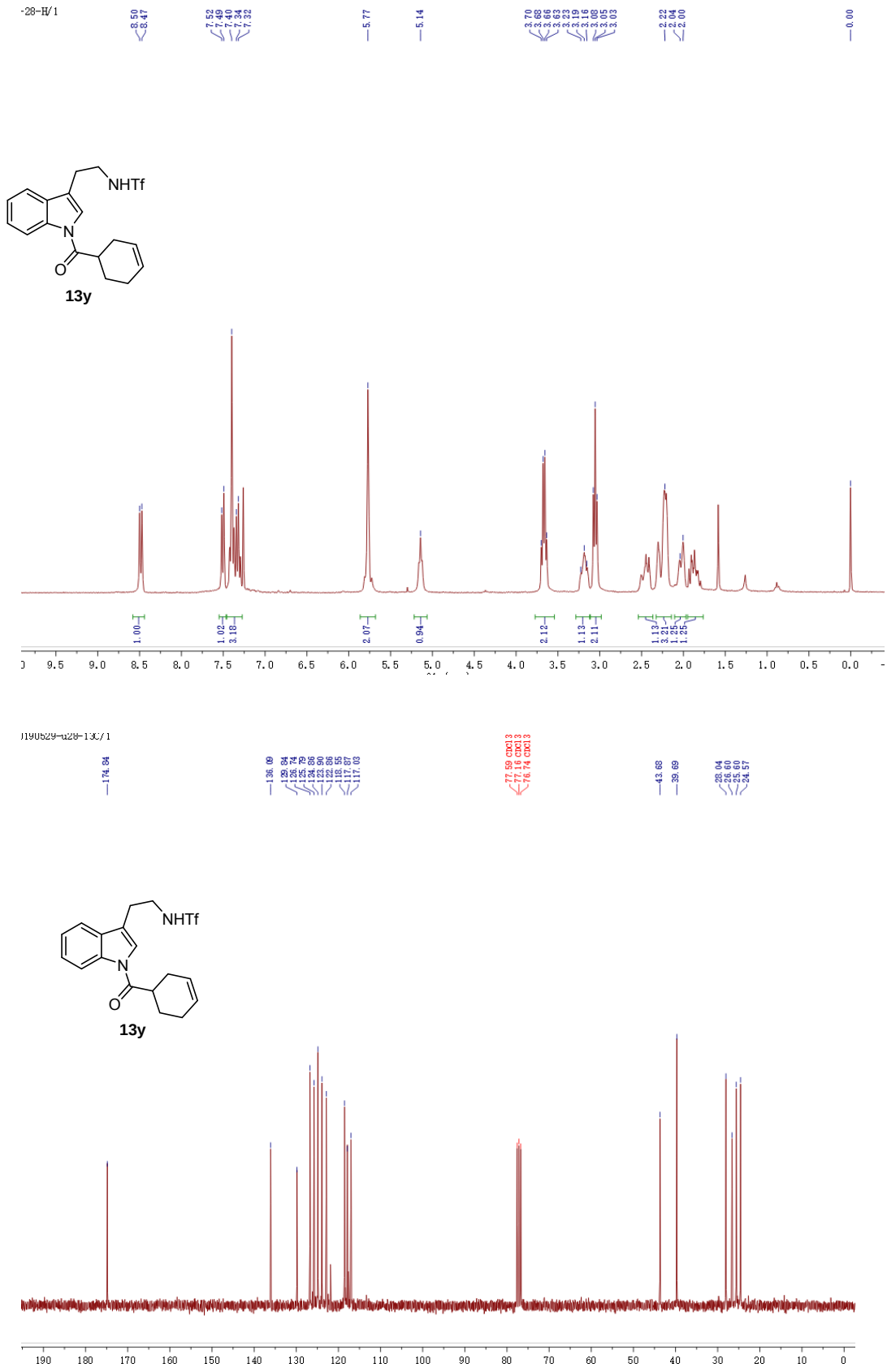

Figure S50. ^{1}H (upper) and ^{13}C-NMR (lower) of compound **13y**, related to **Table 3**

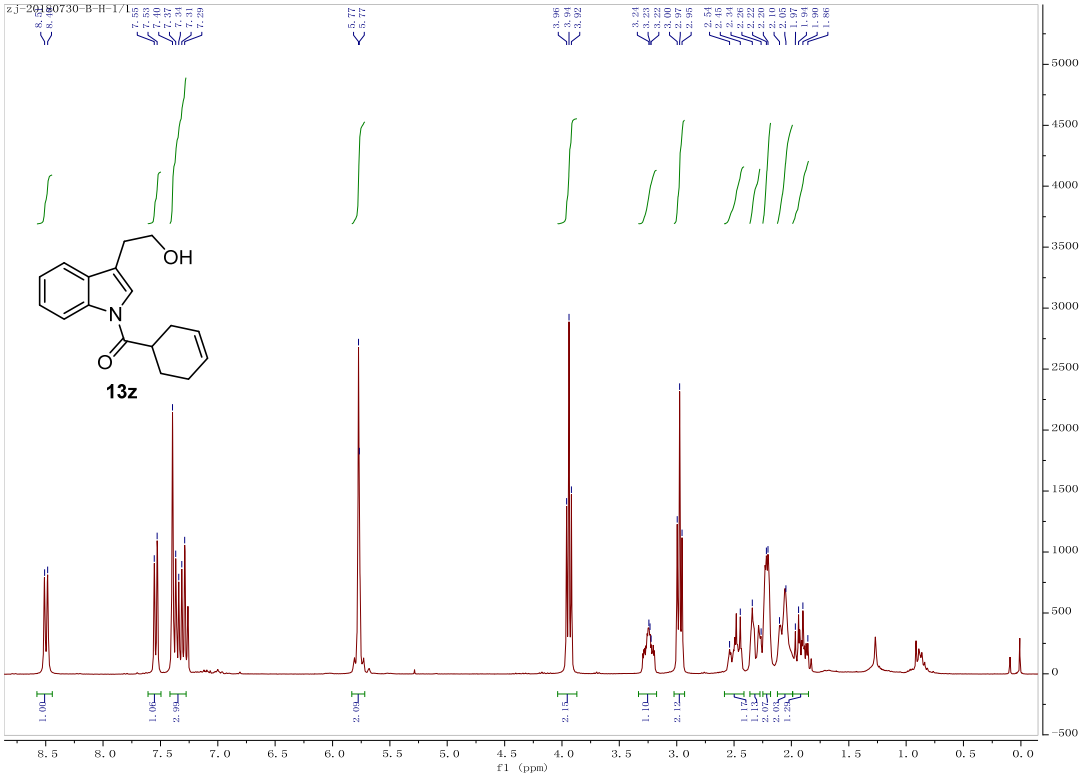

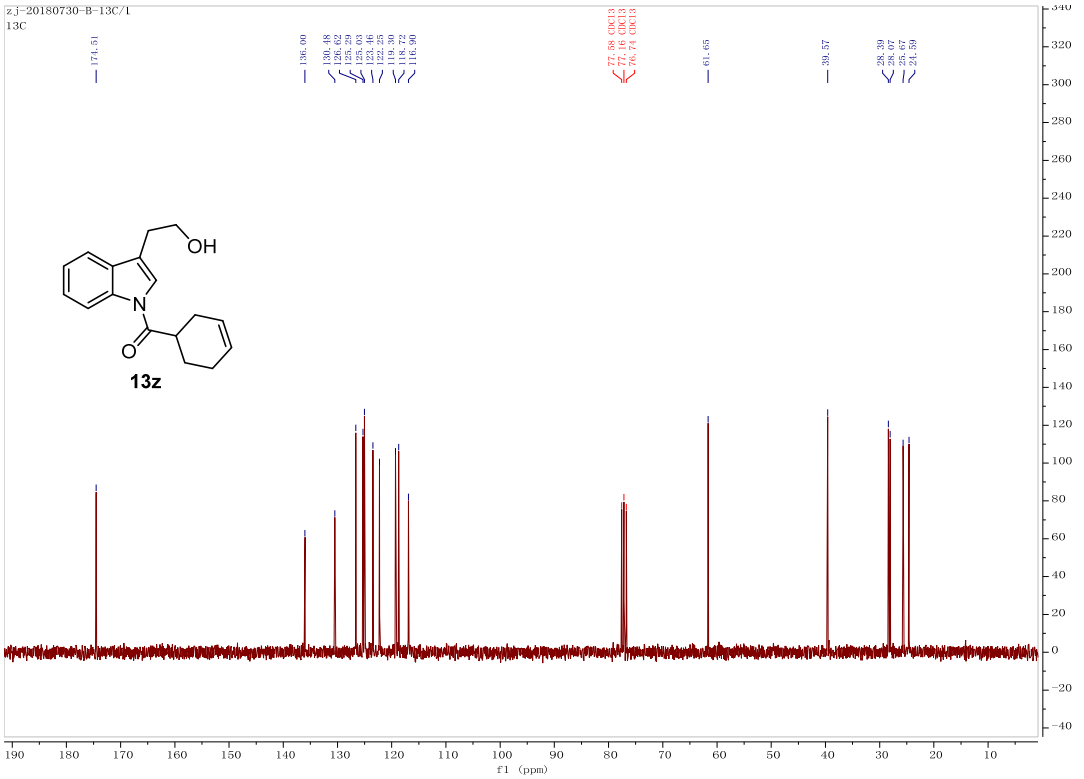

Figure S51. ^{1}H (upper) and ^{13}C-NMR (lower) of compound **13z**, related to **Table 3**

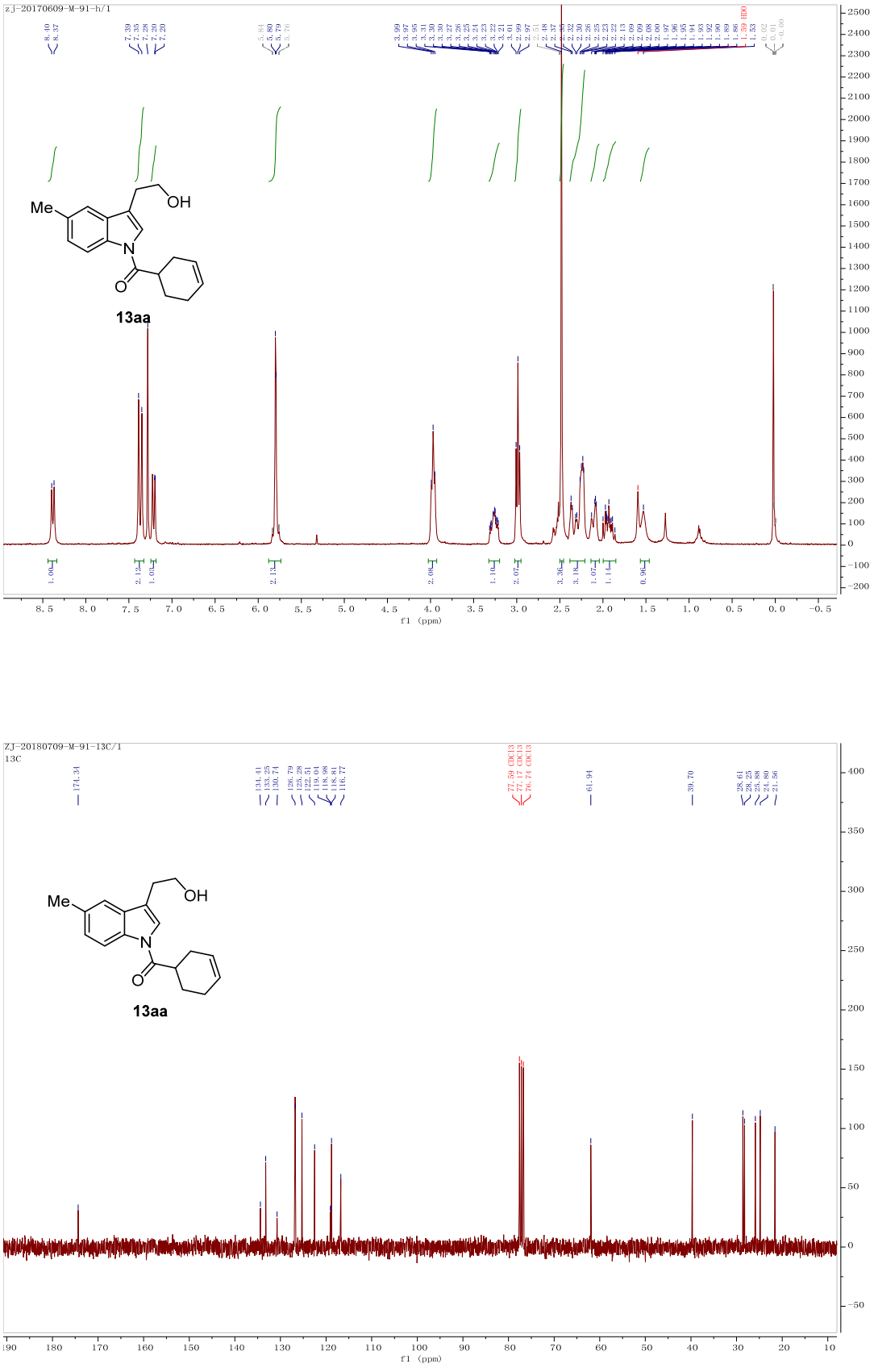

Figure S52. ^{1}H (upper) and ^{13}C-NMR (lower) of compound **13aa**, related to **Table 3**

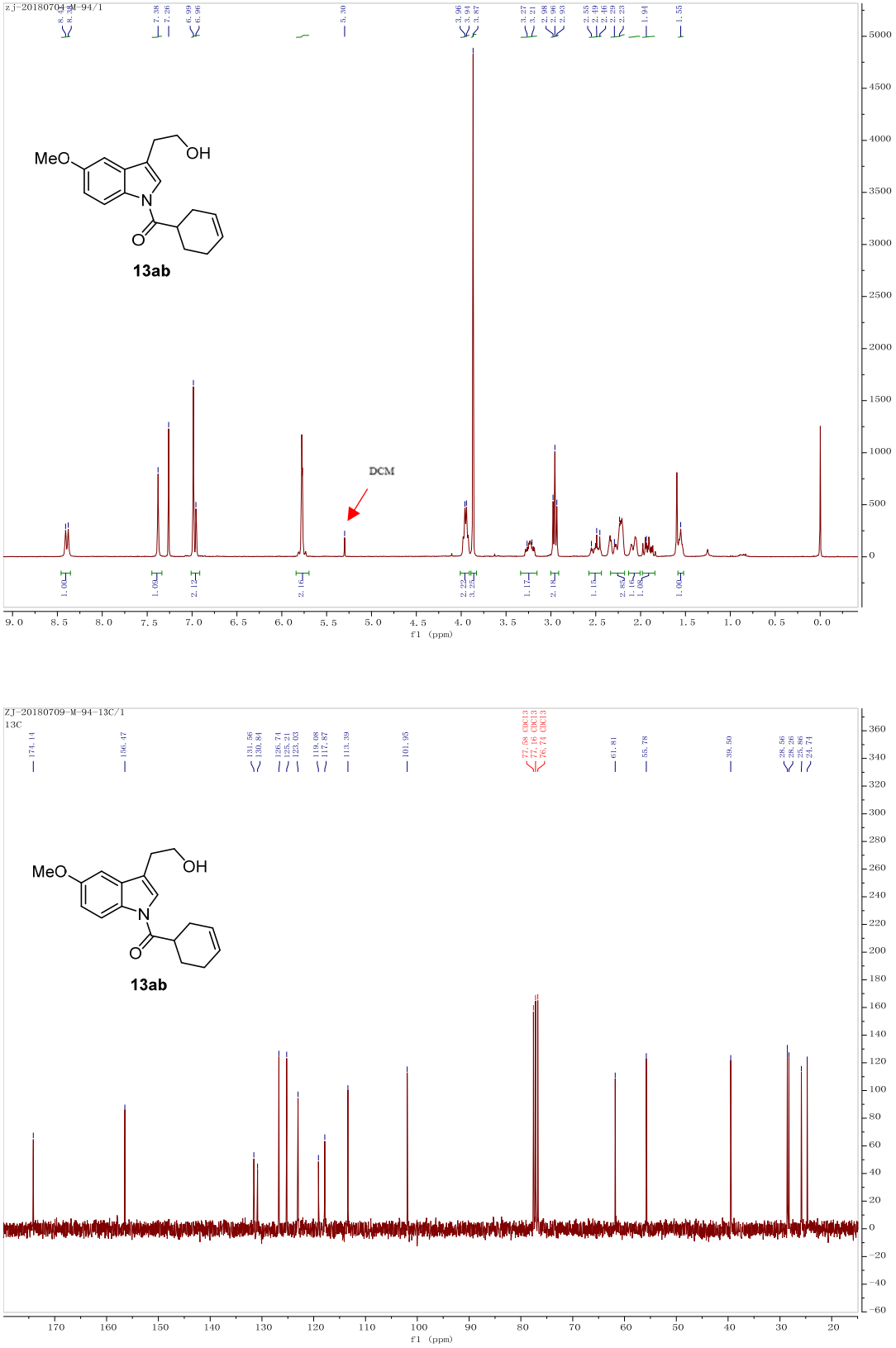

Figure S53. ^{1}H (upper) and ^{13}C-NMR (lower) of compound **13ab**, related to **Table 3**

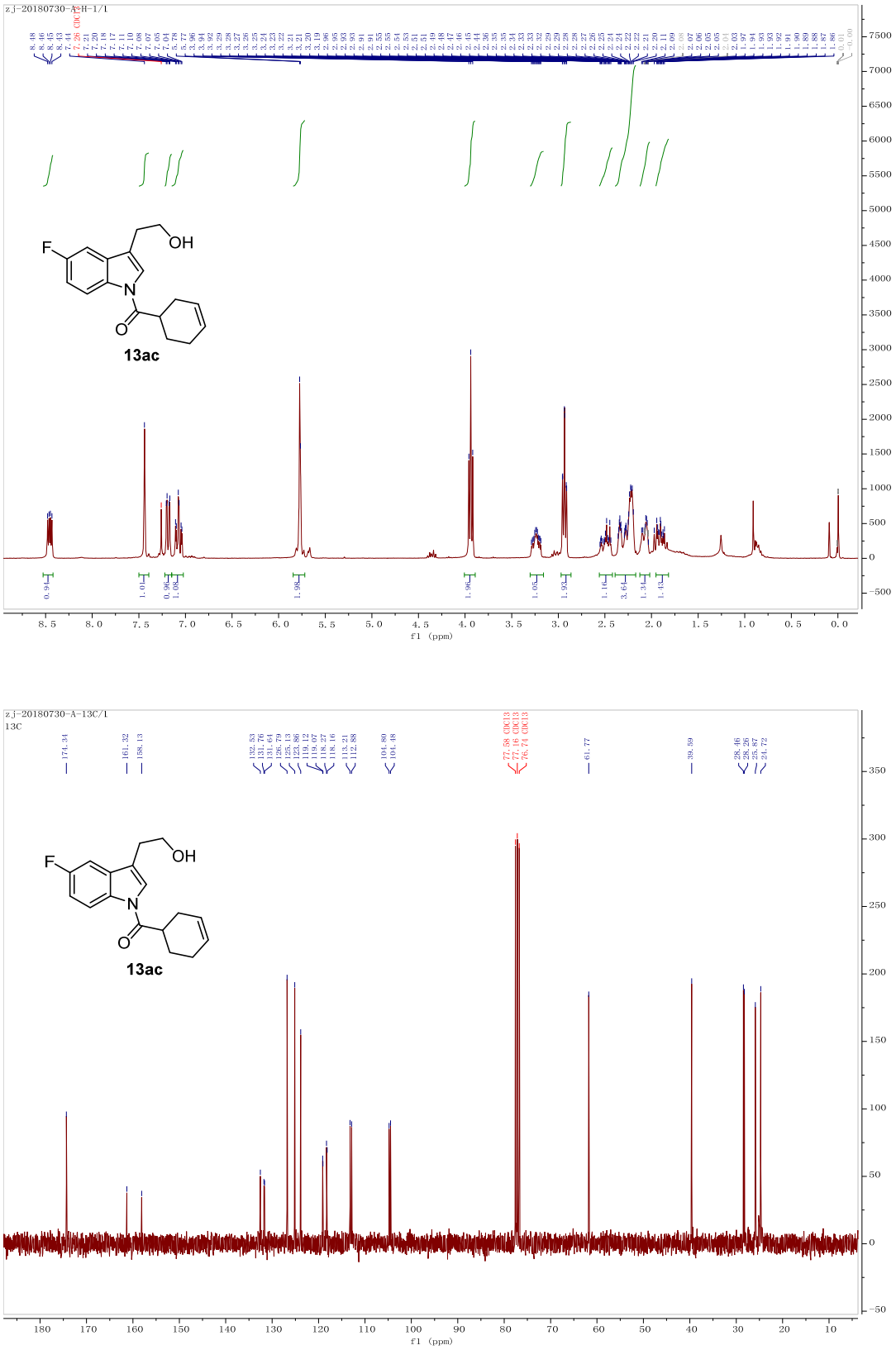

Figure S54. ^{1}H (upper) and ^{13}C-NMR (lower) of compound **13ac**, related to **Table 3**

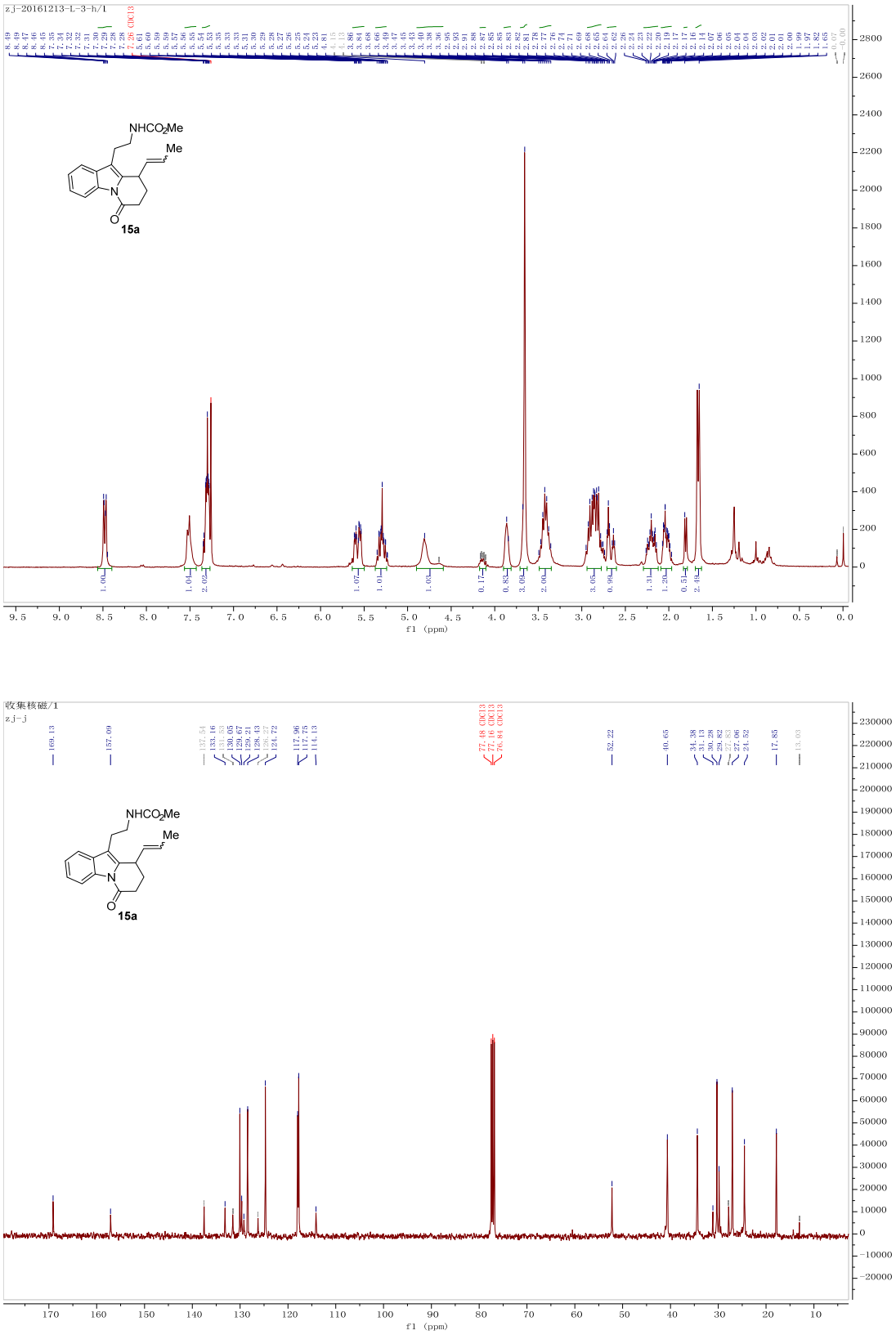

Figure S55. ^{1}H (upper) and ^{13}C-NMR (lower) of compound **15a**, related to **Table 1**

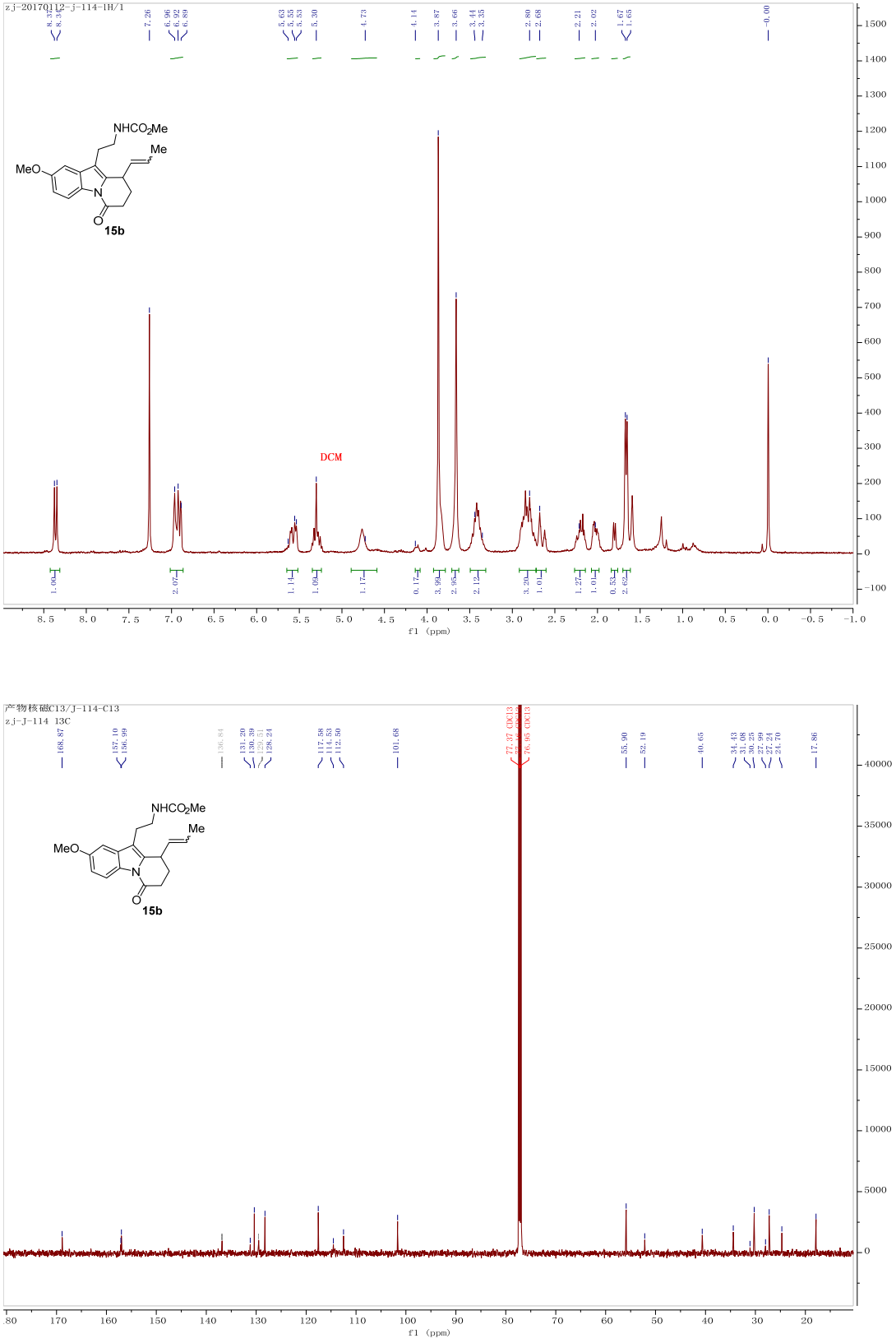

Figure S56. ^{1}H (upper) and ^{13}C-NMR (lower) of compound **15b**, related to **Table 2**

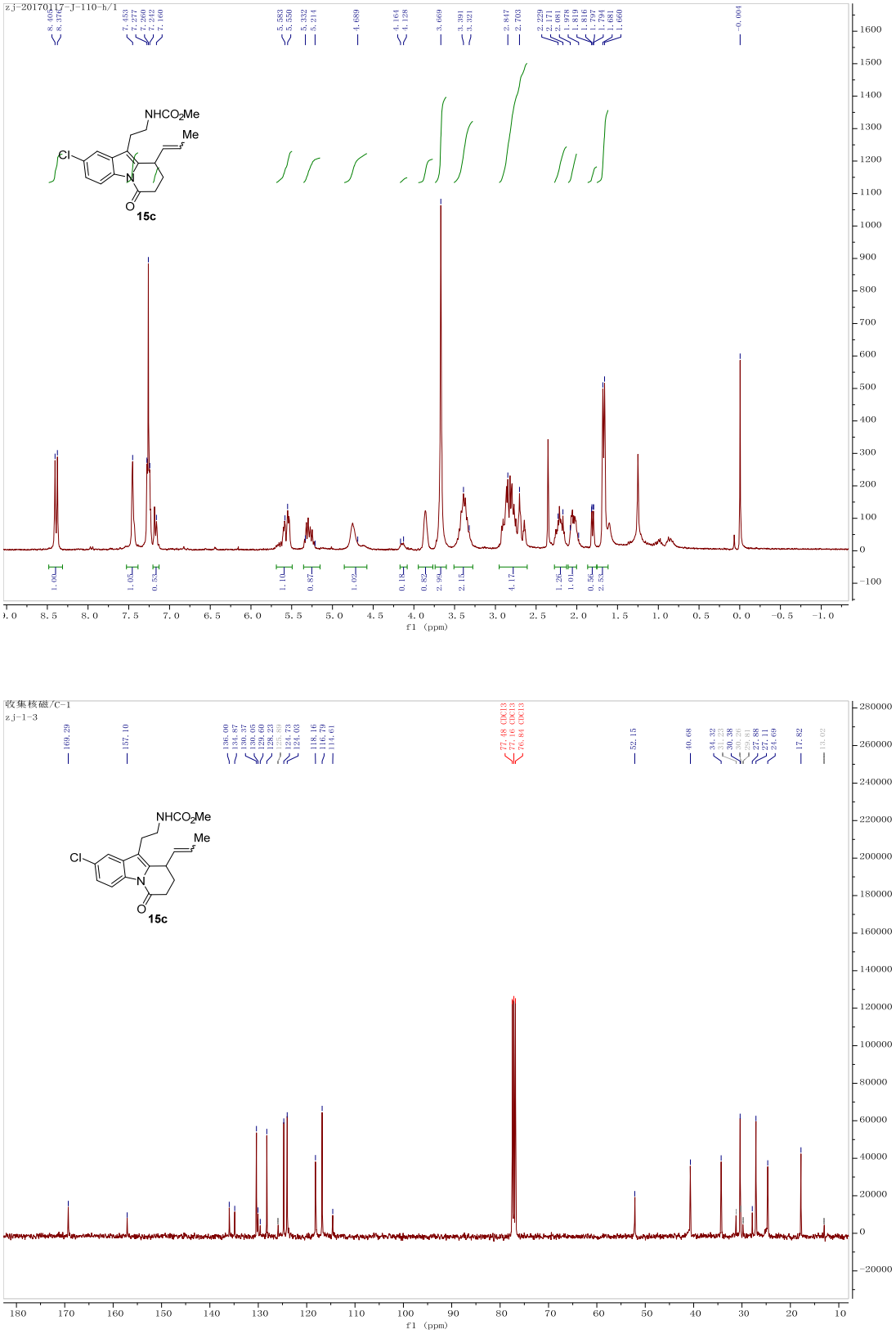

Figure S57. ^{1}H (upper) and ^{13}C-NMR (lower) of compound **15c**, related to **Table 2**

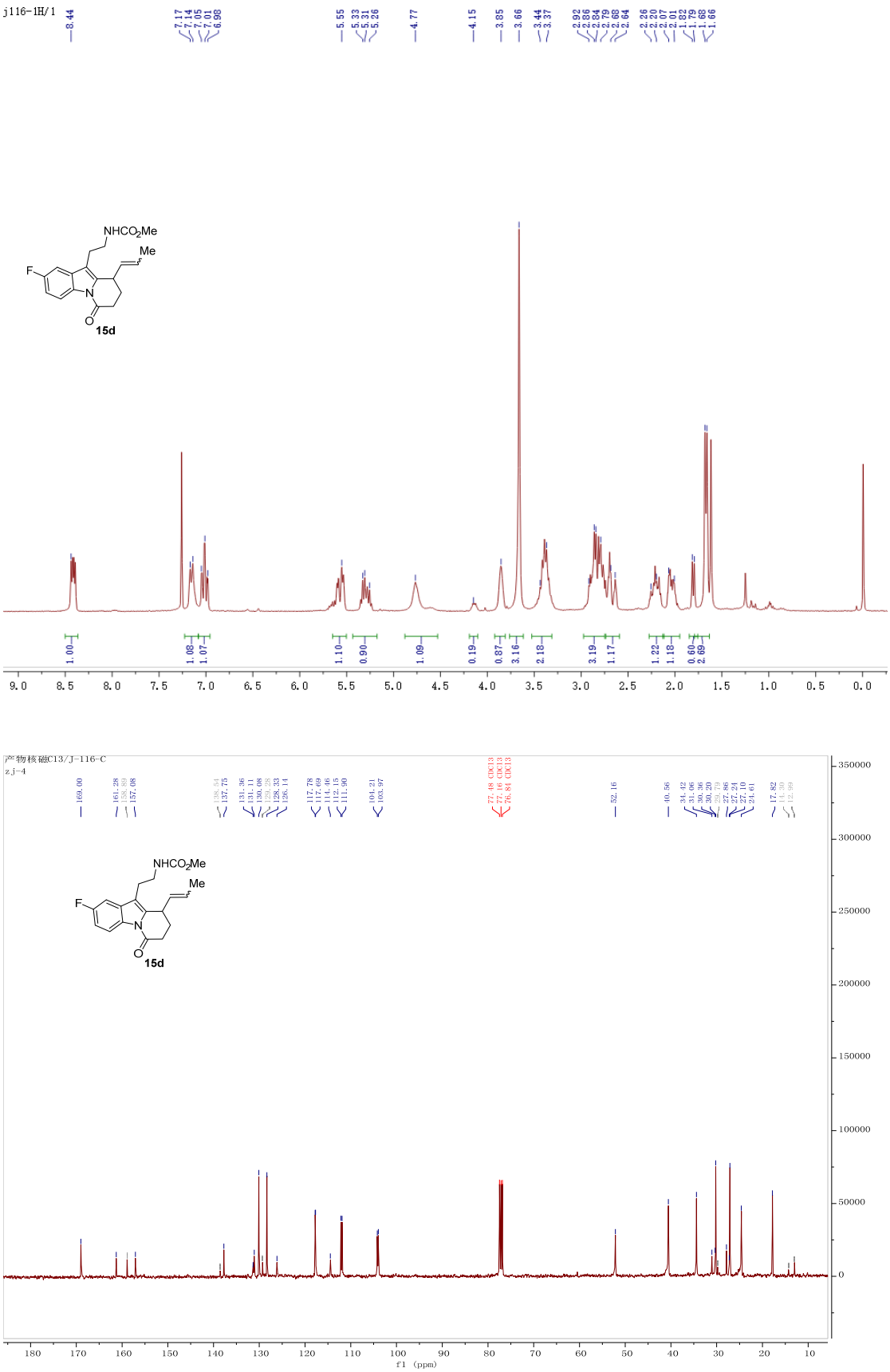

Figure S58. ^{1}H (upper) and ^{13}C-NMR (lower) of compound **15d**, related to **Table 2**

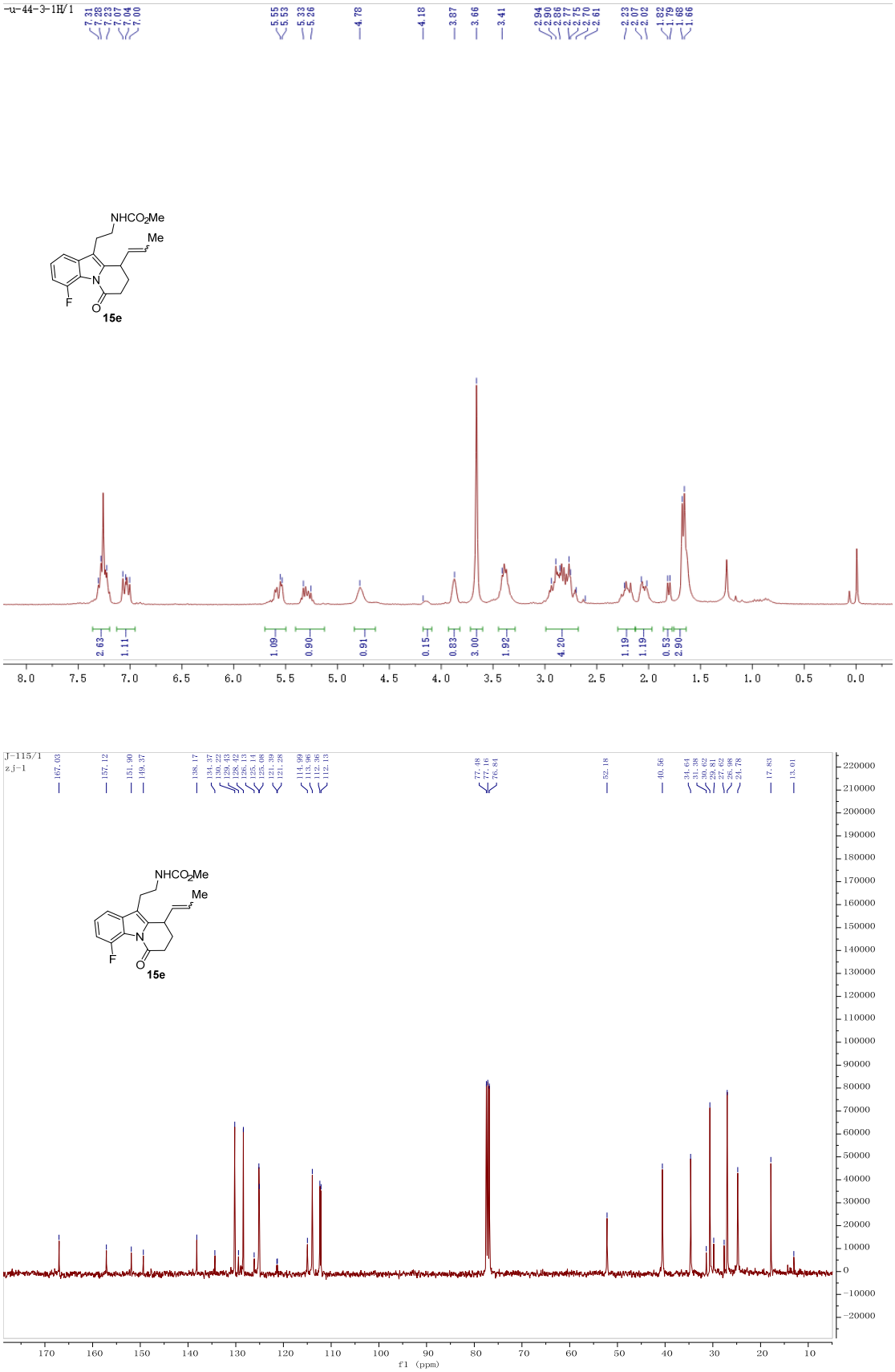

Figure S59. ^{1}H (upper) and ^{13}C-NMR (lower) of compound **15e**, related to **Table 2**

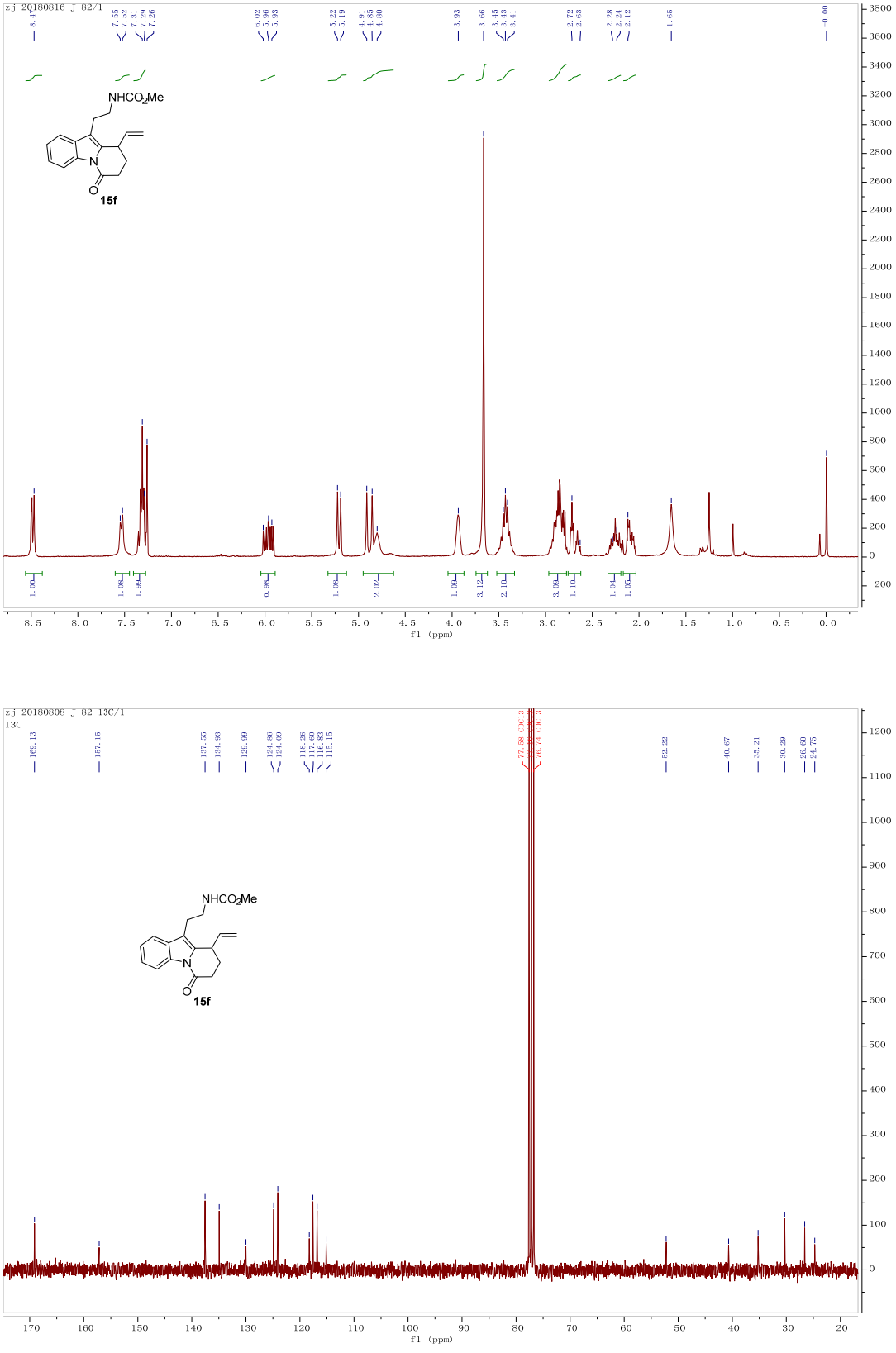

Figure S60. ^{1}H (upper) and ^{13}C-NMR (lower) of compound **15f**, related to **Table 2**

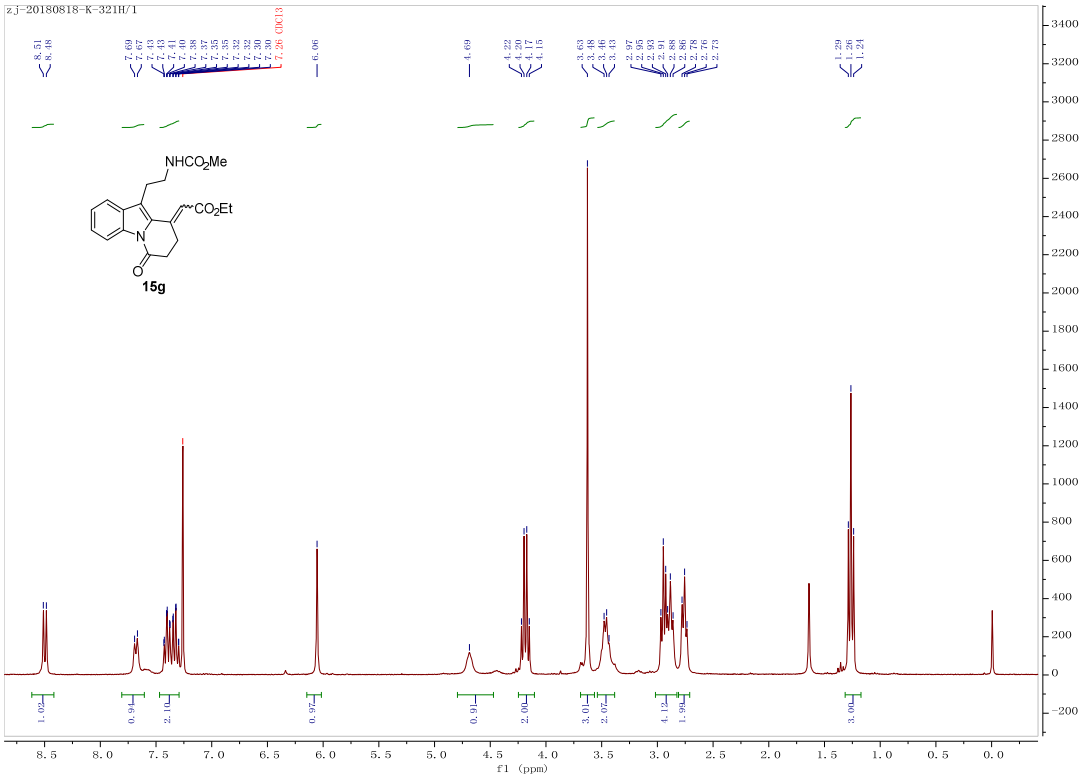

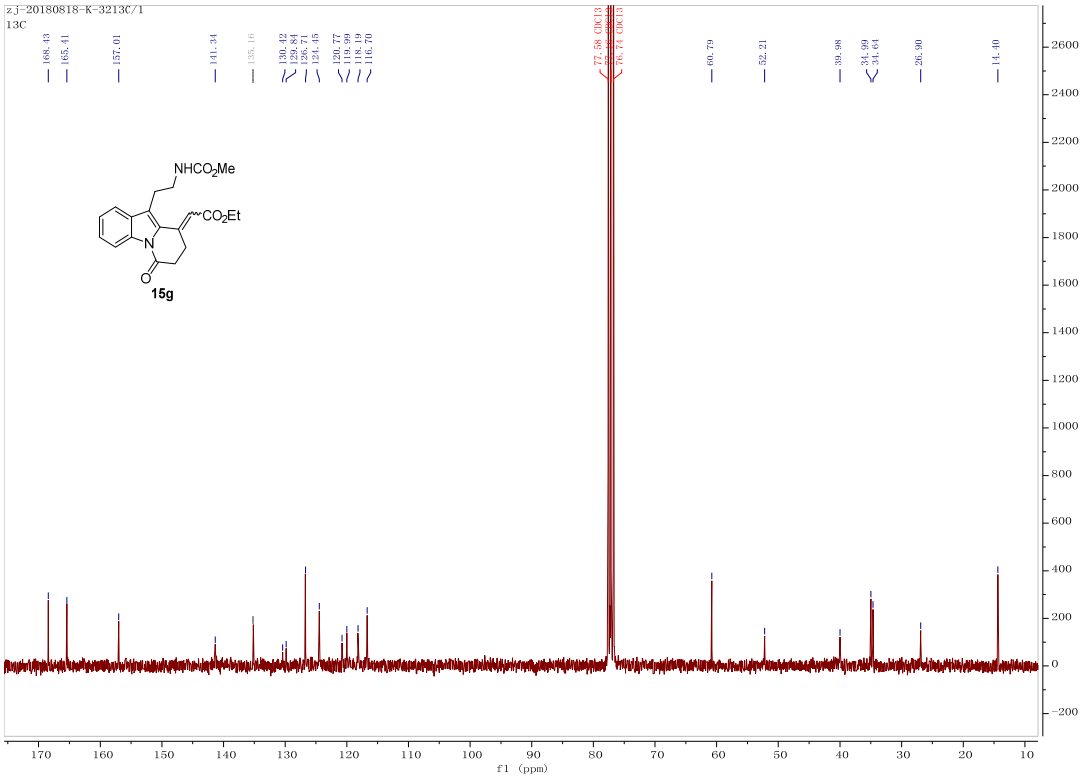

Figure S61. ^{1}H (upper) and ^{13}C-NMR (lower) of compound **15g**, related to **Table 2**

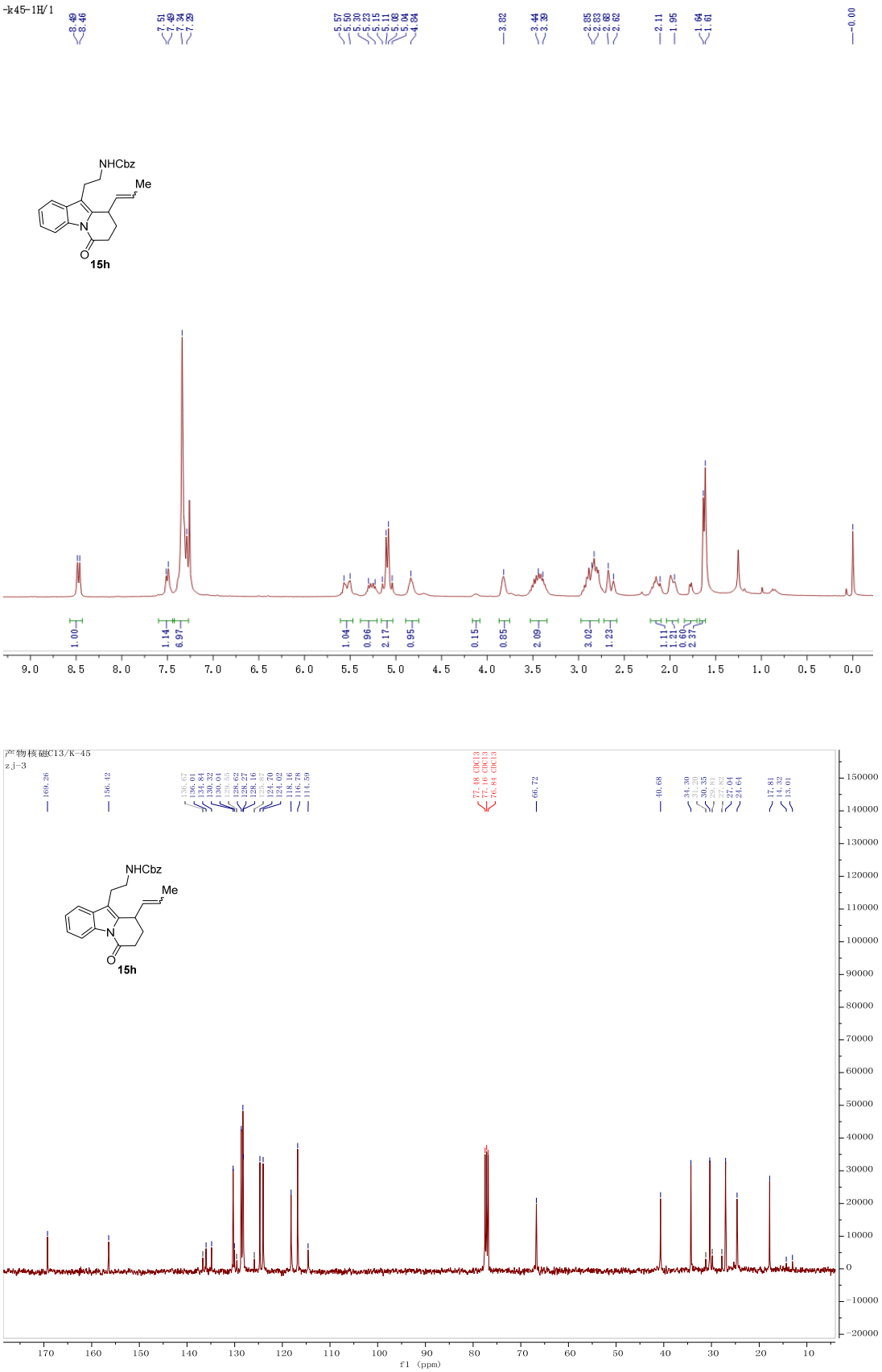

Figure S62. ^{1}H (upper) and ^{13}C-NMR (lower) of compound **15h**, related to **Table 2**

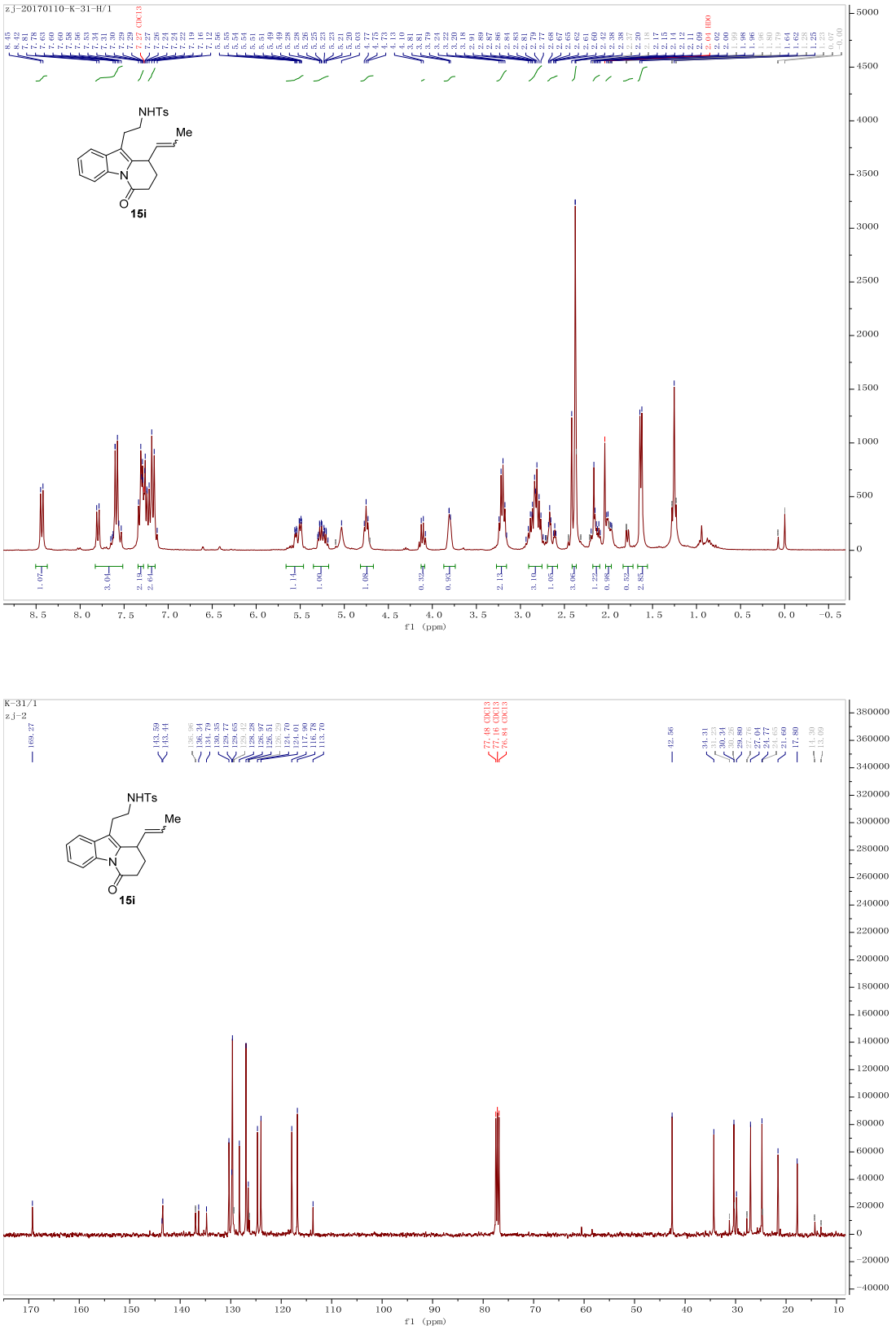

Figure S63. ^{1}H (upper) and ^{13}C-NMR (lower) of compound **15i**, related to **Table 2**

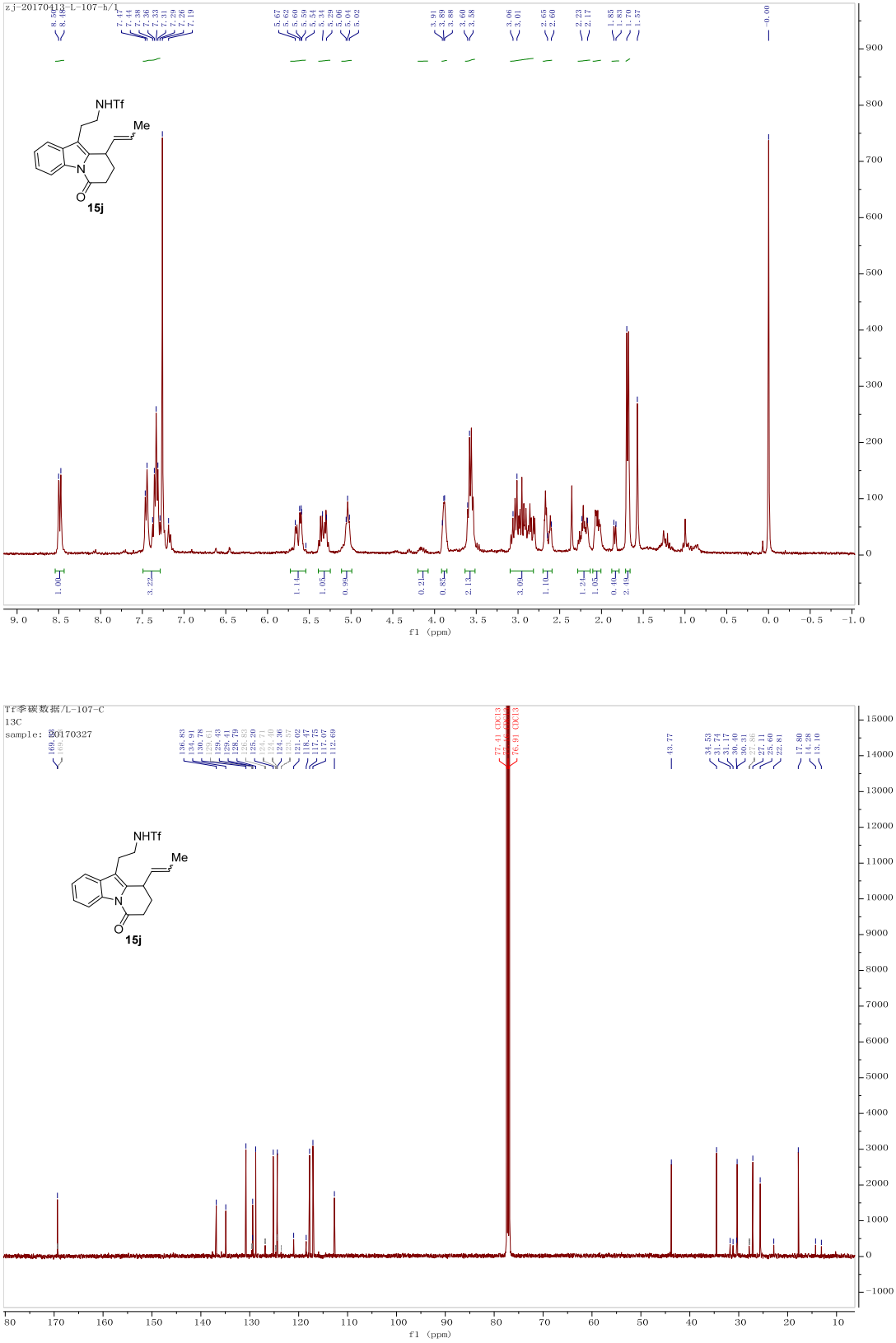

Figure S64. ^{1}H (upper) and ^{13}C-NMR (lower) of compound **15j**, related to **Table 2**

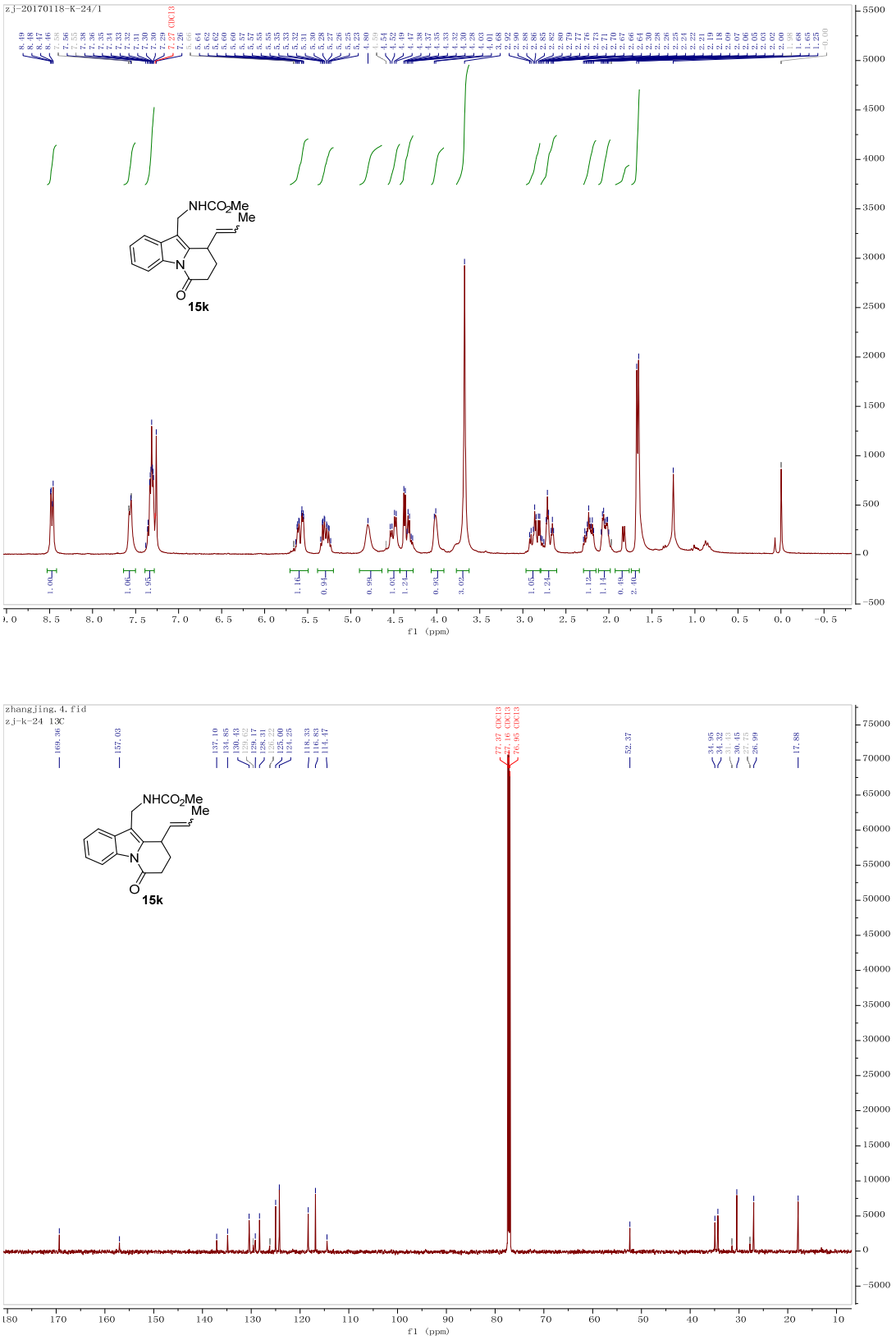

Figure S65. ^{1}H (upper) and ^{13}C-NMR (lower) of compound **15k**, related to **Table 2**

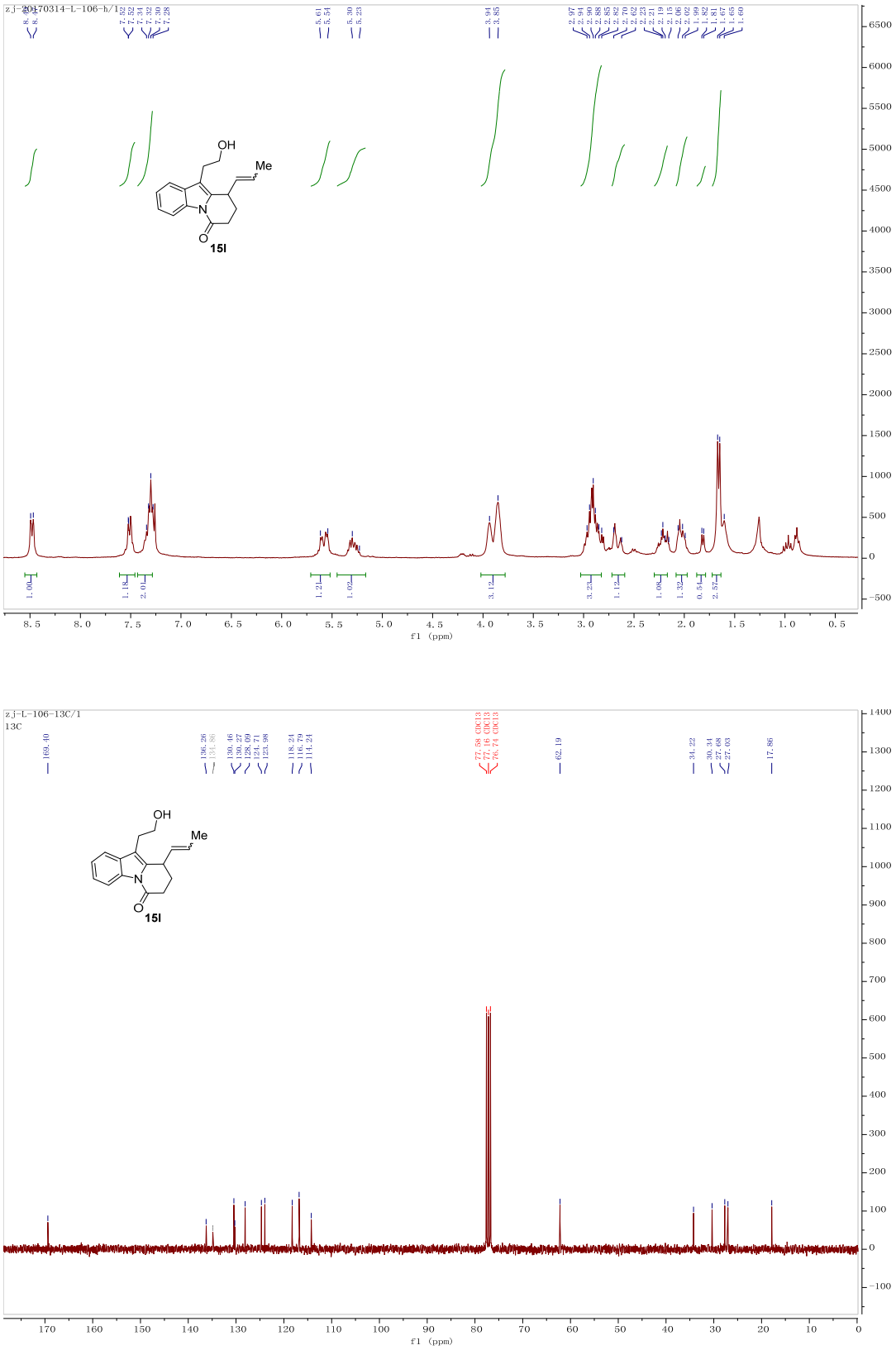

Figure S66. ^{1}H (upper) and ^{13}C-NMR (lower) of compound **15l**, related to **Table 2**

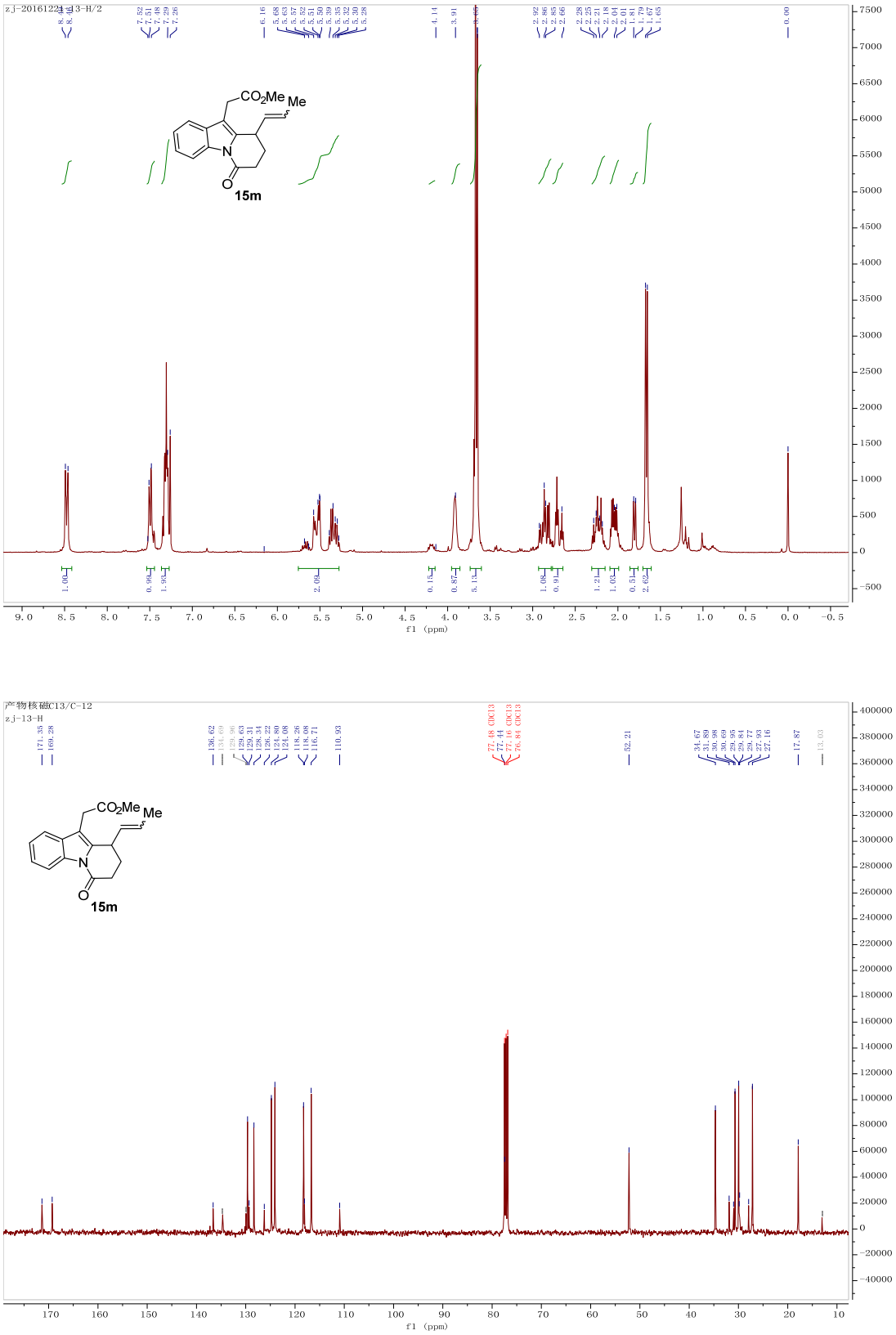

Figure S67. ^{1}H (upper) and ^{13}C-NMR (lower) of compound **15m**, related to **Table 2**

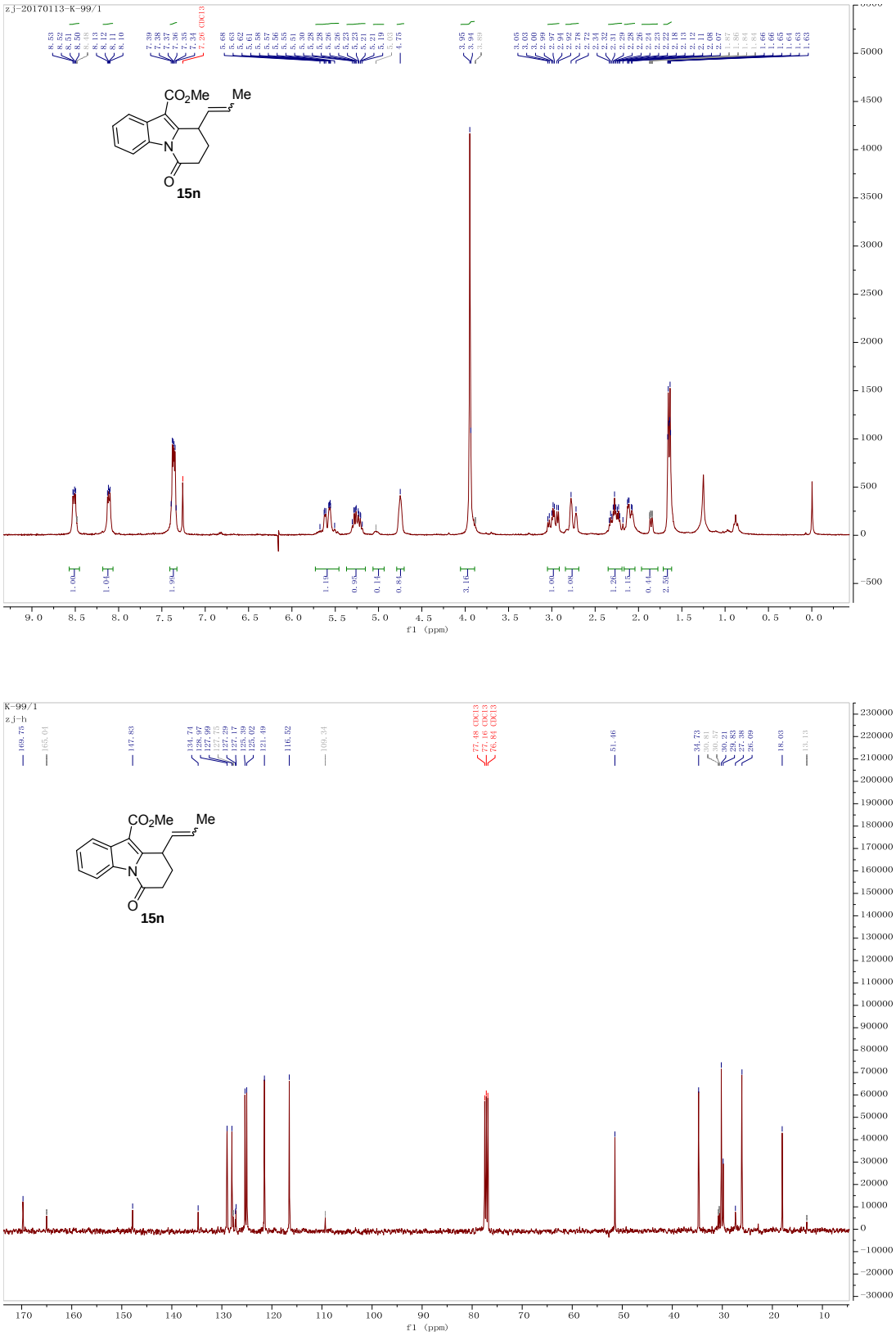

Figure S68. ^{1}H (upper) and ^{13}C-NMR (lower) of compound **15n**, related to **Table 2**

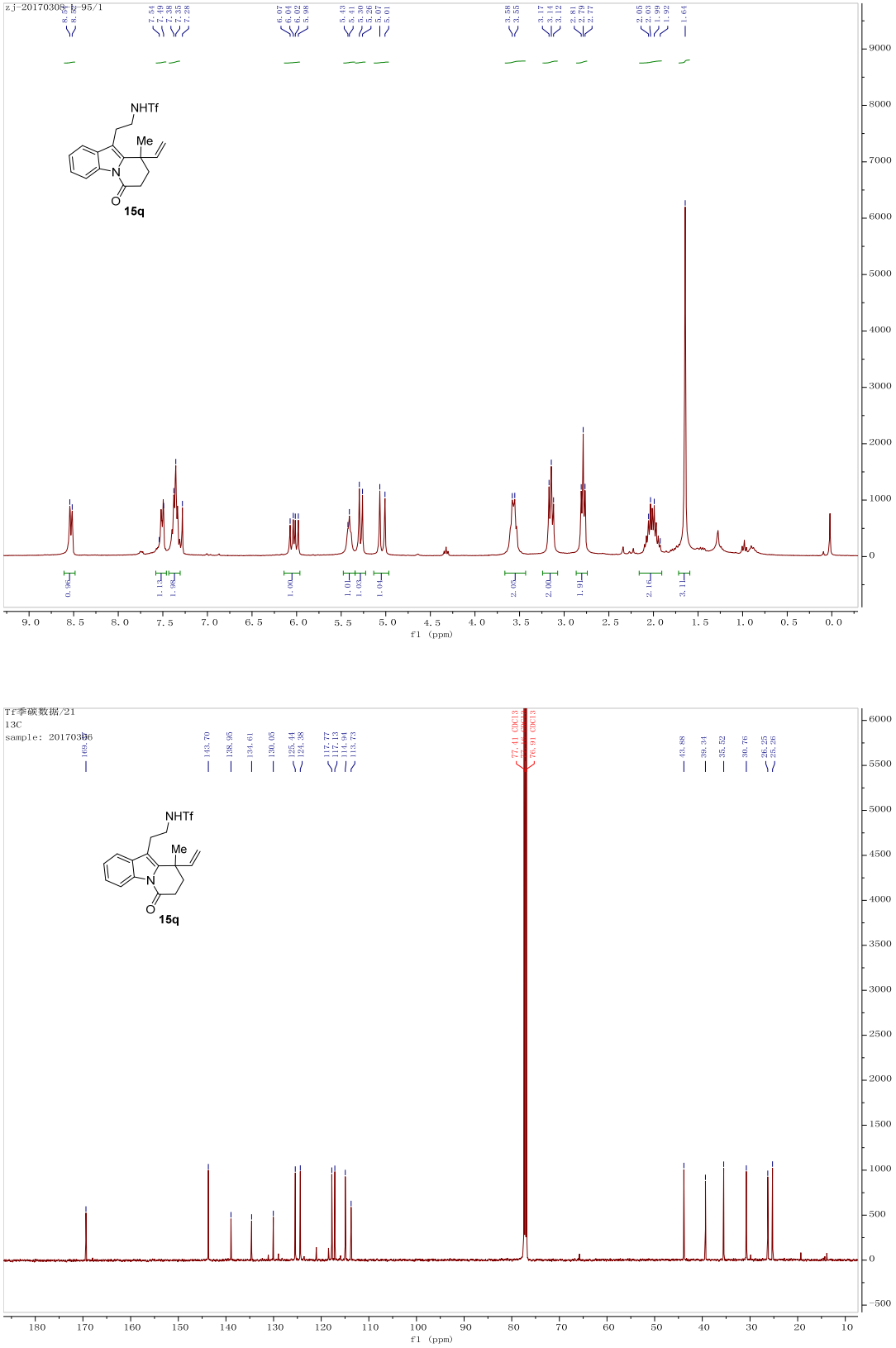

Figure S69. ^{1}H (upper) and ^{13}C-NMR (lower) of compound **15q**, related to **Table 3**

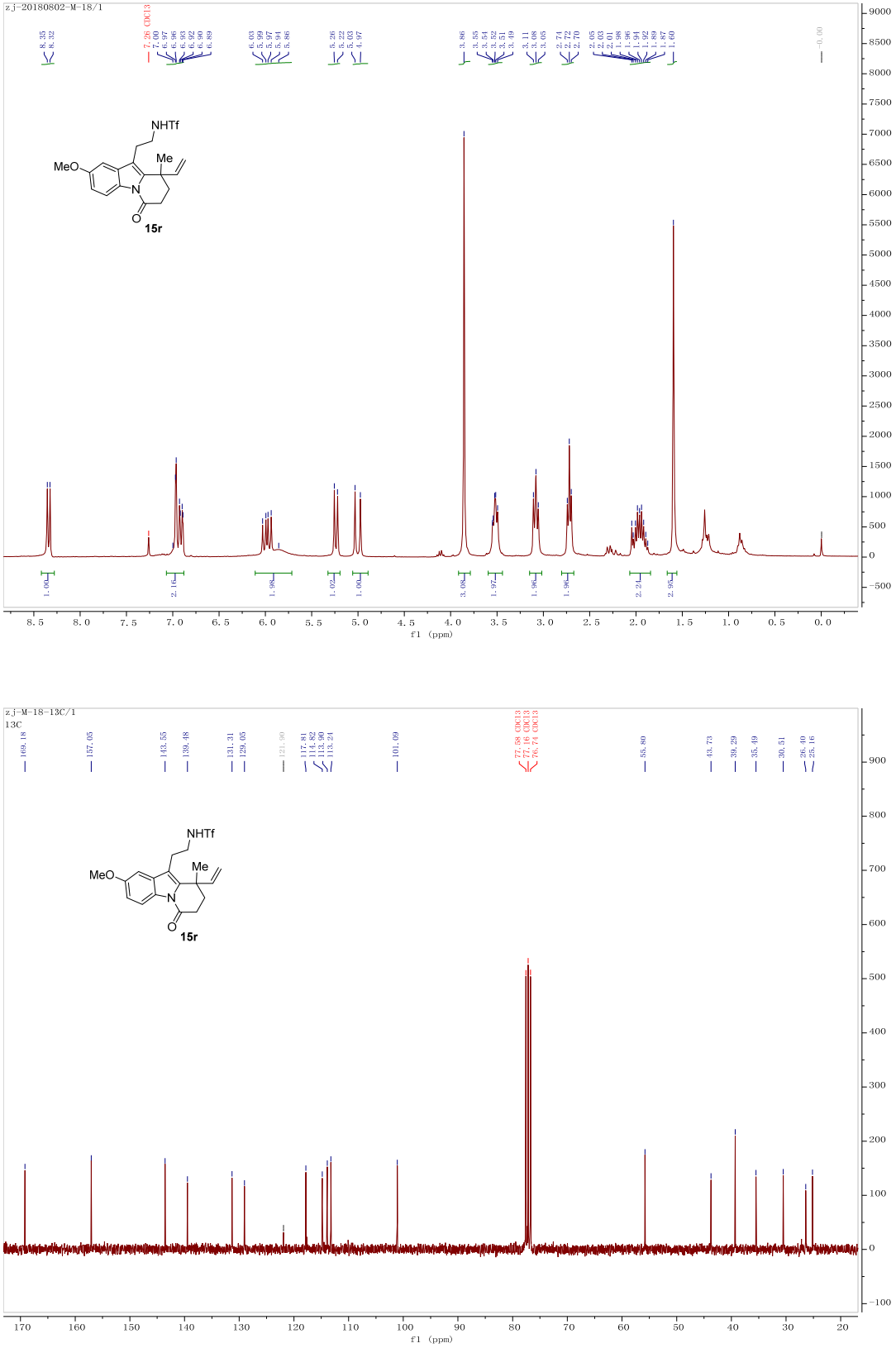

Figure S70. ^{1}H (upper) and ^{13}C-NMR (lower) of compound **15r**, related to **Table 3**

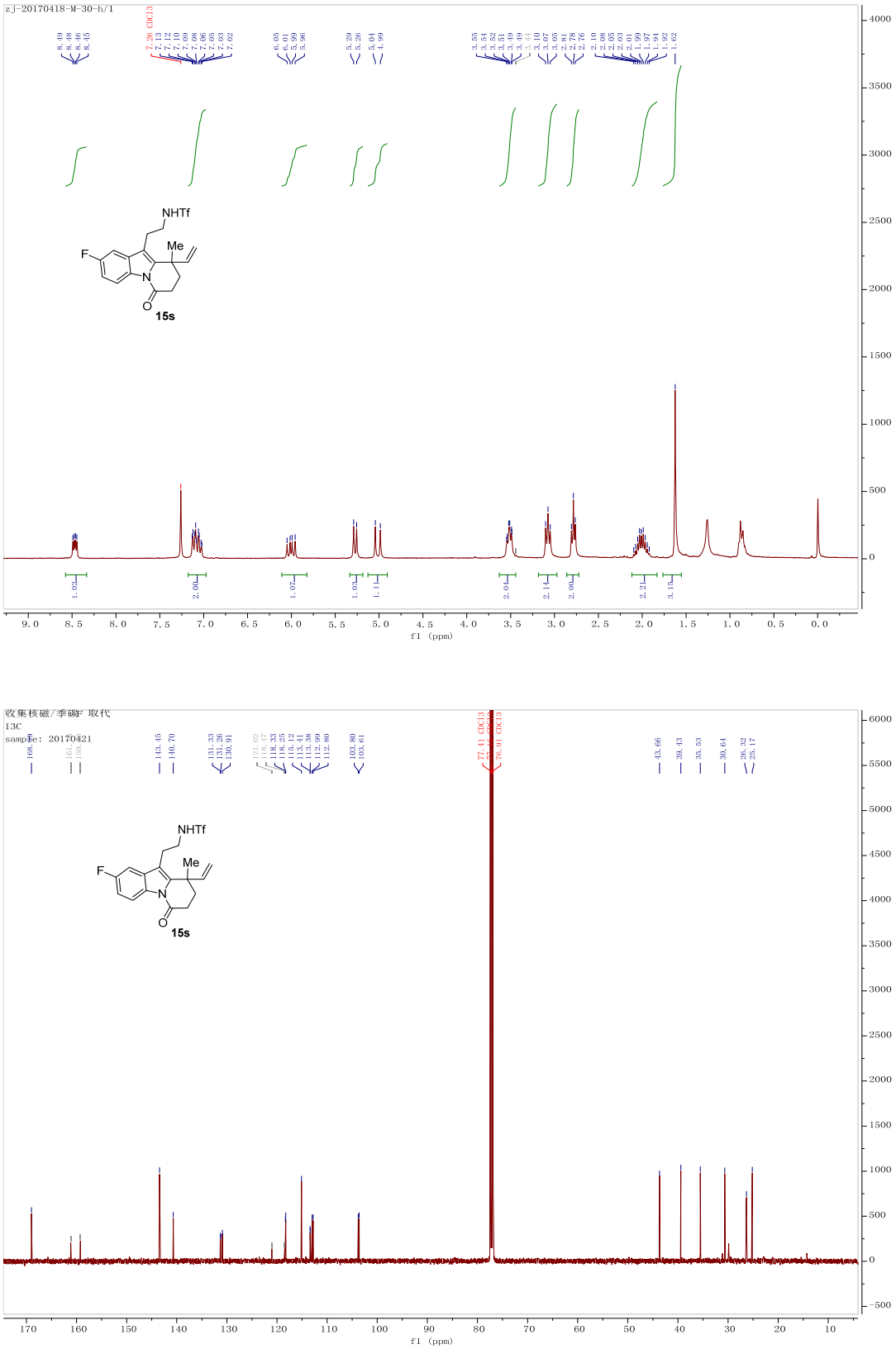

Figure S71. ^{1}H (upper) and ^{13}C-NMR (lower) of compound **15s**, related to **Table 3**

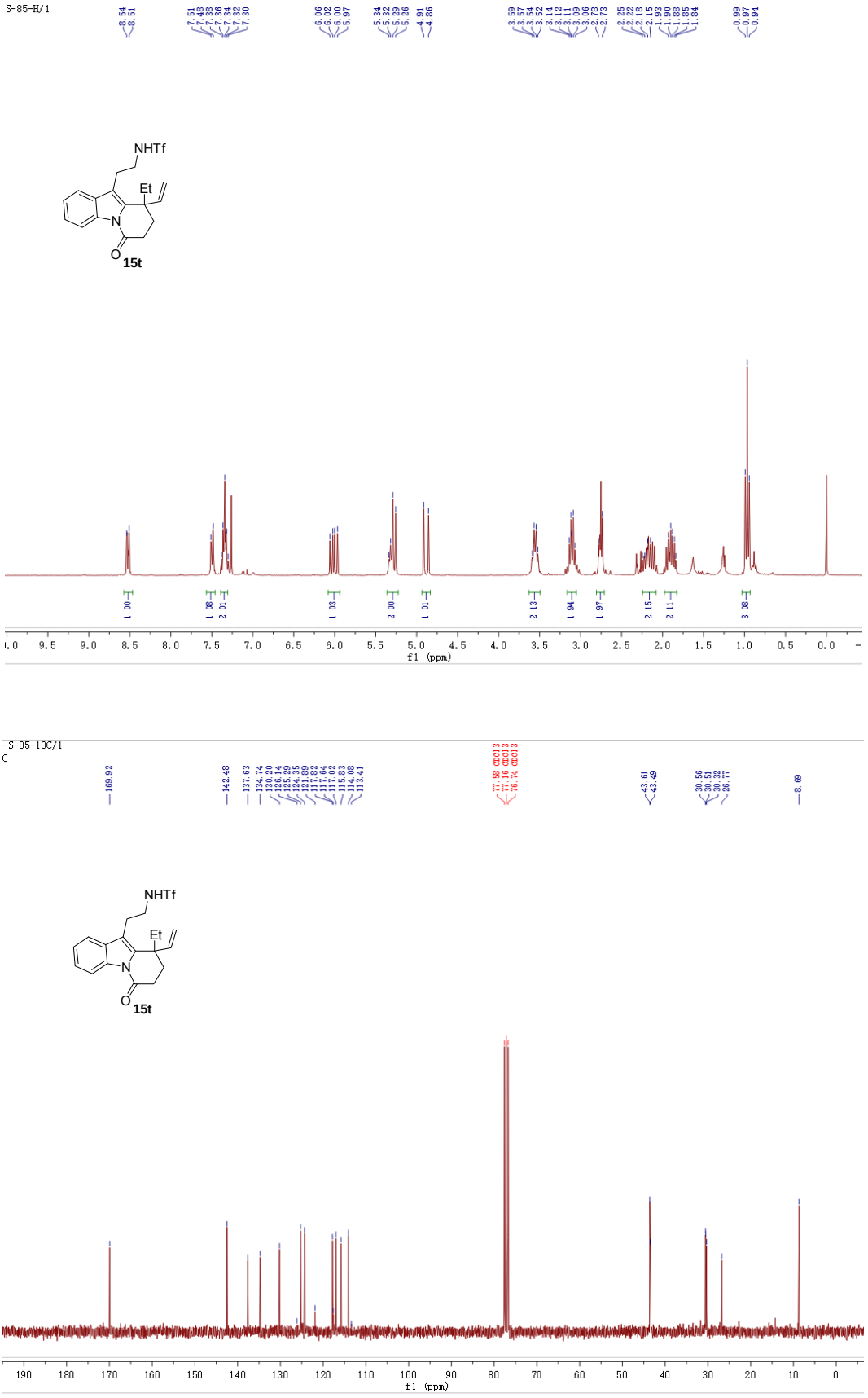

Figure S72. ^{1}H (upper) and ^{13}C-NMR (lower) of compound **15t**, related to **Table 3**

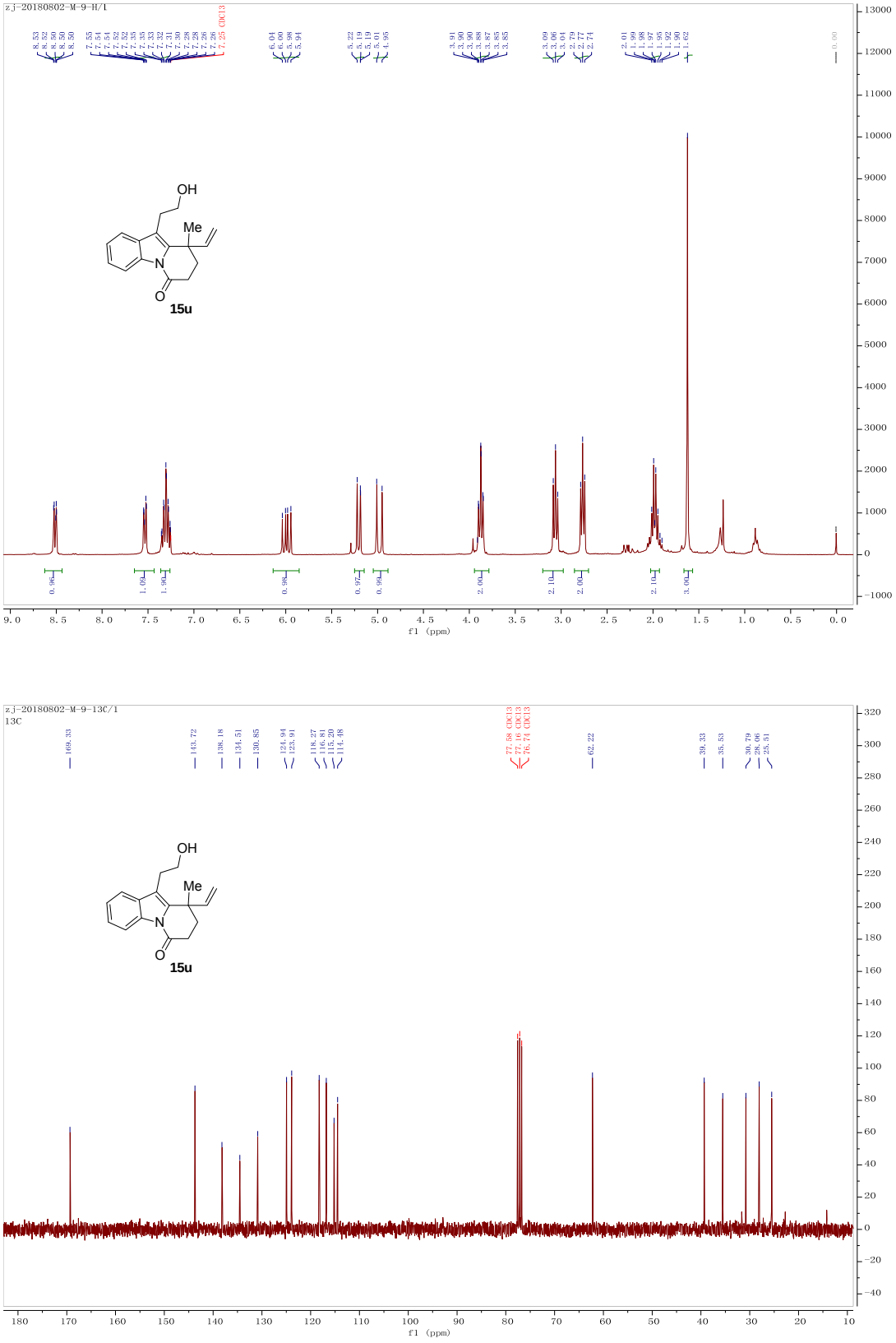

Figure S73. ^{1}H (upper) and ^{13}C-NMR (lower) of compound **15u**, related to **Table 3**

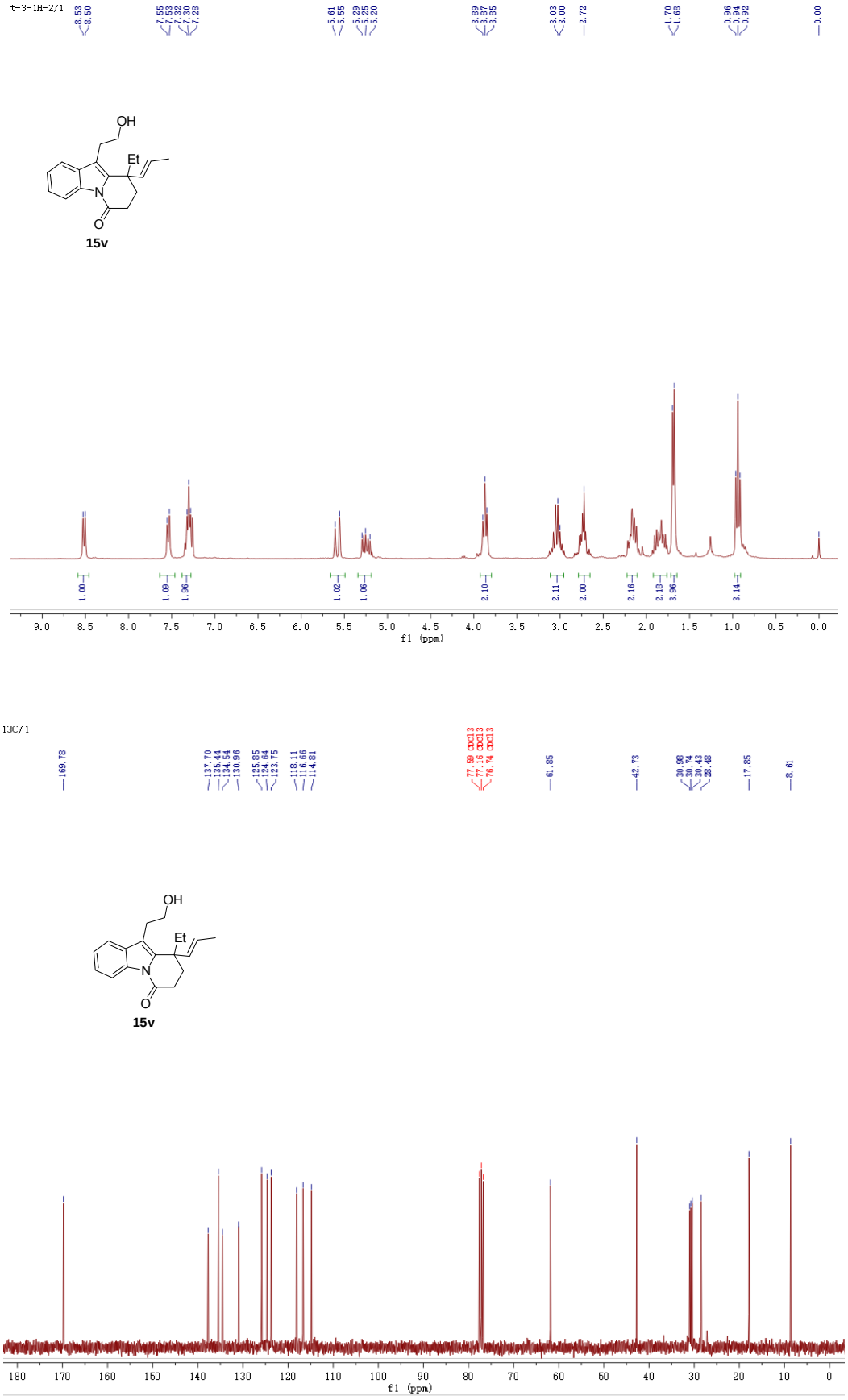

Figure S74. ^{1}H (upper) and ^{13}C-NMR (lower) of compound **15v**, related to **Table 3**

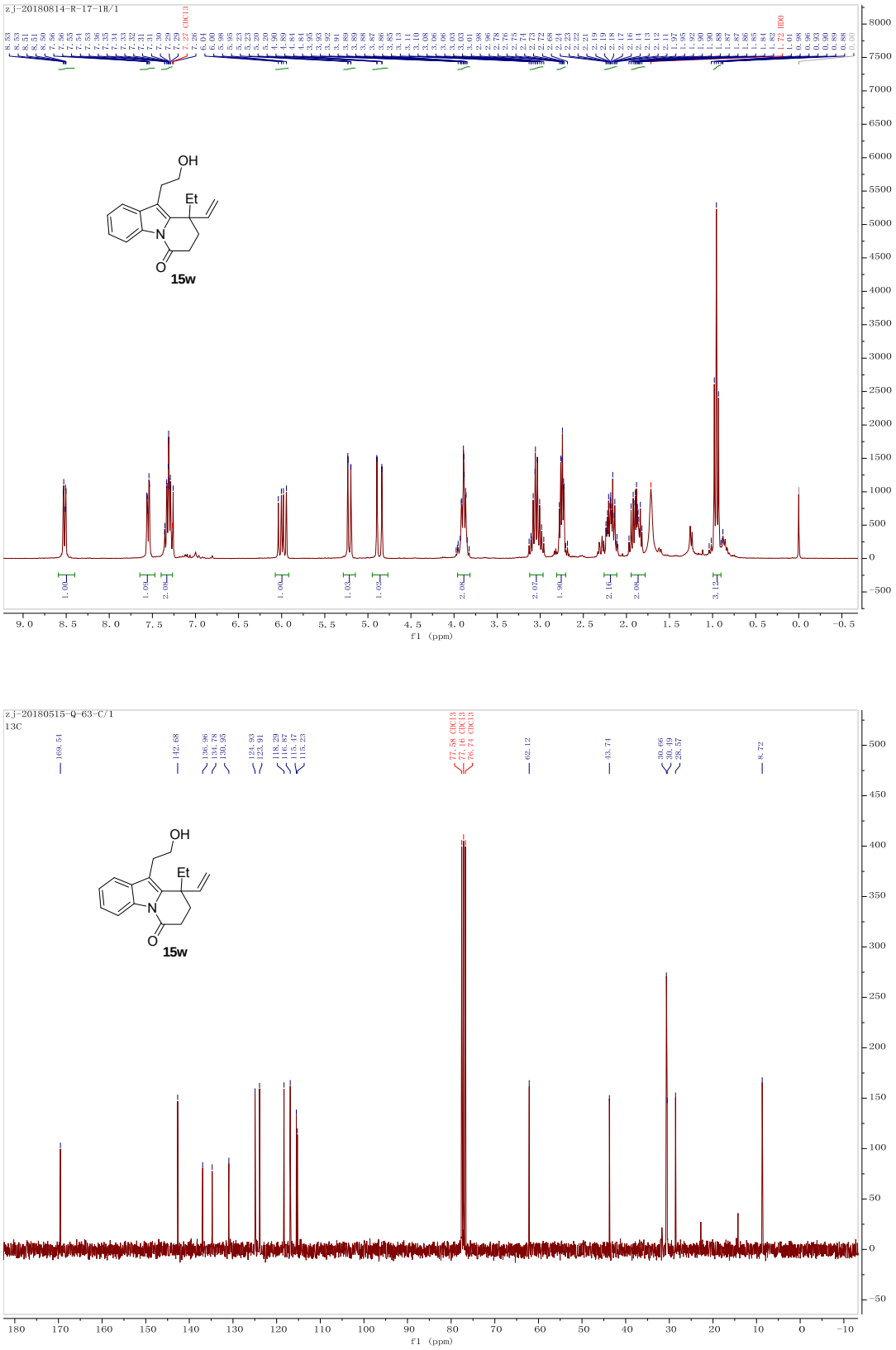

Figure S75. ^{1}H (upper) and ^{13}C-NMR (lower) of compound **15w**, related to **Table 3**

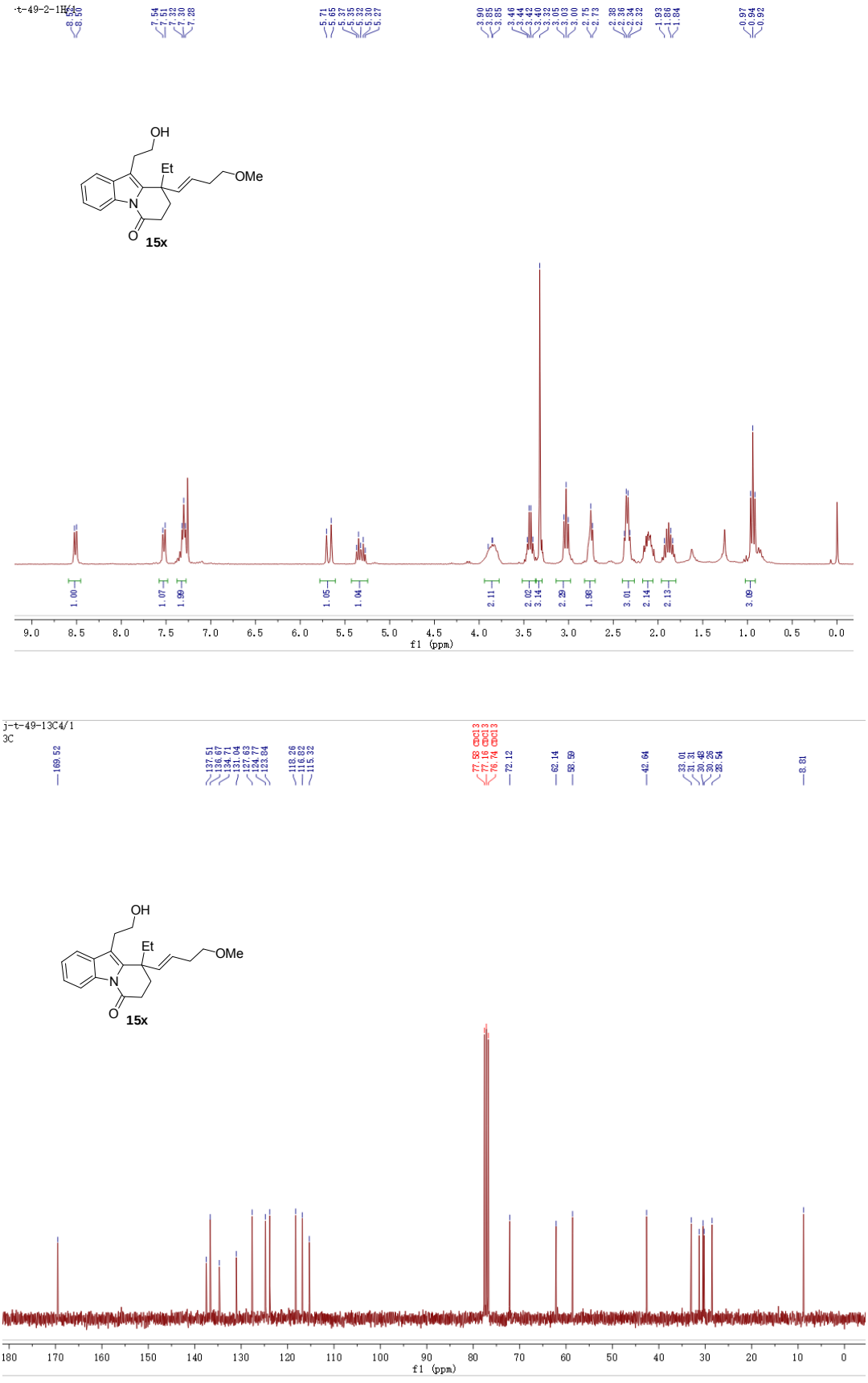

Figure S76. ^{1}H (upper) and ^{13}C-NMR (lower) of compound **15x**, related to **Table 3**

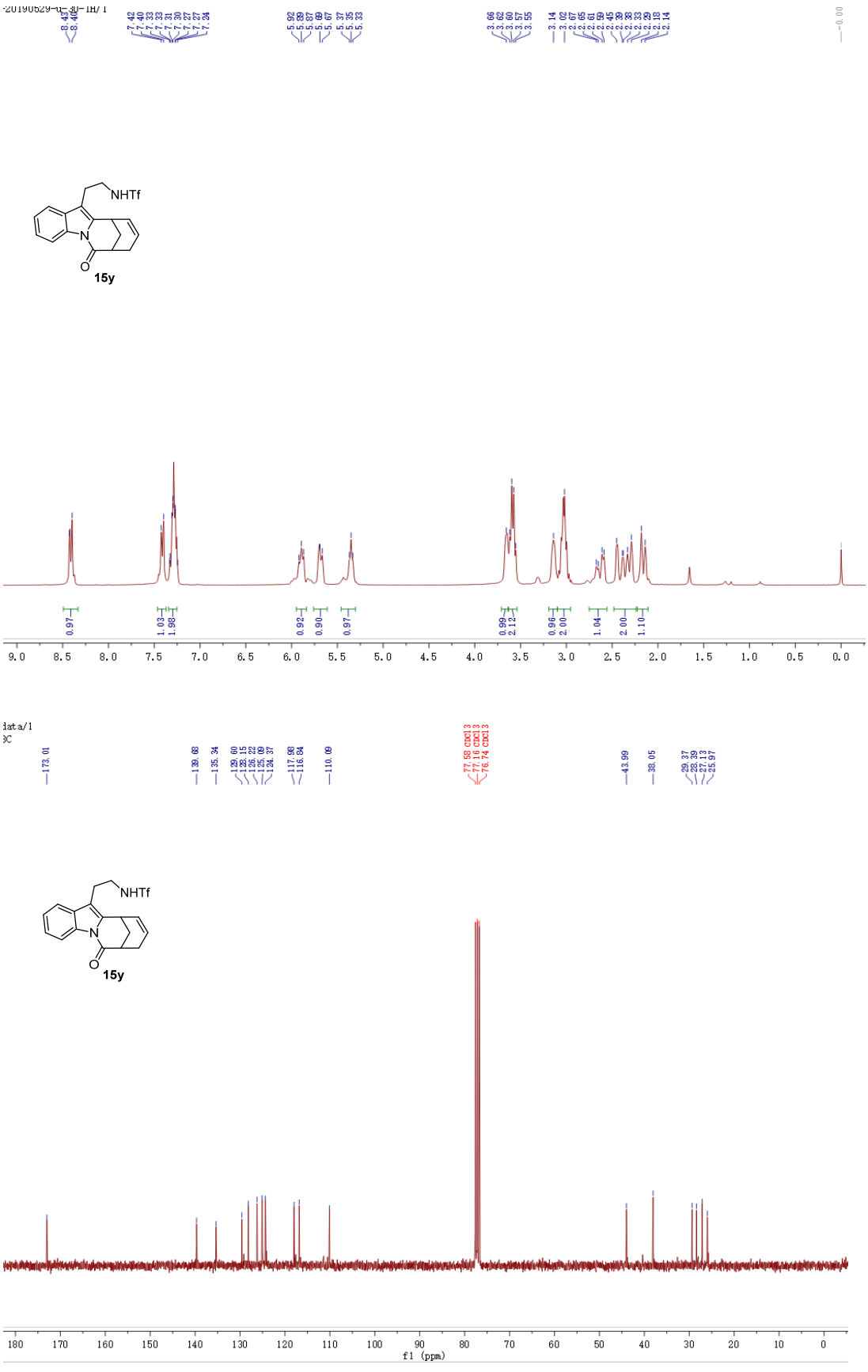

Figure S77. ^{1}H (upper) and ^{13}C-NMR (lower) of compound **15y**, related to **Table 3**

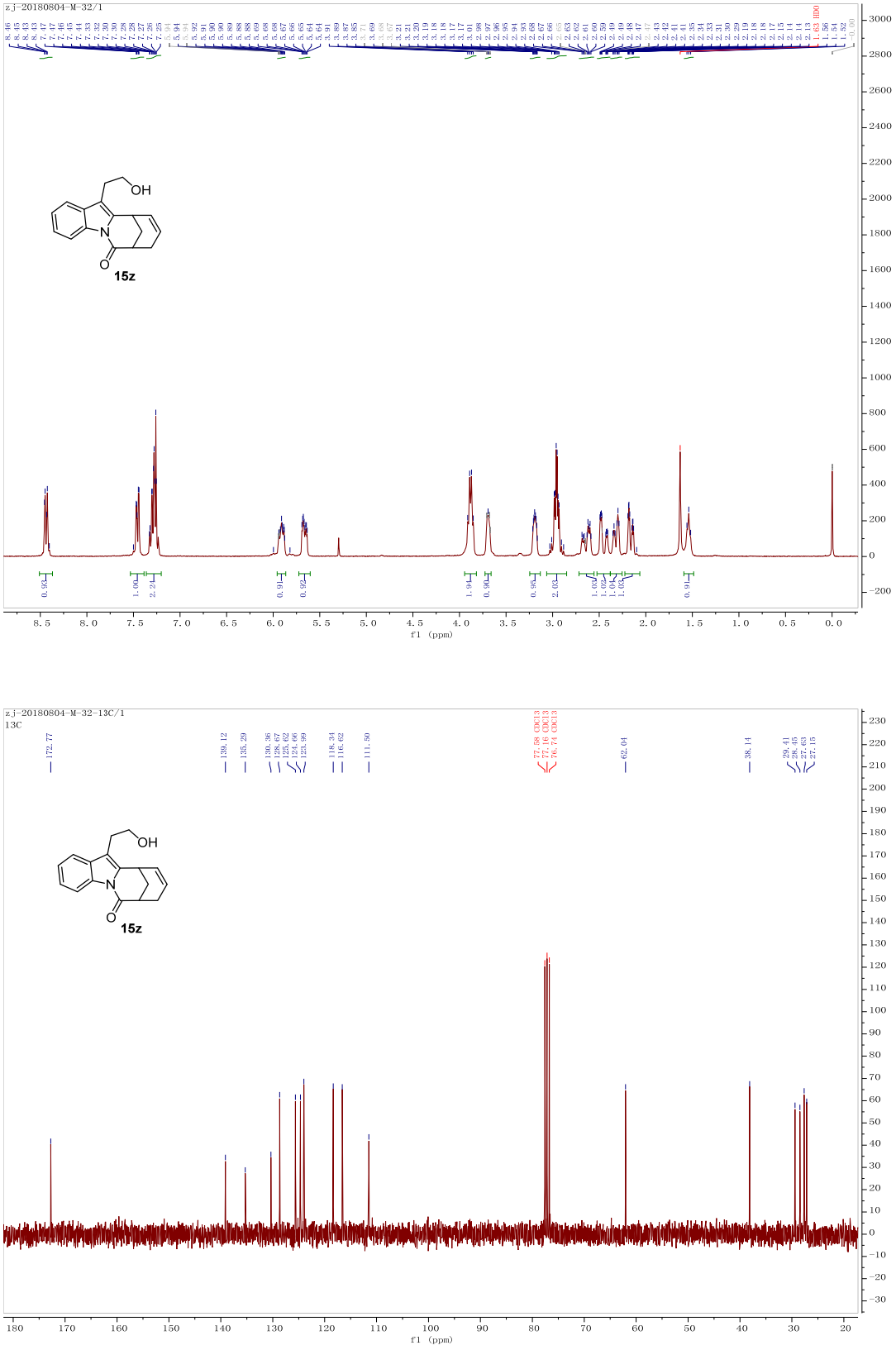

Figure S78. ^{1}H (upper) and ^{13}C-NMR (lower) of compound **15z**, related to **Table 3**

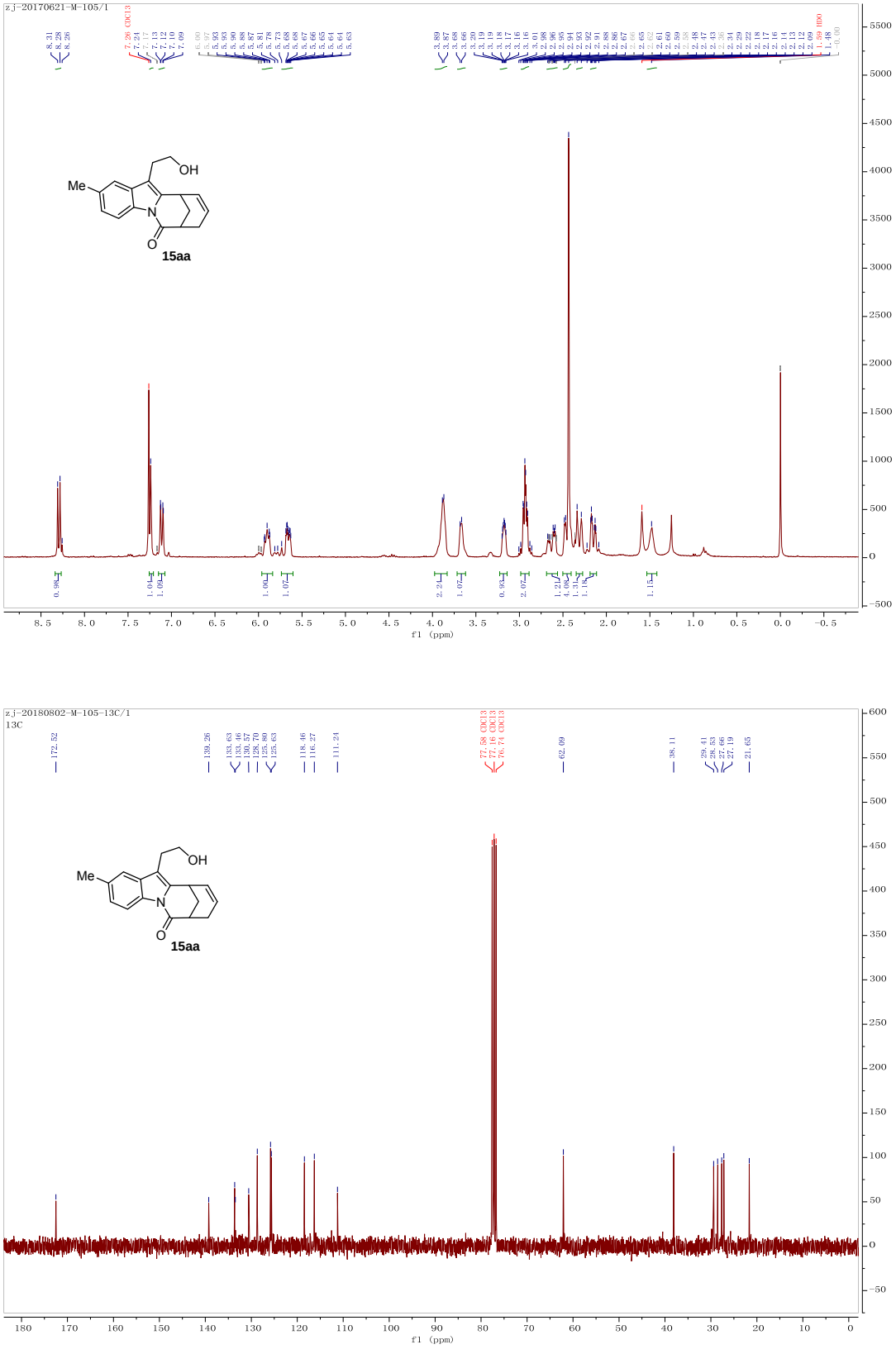

Figure S79. ^{1}H (upper) and ^{13}C-NMR (lower) of compound **15aa**, related to **Table 3**

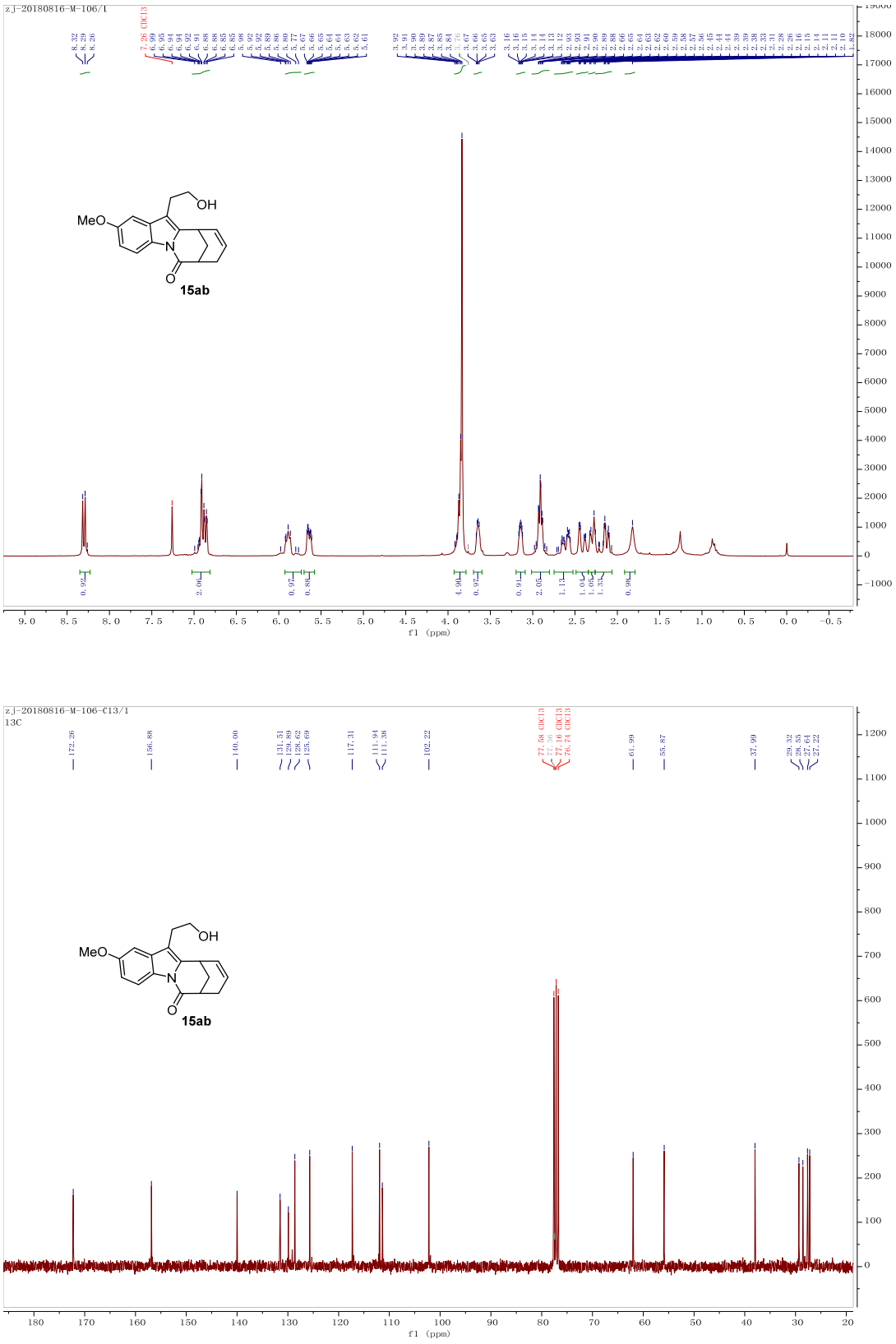

Figure S80. ^{1}H (upper) and ^{13}C-NMR (lower) of compound **15ab**, related to **Table 3**

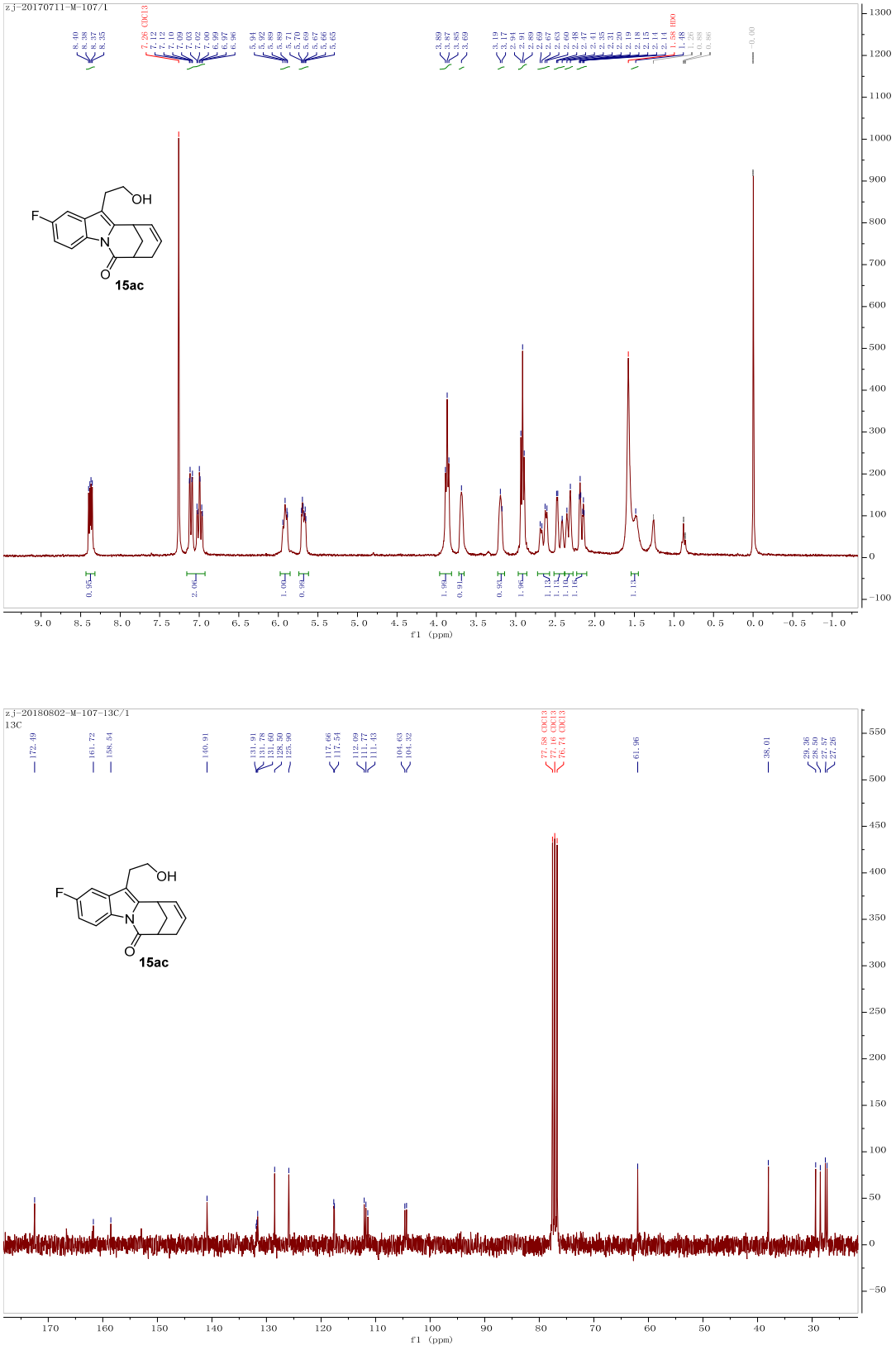

Figure S81. ^{1}H (upper) and ^{13}C-NMR (lower) of compound **15ac**, related to **Table 3**

8. References

1. Hartung, C.-G., Fecher, A., Chapell, B., and Snieckus, V. (2003). Direct ortho metalation approach to C-7-substituted indoles. Suzuki-Miyaura cross-coupling and the synthesis of pyrrolophenanthridone alkaloids. Org. Lett. *5*, 1899.

2. Liu, B.-Q., Song, C., Sun, C., Zhou, S- J., and Zhu, J. (2013). Rhodium(III)-catalyzed indole synthesis using N–N bond as an internal oxidant. J. Am. Chem. Soc. 135, 16625.

3. Pan, S., Ryu, N., and Shibata, T. (2012). Ir(I)-catalyzed C–H bond alkylation of C2-position of indole with alkenes: selective synthesis of linear or branched 2-alkylindoles. J. Am. Chem. Soc. *134*, 17474.

4. Powers, D. C. and Ritter, T. (2009). Bimetallic Pd(III) complexes in palladium catalysed carbon-heteroatom bond dormaiton. Nat. Chem. *1*, 302.